

REPORT DOCUMENTATION PAGE			Form Approved OMB NO. 0704-0188		
<p>The public reporting burden for this collection of information is estimated to average 1 hour per response, including the time for reviewing instructions, searching existing data sources, gathering and maintaining the data needed, and completing and reviewing the collection of information. Send comments regarding this burden estimate or any other aspect of this collection of information, including suggestions for reducing this burden, to Washington Headquarters Services, Directorate for Information Operations and Reports, 1215 Jefferson Davis Highway, Suite 1204, Arlington VA, 22202-4302. Respondents should be aware that notwithstanding any other provision of law, no person shall be subject to any penalty for failing to comply with a collection of information if it does not display a currently valid OMB control number.</p> <p>PLEASE DO NOT RETURN YOUR FORM TO THE ABOVE ADDRESS.</p>					
1. REPORT DATE (DD-MM-YYYY) 13-09-2011		2. REPORT TYPE Final Report		3. DATES COVERED (From - To) 29-May-2008 - 31-Jul-2011	
4. TITLE AND SUBTITLE Phase II: Programmable Matter Creating Systems that Can Think, Talk, and Morph Autonomously			5a. CONTRACT NUMBER W911NF-08-1-0228		
			5b. GRANT NUMBER		
			5c. PROGRAM ELEMENT NUMBER 8D10AN		
6. AUTHORS Daniela Rus			5d. PROJECT NUMBER		
			5e. TASK NUMBER		
			5f. WORK UNIT NUMBER		
7. PERFORMING ORGANIZATION NAMES AND ADDRESSES Massachusetts Institute of Technology (MIT) Office of Sponsored Programs Bldg. E19-750 Cambridge, MA 02139 -4307			8. PERFORMING ORGANIZATION REPORT NUMBER		
9. SPONSORING/MONITORING AGENCY NAME(S) AND ADDRESS(ES) U.S. Army Research Office P.O. Box 12211 Research Triangle Park, NC 27709-2211			10. SPONSOR/MONITOR'S ACRONYM(S) ARO		
			11. SPONSOR/MONITOR'S REPORT NUMBER(S) 54547-MS-DRP.1		
12. DISTRIBUTION AVAILABILITY STATEMENT Approved for Public Release; Distribution Unlimited					
13. SUPPLEMENTARY NOTES The views, opinions and/or findings contained in this report are those of the author(s) and should not be construed as an official Department of the Army position, policy or decision, unless so designated by other documentation.					
14. ABSTRACT This report covers the coordinated activities from MIT (PIs Daniela Rus and Erik Demaine), Berkeley University (PIs Ron Fearing and Ali Javey), Harvard University (PI Rob Wood), and the University of Pennsylvania (PIs Vijay Kumar and Mark Yim). Our vision is to create programmable matter analogous to a bag of "smart sand" or stack of "smart paper" that will be light and compact and which configures itself into a desired form as needed. We will achieve programmable					
15. SUBJECT TERMS programmable matter, origami robots					
16. SECURITY CLASSIFICATION OF:		17. LIMITATION OF ABSTRACT		15. NUMBER OF PAGES	
a. REPORT UU	b. ABSTRACT UU	c. THIS PAGE UU	UU	19a. NAME OF RESPONSIBLE PERSON Daniela Rus	
				19b. TELEPHONE NUMBER 617-258-7567	

Report Title

Phase II: Programmable Matter Creating Systems that Can Think, Talk, and Morph Autonomously

ABSTRACT

This report covers the coordinated activities from MIT (PIs Daniela Rus and Erik Demaine), Berkeley University (PIs Ron Fearing and Ali Javey), Harvard University (PI Rob Wood), and the University of Pennsylvania (PIs Vijay Kumar and Mark Yim).

Our vision is to create programmable matter analogous to a bag of “smart sand” or stack of “smart paper” that will be light and compact and which configures itself into a desired form as needed. We will achieve programmable matter using the paradigm of physically connected small robotic modules which can autonomously reconfigure into a desired goal shape. Programmable matter will enable warfighters to create parts (e.g. wrench, antenna, bench, cup, tripod, splint) on demand. When use is completed, the same material is reconfigured to make new parts with different shapes and functionalities, thus minimizing the overall load on the warfighter. The ability to make generically what is needed, when it is needed, is a ground-breaking leap forward in equipping warfighters for warfare scenarios because the packing list is simplified, the load lightened, and the capabilities increased. Areas of application include construction assembly and repair on the battlefield, the creation of temporary structural support for logistics, adaptive and interchangeable tooling for human assistance, and active formation of sensors, communication, and actuator arrays.

We are exploring two different concepts for achieving programmable matter: (1) a subtraction approach inspired by creating functional objects by sculpting and (2) a folding approach inspired by creating functional objects by origami. These are the most promising approaches to making programmable matter that were identified by the team’s prior research into modular small-scale robots and connectors, self-assembly strategies, and information flow. In Phase I and II we are studying the range of shapes achievable by each approach and experiment with fabrication of sub-cm scale unit-modules.

The centerpiece of our research focuses on the development of a smart light-weight material that integrates Sensing, Actuation, Computation, Communication, and Connectors and is called SAC3. We are also developing supporting algorithms for creating programmable matter by folding and subtraction, simulation infrastructure, and task specifications for achieving programmable matter from SAC3.

Enter List of papers submitted or published that acknowledge ARO support from the start of the project to the date of this printing. List the papers, including journal references, in the following categories:

(a) Papers published in peer-reviewed journals (N/A for none)

<u>Received</u>	<u>Paper</u>
-----------------	--------------

TOTAL:

Number of Papers published in peer-reviewed journals:

(b) Papers published in non-peer-reviewed journals (N/A for none)

<u>Received</u>	<u>Paper</u>
-----------------	--------------

TOTAL:

Number of Papers published in non peer-reviewed journals:

(c) Presentations

Number of Presentations: 0.00

Non Peer-Reviewed Conference Proceeding publications (other than abstracts):

Received Paper

TOTAL:

Number of Non Peer-Reviewed Conference Proceeding publications (other than abstracts):

Peer-Reviewed Conference Proceeding publications (other than abstracts):

Received Paper

TOTAL:

Number of Peer-Reviewed Conference Proceeding publications (other than abstracts):

(d) Manuscripts

Received Paper

TOTAL:

Number of Manuscripts:

Books

Received

Paper

TOTAL:

Patents Submitted

Patents Awarded

Awards

Graduate Students

<u>NAME</u>	<u>PERCENT SUPPORTED</u>
FTE Equivalent:	
Total Number:	

Names of Post Doctorates

<u>NAME</u>	<u>PERCENT SUPPORTED</u>
FTE Equivalent:	
Total Number:	

Names of Faculty Supported

<u>NAME</u>	<u>PERCENT SUPPORTED</u>
FTE Equivalent:	
Total Number:	

Names of Under Graduate students supported

<u>NAME</u>	<u>PERCENT SUPPORTED</u>
FTE Equivalent:	
Total Number:	

Student Metrics

This section only applies to graduating undergraduates supported by this agreement in this reporting period

- The number of undergraduates funded by this agreement who graduated during this period: 0.00
- The number of undergraduates funded by this agreement who graduated during this period with a degree in science, mathematics, engineering, or technology fields:..... 0.00
- The number of undergraduates funded by your agreement who graduated during this period and will continue to pursue a graduate or Ph.D. degree in science, mathematics, engineering, or technology fields:..... 0.00
- Number of graduating undergraduates who achieved a 3.5 GPA to 4.0 (4.0 max scale):..... 0.00
- Number of graduating undergraduates funded by a DoD funded Center of Excellence grant for Education, Research and Engineering:..... 0.00
- The number of undergraduates funded by your agreement who graduated during this period and intend to work for the Department of Defense 0.00
- The number of undergraduates funded by your agreement who graduated during this period and will receive scholarships or fellowships for further studies in science, mathematics, engineering or technology fields: 0.00

Names of Personnel receiving masters degrees

<u>NAME</u>
Total Number:

Names of personnel receiving PHDs

<u>NAME</u>
Total Number:

Names of other research staff

<u>NAME</u>	<u>PERCENT SUPPORTED</u>
FTE Equivalent:	
Total Number:	

Sub Contractors (DD882)

Inventions (DD882)

Scientific Progress

please see the attached report
no inventions

Technology Transfer

A Final Report to DARPA on Project
Phase II: Programmable Matter
Creating Systems that Can Think, Talk, and
Morph Autonomously
Award W911NF-08-1-0228,
Army Research Office
Final Report

PI: Daniela Rus, MIT CSAIL

Contents

1	Overall Project Goals	3
2	Activities and Findings	3
2.1	Mechanics, electronics, and actuation	4
2.1.1	Participants	4
2.1.2	Highlights	4
2.1.3	Collaborations	4
2.1.4	Approach	4
2.1.5	Implementation	5
2.1.6	Experiments	7
2.1.7	Findings	11
2.2	Nanowire connectors	12
2.2.1	NIPAM Programmable Materials	12
2.2.2	Participants	13
2.2.3	Highlights	13
2.2.4	Collaborations	13
2.2.5	Approach	13
2.2.6	Implementation	14
2.2.7	Characterization	15
2.2.8	Theory	15
2.2.9	Integration	16
2.2.10	Findings	16
2.3	Nanowire connector integration	17
2.3.1	Highlights	17
2.3.2	Collaborations	17
2.3.3	Approach	18
2.3.4	Implementation	18
2.3.5	Findings	18
2.4	Polymer microfiber connectors	19
2.4.1	Highlights	19
2.4.2	Approach	19
2.4.3	Implementation	19
2.4.4	Findings	19
2.5	Magnetic metal spikes	19
2.5.1	Highlights	20
2.5.2	Collaborations	20
2.5.3	Approach	20
2.5.4	Implementation	20
2.5.5	Findings	21
2.6	Microconnectors for reconfigurable millirobots	21
2.6.1	Highlights	21

2.6.2	Approach	22
2.6.3	Implementation	23
2.6.4	Findings	25
2.7	Low-Stiffness Conformal Backing	26
2.7.1	Highlights	26
2.7.2	Approach	27
2.7.3	Implementation	27
2.7.4	Findings	28
2.8	Magnetic Connectors and Smart Sand	28
2.8.1	Collaborations	29
2.8.2	Highlights	29
2.8.3	Approach	29
2.8.4	Findings	33
2.9	Algorithms	34
2.9.1	Highlights	34
2.9.2	Collaborations	34
2.9.3	Approach	34
2.9.4	Findings	35
2.10	Simulation and Task Specification	36
2.10.1	Highlights	36
2.10.2	Collaborations	37
2.10.3	Approach	37
2.10.4	Implementation	37
2.10.5	Findings	38
2.11	Papers	39

1 Overall Project Goals

This report covers the coordinated activities from MIT (PIs Daniela Rus and Erik Demaine), Berkeley University (PIs Ron Fearing and Ali Javey), Harvard University (PI Rob Wood), and the University of Pennsylvania (PIs Vijay Kumar and Mark Yim).

Our vision is to create programmable matter analogous to a bag of “smart sand” or stack of “smart paper” that will be light and compact and which configures itself into a desired form as needed. We will achieve programmable matter using the paradigm of physically connected small robotic modules which can autonomously reconfigure into a desired goal shape. Programmable matter will enable warfighters to create parts (e.g. wrench, antenna, bench, cup, tripod, splint) on demand. When use is completed, the same material is reconfigured to make new parts with different shapes and functionalities, thus minimizing the overall load on the warfighter. The ability to make generically what is needed, when it is needed, is a ground-breaking leap forward in equipping warfighters for warfare scenarios because the packing list is simplified, the load lightened, and the capabilities increased. Areas of application include construction assembly and repair on the battlefield, the creation of temporary structural support for logistics, adaptive and interchangeable tooling for human assistance, and active formation of sensors, communication, and actuator arrays.

We are exploring two different concepts for achieving programmable matter: (1) a subtraction approach inspired by creating functional objects by sculpting and (2) a folding approach inspired by creating functional objects by origami. These are the most promising approaches to making programmable matter that were identified by the team’s prior research into modular small-scale robots and connectors, self-assembly strategies, and information flow. In Phase I and II we are studying the range of shapes achievable by each approach and experiment with fabrication of sub-cm scale unit-modules.

The centerpiece of our research focuses on the development of a smart light-weight material that integrates **S**ensing, **A**ctuation, **C**omputation, **C**ommunication, and **C**onnectors and is called **SAC**³. We are also developing supporting algorithms for creating programmable matter by folding and subtraction, simulation infrastructure, and task specifications for achieving programmable matter from *SAC*³.

2 Activities and Findings

1. Mechanics, electronics, and actuation for folding
2. Connectors.
3. Algorithms
4. Simulation and Characterization.

In each of these areas we have innovated and obtained novel results in the span of a short time. Our efforts are described in detail below. Many of these results are in the process of being disseminated in the form of refereed papers.

2.1 Mechanics, electronics, and actuation

2.1.1 Participants

Robert Wood, Jamie Paik, Byoung An, Daniela Rus

Several aspects in the fabrication of the robotic origami have been investigated as follows:

- Substrate fabrication
- Stretchable circuits
- Low profile torsional actuators
- Integration and folding experiments

2.1.2 Highlights

Our biggest highlight is the development of a process to fabricate and assembly all the mechanical components of a self-folding robotic origami. The robotic origami consists of a substrate with a universal folding pattern, newly developed stretchable circuits, and high-torque low-profile folding actuators.

2.1.3 Collaborations

- We have worked with the Rus group to develop universal circuit patterns and demonstrations to simplify programming of the self-folding sheets.
- We have also worked with the Rus group on fabrication and sheet design.

2.1.4 Approach

In phase I, we defined one of the concepts for programmable matter as a reconfigurable self-folding sheet. Thus, our work in phase II concentrated on the elements of a self folding sheet. These include:

- Fabrication techniques for tiled substrates with flexible and extensible mechanical interconnections.
- Power and control circuits which are also flexible and extensible.
- Low-profile, high torque density torsional actuators to power folding.

In addition to the topics listed above, we have addressed integration issues to make the overall assembly of the self folding sheets and rapid as possible.

2.1.5 Implementation

Our first task was to define a fabrication process for the folding sheet substrate that would be flexible enough to allow rapid prototyping of various designs. The requirements for the substrate are simple: provide a rigid substrate for the connection of all components of the self-folding sheet and include flexible and extensible joints to accommodate the folds that define the 3D folded shapes. The sheets are created as a combination of micro-machining and molding. First, layers of fiberglass composite sheets, chosen for high strength, low density, and dielectric properties, are laminated to form a single rigid sheet approximately $200\mu\text{m}$ thick. This sheet is then micro-machined using a diode-pumped solid-state (DPSS) laser while on a tacky carrier. This step creates the tiling pattern as well as other mechanical features such as mounting holes for the actuators. In previous fabrication methods, the subsequent step would be casting a silicone elastomer layer onto the machined tiles and curing to form the joints of the folding sheet. The silicone elastomers can be very low modulus and accommodate folding and stretching - the latter being necessary for ‘compound folds’ which occur when multiple successive folds are performed using the same sheet. The silicone elastomers also bond well to glass fiber composites. However, we have recently switched to a process of encapsulation wherein after machining the tiles, the circuit layer is laminated to the tiles, then encapsulated with two layers of thermoplastic polyurethane under a controlled pressure and temperature profile. The circuit layer is created in one of two ways. The first method involves direct-write lithography using the same DPSS laser system. The circuit is created from a polyimide/copper composite which is covered with a resist, exposed using the DPSS laser, developed, and etched. The circuit is then re-aligned to the laser which performs a final machining step, this time to create a mesh pattern transversely to the path of the conductive trace at each point where the trace crosses a joint. This patterning converts axial stresses from joint extension into local bending moments in the metal traces thereby effectively increasing the maximum strain that the trace can withstand before mechanical failure from a few percent to over 50%. The final thermoplastic lamination step protects the delicate features in the copper mesh. An alternative method uses micro-channels in a thin elastomer filled with liquid metals (eutectic Gallium Indium, eGaIn). Although not as conductive as copper, eGaIn can still manage a high current density with inter-tile resistances in the tenths of ohms. Micro-channels are formed in an elastomer substrate (PDMS) using microfluidics techniques and filled with eGaIn using syringes. Once sealed, the soft circuit is laminated to the surfaces of the tiles and chemically bonded. The eGaIn soft circuits can withstand over 100% strain and can also include a variety of sensors (e.g. for joint angle proprioception).

The above process creates a tiled sheet that is mechanically and electrically interconnected. A major challenge for a self folding sheet is actuation. The actuation needs of the robotic origami form a paradox: the joints require high torques, which are typically obtained using an extended moment arm, however the low profile requirement eliminates this possibility. Therefore, we require actuators with a high torque density. After exploring many options including electromagnetic, electrostatic, and electroactive polymers, we settled on shape memory alloys. Although these actuators suffer from low electromechanical efficiency

(on the order of 5%), their energy density is extremely high (approximately 1kJ/kg). Furthermore, there is a large space of geometric designs one can choose from including wire, coil, and sheets, and all materials can be formed into arbitrary shapes through a process of fixturing and annealing. For folding actuators, we start with thin sheets of nickel titanium shape memory alloy, laser machine into the desired platform shape, and fix into a ‘closed’ fold. The sheet is annealed while folded at a temperature well above the transition temperature for the material. This forms a new ‘memorized’ shape. After annealing, the actuator is manually unfolded and fixed to the tiles using either sum-millimeter bolts or hooks built into the actuator geometry. Once heated above the transition temperature, the actuator reverts to its memorized folded shape, thereby applying a torque about the folding axis. We have demonstrate folding actuators with a 180 degree folding range and between 30-50mNm of blocked torque in a 500 μ m thick package. We have also explored the ability to reduce actuation time constants and increase efficiency by using external heating elements. The typical mode for heating a shape memory actuator is by Joule heating by passing a current through the body of the actuator. Since the alloys are typically low resistivity, this can be wasteful since heating the entire actuator is not necessary given a relatively small active area relative to the overall area of the actuator. Furthermore, large currents are required to raise the temperature above the transition temperature which could cause wasteful dissipation by I^2R losses in surrounding circuitry. One way to alleviate this is to pattern the actuator sheet to create more narrow current paths in the active area, but this has the drawback of reducing torque capabilities and robustness. Instead, we have concentrated on an external heating element using patterned nickel chrome sheets bonded to the active areas of the actuator with a polyimide carrier. This increases the resistance by approximately one order of magnitude compared to Joule heating, thereby dramatically reducing the current (at a higher voltage) and therefore reducing the losses in surrounding circuits. Additionally, the thermal mass is lower which decreases the time constant for the actuator transition. All of the above discussion has described a unidirectional actuator. We have also explored a bidirectional version which has demonstrated the ability to create decoupled folds in either direction.

Finally, we have performed a large integration effort aimed at seamless assembly of all the components of the robotic origami. The long term vision for programmable matter by folding is to use parallel processes for molding and machining and roll-to-roll population of discrete components similar to printed circuit boards. In phase II we have established the ability to fabricate the sheets and actuators and explored methods to assemble the actuators onto the tiles. This has a number of difficulties due to the high torque of the actuators and strong oxide that form on the surface of the nickel titanium alloy. The former implies that chemical bonds (e.g. epoxies) may not be sufficient while the latter means that soldering is extremely difficult. We have experimented with mechanical connections (bolts and tabs and slots) as well as micro-welding. Electrical connections are made either simultaneously with the mechanical connection or by laser welding to the heater electrodes.

Table 1: Overview of 4×4 and 8×8 self-folding sheets

	4×4 sheet	8×8 sheet
Crease Pattern	4×4 Box-Pleated	8×8 Box-Pleated
Total # of Edges	40	176
Total # of Actuators	40	36
Current	1.5 A	5.0 A
Ave. Folding Time	21.6 s	5.0 s
Sticker Controller	Sticker Controller	Socket Controller
Reprogram	Very Easy	Easy
Body	LP Body	LP Body
Actuator	Y-type Actuator	Y-type Actuator
Sticker Programming	By Sticker Programming Algorithm	By Sticker Programming Algorithm

Table 2: Origami Planning Time for Vertical and Diagonal folding

Single Origami Planing Analysis Time (Vertical)	3.6 s (3600 ms)
Single Origami Planing Building Time (Vertical)	17 ms
Single Origami Planing Analysis Time (Diagonal)	4.2 s (4200 ms)
Single Origami Planing Building Time (Diagonal)	16 ms
CPU	Intel Core 2 Quad 2.83GHz (Q9550)
Storage	3 GB RAM, Seagate 750GB 300MBps 7200rpm HDD
Graphics	NVIDIA Quadro FX 1700

2.1.6 Experiments

We have built the 4×4 and 8×8 self-folding sheets and executed three programs on them; Table 1 shows the overview of the target sheets.

Self-folding sheets are composed of four parts : a body, actuators, a controller, and a sticker program (see attached Figures). The 4×4 sheet and the 8×8 sheet have the same body and actuators but different controllers which are implemented as different circuits. However, the controllers for both the 4×4 and the 8×8 sheets are implemented using the sticker controller architecture.

The 4×4 self-folding sheet runs two basic motion: vertical and diagonal folding (Fig ??) (see attached figures).

We implemented and evaluated the following four steps:

1. we generated two executable sticker designs for the vertical shape and diagonal shape.
2. we placed and executed the executable sticker for the vertical folding.
3. we removed the executable sticker.
4. we placed and executed the executable sticker for the diagonal folding.

Table 2 shows the planning times on hardware.

Table 3: Actuators of 4×4 Sheet

	Folding Actuators	Total Actuators	Total Edges	Folding Actuators / Total Actuators	Total Actuators / Total Edges
Vertical	12	40	40	30.0%	100.0%
Diagonal	10	40	40	25.0%	100.0%
Total	11	40	40	42.5%	100.0%

Table 4: Folding Time and Current of 4×4 Sheet

	# of Runs	Current	Ave. Folding Time
Vertical	14	1.5 A	21.0 s \pm 26.7%
Diagonal	13	1.5 A	22.4 s \pm 17.9%
Total	27	1.5 A	21.6 s \pm 22.5%

The 4×4 sheet has 40 actuators and 40 edges. 42.5% of the actuators are the actuators were used for each of the two shapes (Table 3).

First, we executed the vertical folding program on the 4×4 self-folding sheet 14 times. Second, we removed the program and reprogrammed the sheet diagonal folding program on the sheet. Then we executed the diagonal folding 13 times. The 4×4 sheet achieved the vertical and diagonal folding reliably (Fig. ??, ??). The 4×4 self-folding sheet runs with current set at 1.5 A. The average folding time of both shapes is 21.6 s (Table 4).

The average angle¹ of the basic folding motion is $134.0^\circ \pm 12.1\%$. Our target folding angle for the basic folding motion was 180.0° . We achieved 74.5% of the target angle.

The error of the diagonal folding angle is 2.1 times bigger than the error of the vertical folding. The diagonal folding is achieved by folding three straight-lines. Each line are the same length and has the same number of the actuators. But, diagonal folding is achieved by folding one long center-line and two short side-lines. Although the center-line carried more weight than the side-line, the center-line achieved better folding than on the side-line. Four actuators are on the center-line while Two actuators on each side-line.

While we folded the 4×4 sheet 27 times, the experiment failed to meet the goal three times (Table 6). Most of failures were due to broken or weak connection between the socket and

¹The angles might not be accurate. We measured the angles by video analysis after the experiments. We picked and analyzed three angles from the first videos of each experiment.

Table 5: Folding Angle and Folding Achievement of 4×4 Sheet

	Ave. Folding Angles ¹	Target Angles	Folding Achievement (Folding Angle / Target Angle)
Vertical	$141.6^\circ \pm 7.9\%$	180.0°	78.7%
Diagonal	$126.4^\circ \pm 16.3\%$	180.0°	70.2%
Total	$134.0^\circ \pm 12.1\%$	180.0°	74.5%

Table 6: Failure of 4×4 Sheet

	# of Runs	# of Failure	Ave. Failure
Vertical	14	1 (of 14 runs)	0.7 (of 10 runs)
Diagonal	13	2 (of 13 runs)	1.5 (of 10 runs)
Total	27	3 (of 27 runs)	1.1 (of 10 runs)

Table 7: Disabled Actuators of 4×4 Sheet

	Ave. # of Disabled Actuators	Folding Actuators	Disabled Actuators / Folding Actuators	Disabled Actuators / Total Actuators
Vertical	0.77	12	6.4 %	1.9 %
Diagonal	1.36	10	13.6 %	3.4 %
Total	1.04	11	9.7 %	2.6 %

the actuator. SMA is a material that is hard to solder. We made the electronic connection not only with solder but also with conductive bolts and nuts. However, while the sheet folded several times, the electronic connection was weak. Once the connection was loose, the socket was hard to recover. In this case, we fixed the system by disabling the broken actuator.

The average number of disabled actuators was 1.04 (Table 7). The sheet achieved their shapes reliably with this number of the disabled actuators.

Most of the results of the two basic shapes on the 4×4 sheet are similar. However, the resistance was 19.1Ω for vertical folding while the resistance was 28.9Ω for diagonal folding. The resistance of the sheet increased 1.5 times after we reprogrammed the sheet. (Table 8). Because the number of folding actuators is almost same in the two experiments, we can say the connectivity decreases after reprogramming the sheet.

We designed the 8×8 sheet to test self-folding planning for more complex shapes. We selected a space shuttle-like shape and a hat-like shape (see attached figures).

We did implemented and evaluated the following four steps:

1. we generated an executable sticker design for the space shuttle and hat shapes.
2. we placed the executable sticker for the two shapes.
3. we executed the executable sticker for the space shuttle shape.
4. we executed the executable sticker for the hat shape.

Table 8: Resistance of 4×4 Sheet

	Ave. Resistance (R)
Vertical	19.1Ω
Diagonal	28.9Ω
Total	23.6Ω

Table 9: Actuators of 8×8 Sheet

	Folding Actuators	Total Actuators	Total Edges	Folding Actuators / Total Actuators	Total Actuators / Total Edges
Space Shuttle (Group 1, 2)	20	36	176	55.6%	20.5%
Hat (Group 1, 3)	24	36	176	66.7%	20.5%
Total	22	36	176	61.1%	20.5%

Table 10: Folding Time and Current of 8×8 Sheet

	# of Runs	Current	Ave. Folding Time
Space Shuttle (Group1, 2)	14	5.0 A	5.9 s \pm 16.9%
Hat (Group1, 3)	12	5.0 A	4.5 s \pm 23.4%
Total	26	5.0 A	5.0 s \pm 19.9%

The 8×8 sheet has 36 actuators and 176 edges. The socket controller controlled the 8×8 sheet with the relatively small number of actuators (only 20.5% of edges have the actuators). 61.1% of the actuators are used, when the sheet transformed into the both shapes (Table 9).

We executed the space shuttle shape folding on the 8×8 device 14 times. Then, we executed the folding of hat shape 12 times. The 8×8 sheet achieved the space shuttle and hat shapes reliably with the optimized number of actuators (Fig. ??, ??). The 8×8 self-folding sheet runs with current set at 5.0 A. The average folding time was 5.0 s (Table 10).

While we folded the 8×8 sheet 26 times with the two complex shapes, the experiment failed five times (Table 11). Like the 4×4 sheet, most of the failures were due to broken or weak connections between a socket and an actuator. We resolved these failures by disabling the broken actuator.

The average number of disabled actuators (for fix) was 0.81. It is 3.7 % of the folding actuators and 2.2 % of the total actuators (Table 12). The sheet achieved their shapes

Table 11: Failure of 8×8 Sheet

	# of Runs	# of Failure	Ave. Failure
Space Shuttle (Group1, 2)	14	3 (of 14 runs)	2.1 (of 10 runs)
Hat (Group1, 3)	12	2 (of 12 runs)	1.6 (of 10 runs)
Total	26	5 (of 26 runs)	1.9 (of 10 runs)

Table 12: Disabled Actuators of 8×8 Sheet

	Ave. # of Disabled Actuators	Folding Actuators	Disabled Actuators / Folding Actuators	Disabled Actuators / Total Actuators
Space Shuttle (Group1, 2)	0.82	20	4.1 %	2.3 %
Hat (Group1, 3)	0.80	24	3.3 %	2.2 %
Total	0.81	22	3.7 %	2.2 %

Table 13: Resistance of 8×8 Sheet

	Ave. Resistance Group1, Group2, Group3	Ave. Resistance of Folding Groups
Space Shuttle (Group1, 2)	44.8 Ω , 34.8k Ω , 1.71M Ω	17.4k Ω
Hat (Group1, 3)	109.3 Ω , 14.7k Ω , 51.0 Ω	80.15 Ω
		(Group1 + Group2) / 2
		(Group1 + Group3) / 2

reliably with this number of the disabled actuators.

We enabled the actuator group 1 and 2 for the space shuttle-like shape. The resistance for the space shuttle shape was 17.4k Ω . We enabled the actuator group 1 and 3 for the hat-like shape. The resistance for the hat shape was 80.15 Ω . While we executed the space shuttle shape, the average resistance of group 3 was 1.71M Ω . However, because we did not use the group 3 for the space shuttle shape, there was no problem to archive the shape.

2.1.7 Findings

- We have established a complete fabrication process which enables the creation of self-folding sheets of robotic origami.
- We have created two types of stretchable circuits which can withstand the elongation associated with compound folds of the robotic origami.
- We have demonstrated both unidirectional and bidirectional actuators using folded and annealed shape memory alloys. These actuators are capable of greater than 30mNm of blocked torque and 180 degrees of folding.
- We have established a new way to control shape memory alloy actuators using an external heating element which improves energy efficiency and reduces the actuation time constant.
- We have combined all of these components into a demonstration of programmable matter by folding which can achieve multiple shapes on command.

2.2 Nanowire connectors

This project investigated connectors and actuators which could be used to join programmable matter components. These connectors were made from a variety of materials and technologies, with the goals of creating new connector technologies which are strong, reusable, and low cost. The technologies explored are listed here:

- NIPAM Programmable Materials
- Nanowire connector integration
- Polymer microfiber connectors
- Magnetic metal spikes
- Microconnectors for reconfigurable millirobots
- Low-Stiffness Conformal Backing

These are described in detail in each section below.

2.2.1 NIPAM Programmable Materials

Our goals for Phase II have been to create programmable materials based on thermally and optically responsive actuators. The UC Berkeley team has been developing carbon nanotube and poly NIPAM composite materials for making programmable matter which meets these requirements.

Several aspects of the CNT-pNIPAM actuators have been investigated as follows:

- Lower Critical Transition Temperature(LCST) of the CNT-pNIPAM composites.
- Strain change of CNT-pNIPAM hydrogel at LCST.
- Fabrication of LDPE/CNT-pNIPAM bilayer actuator.
- Reversible folding and unfolding actuation properties in water.
- Fabrication of folding and unfolding cubes based on the CNT-pNIPAM actuator.
- Integration of pNIPAM and CNT-pNIPAM for making folding and unfolding flowers.
- Demonstration of near IR responsive properties for CNT-pNIPAM composites .

2.2.2 Participants

The participants in this part of the project have been:

Prof. Ronald Fearing, Dept. of EECS, UCB

Prof. Ali Javey, Dept. of EECS, UCB

Post Doc:

Dr. Hyunhyub Ko

Graduate Students:

Bryan Schubert (EECS)

Andrew Gillies (EECS)

Min Hyung Lee (EECS)

Undergraduate Students:

Michael J. Cohen (BioE)

2.2.3 Highlights

A simple approach is described to fabricate reversible, thermally- and optically-responsive actuators utilizing composites of poly N-isopropylacrylamide (pNIPAM) loaded with single-walled carbon nanotubes. With nanotube loading at concentrations of 0.75mg/mL , we demonstrate up to 5 times enhancement to the thermal response time of the nanotube-pNIPAM hydrogel actuators caused by the enhanced mass transport of water molecules. Additionally, we demonstrate the ability to obtain ultrafast near-infrared optical response in nanotube-pNIPAM hydrogels under laser excitation enabled by the strong absorption properties of nanotubes. The work opens the framework to design complex and programmable self-folding materials, such as cubes and flowers, with advanced built-in features, including tunable response time as determined by the nanotube loading.

2.2.4 Collaborations

We are working with Prof. Wood's group to integrate nanowire connectors into programmable matter.

2.2.5 Approach

We utilized an aqueous 2 wt.% DOC solution as the surfactant to disperse HiPCO SWNTs at concentrations of up to 1 mg/ml using an ultrasonic bath. Compared to other known surfactants for SWNT dispersion, such as sodium dodecyl sulfate or sodium dodecylbenzene sulfonate, we found DOC to be more stable in NIPAM monomer solutions. In order to fabricate SWNT-pNIPAM hydrogel strips, confinement channels with desired shapes and dimensions were made using Gel-Pak films. Polymerization was performed by UV light

irradiation (365 nm, 18.4W) for two hours, resulting in SWNT-pNIPAM composite strips loaded with varying amount of SWNTs

2.2.6 Implementation

We utilized a SWNT-pNIPAM /LDPE bilayer device scheme. In this device architecture, water loss in the SWNT-pNIPAM layer results in a mechanical strain that causes the actuation of the bilayer at predefined sites. Briefly, a parallel array of 10 hinge lines (depth, 25 μm ; width, 30 μm ; pitch, 80 μm) is patterned on the LDPE substrate using a computer-controlled laser writer to define the actuation sites. Next, an array of holes (diameter, 200 μm ; pitch, 200 μm) are laser cut near the hinge lines in order to serve as anchoring sites for the subsequent deposition and polymerization of SWNT-pNIPAM (Fig. 2a). A thin layer of SWNT-pNIPAM film (0.4 μm thick) was then directly formed onto the anchor holes by depositing the composite solution followed by UV polymerization. This forms a hinge that can fold up to 180° due to the abrupt strain change in the polymer hydrogel above the LCST. The folding dynamics of the hinges when transferred from a 23 °C to 55 °C water bath were characterized for SWNT concentrations of 0-0.75 mg/ml.

The response time, corresponding to the time required to reach a folding angle of 90° is shown in Fig. 2b. The response time is found to linearly change with the SWNT content for the explored concentration range (0-0.75 mg/ml) with a slope of -15sec/(mg/ml). Specifically, in the case of a hydrogel with 0.75 mg/ml of SWNTs, it takes 2.7 sec for the hydrogel hinge to reach a 90 angle, compared to 14 seconds for the hydrogel without SWNTs. This leads to an overall maximum response time enhancement of 5 times through the incorporation of SWNTs into the polymer matrix.

We now demonstrate the ability to make "smart" or programmable devices based on the integration of SWNT-pNIPAM (0.5 mg/ml) hydrogel hinges arranged in complex assemblies. Shown in Figure 3a is the schematic of a cube fabricated using the concept of bilayer hinges (Fig. 2a) made of SWNT-pNIPAM hydrogels. The cube template was fabricated on a laser patterned 50 μm LDPE film followed by the UV polymerization of SWNT-pNIPAM hydrogel patches on the hinges. When placed in warm water (48°C), the strain induced by the shrinking hydrogel patches causes the cooperative folding of each hinge until the equilibrium shape of a cube is obtained. Figure 3a illustrates this process with a scheme, and Fig. 3b and 3c show that optical images of the cube folding and unfolding in a water bath after being heated to 48°C, and subsequently cooled to 20°C, respectively. In this case, the entire process of cube folding takes 35 seconds, which is significantly faster than a similar device with only pNIPAM hydrogel hinges that would take up to 150 seconds to perform the same function. The process is reversible and the closed cube can unfold completely when cooled down in water.

In order to demonstrate the optical response of SWNT -pNIPAM/LDPE bilayer actuators, we utilized a 785 nm laser (spot size 20 μm) excitation with a power of 30 mW. Transmission-mode optical images of a SWNT-pNIPAM hydrogel before, during, and after laser irradiation are captured using a CCD camera. As shown in Fig. 4a, the hydrogel begins to develop a black (i.e., opaque) spot where the laser beam is positioned within 2

seconds of exposure due to the shrinking of the hydrogel by the local heat generated from near-IR absorption of SWNTs. This spot then spreads and reaches an equilibrium size after only 8 seconds of exposure corresponding to the heat transport of the surroundings. Furthermore, after the laser is turned off, the pNIPAM hydrogel exhibits an ultra-fast recovery to its original (transmissive) state within only 0.3 sec. In contrast, control pNIPAM samples without SWNTs did not exhibit near-IR response (data not shown). The switching behavior of pNIPAM-SWNT composites was highly reversible after many cycles of switching; emphasizing that damage is not being incurred by the laser beam. This presents a new hydrogel medium with tremendous potential for ultrafast near-IR optical actuation relevant for numerous emerging biologically-inspired applications.

2.2.7 Characterization

The DOC-SWNTs and NIPAM monomer solutions formed homogenous mixtures that exhibited stability to SWNT flocculation for several weeks. The dispersion quality was characterized by absorption studies. Figure 1c shows the UV-Vis-nIR absorption spectra of as-prepared SWNT-DOC solution and the SWNT-pNIPAM hydrogel after UV polymerization. Both samples exhibit near identical absorption spectra, with the absorption bands for the semiconductor (E11 870-1300 nm and E22 500-800 nm) and metallic SWNTs (E11 400-600 nm) clearly distinguished, confirming the good dispersion at the concentrations studied here. The LCST temperature does not appear to be significantly influenced by the incorporation of SWNTs into the polymer hydrogels. Upon close inspection, it seems that the polymer strips with 1 mg/ml SWNTs have a slight depression of the LCST $1-2^{\circ}C$ compared to the pure pNIPAM strips, but this depression is comparable to the expected fitting error from the measurements. Nonetheless, the fact that the LCST in the SWNT-pNIPAM composites remains well-defined suggests that the incorporation of SWNTs into the polymer hydrogel does not influence the structure and the thermally induced phase transition of the polymer strips.

2.2.8 Theory

Considering the mechanism by which the SWNTs enhance the response time, the result could be related to either one of two possible mechanisms: (i) enhancement of polymer composite thermal conductivity yielding faster heat transfer through the hydrogel, or (ii) enhancement of the mass (water) transport through the hydrogel due to the integration of SWNT fluidic channels in the hydrogel structure. If we assume the thermal conductivity of pNIPAM hydrogel is equal to the thermal conductivity of water, simple heat transport modeling reveals that the inner temperature of the hydrogel reaches the temperature of the hot water ($55^{\circ}C$) from an initial state of $25^{\circ}C$ in less than a second for the specific device dimensions explored here. Thereby, the response time is not limited by the heat transport since the timescale on which variations in thermal conductivity will influence the SWNT-pNIPAM response is significantly less than the actuator response time. Therefore, we propose the response time is instead limited by the mass transport of water and by the polymer

chain reorganization (from hydrophilic to hydrophobic). The addition of SWNTs into the pNIPAM hydrogel provides more porous (nano or micro-scale pores between pNIPAM and SWNTs) structures for enhanced water diffusion. In addition, previous reports have shown that carbon nanotubes can act as efficient channels for water flow driven by the osmotic pressure. Molecular dynamics simulation has shown that the flow rate can be as high as 5.8 molecules per nanosecond per nanotube and almost friction-less. The diffusion coefficient of a hydrogel has been shown to be inversely proportional to the diffusion friction coefficient between the fluid and the network which can be effectively reduced by adding of SWNT as shown here.

2.2.9 Integration

We also demonstrate the ability to exploit the response time enhancement in the SWNT-pNIPAM hydrogels in the framework of a multi-layer actuator architecture. Shown in Fig. 5a is a design scheme for a multi-layered patterned hinge resembling a flower, where the first layer of hinges are designed with a pNIPAM hydrogel (i.e., without SWNTs), whereas the second layer of hinges are composed of a SWNT-pNIPAM hydrogel that exhibits significantly enhanced response time. This allows the actuator device to exhibit an additional level of complexity that resembles the closing or blossoming of a real flower that has some leaves closing (blooming) earlier than others. Figure 5b shows a frame shot of this complex flower that is taken after the flower is placed in warm water ($48^{\circ}C$). In this case, even after 10 seconds of being immersed in the warm water, the hinges with the SWNT-pNIPAM have already reached a folding angle of over $90^{\circ}C$, whereas the hinges with only pNIPAM hydrogels remain only slightly bent ($\approx 30^{\circ}C$). Additionally, Figure 5c shows the reverse process of the flower closing, depicting the process of a flower blooming with the inner "leaves" of the flower blooming faster than the outer leaves due to the enhanced response time of the SWNT-pNIPAM hydrogels compared to pNIPAM hydrogels used on the hinges. It should be noted that in all cases, the folding and unfolding processes were always found to be highly reversible with no noticeable degradation occurring in the thermally driven response for more than 20 cycles.

In addition, the use of SWNTs in the pNIPAM hydrogel templates yields an excellent route toward near-IR optically responsive hydrogel materials. pNIPAM is transparent in this wavelength range, and therefore unresponsive to near-IR irradiation. SWNTs have a well-defined near-IR optical absorption, specifically ideal for biocompatible devices such as drug delivery mediums or biological connector devices, since tissue and blood have a minimal near-IR absorptivity.

2.2.10 Findings

- The CNT can be uniformly dispersed into NIPAM monomer solution with 2% DOC surfactant. The uniform solution is stable over several months. The uniformity of the CNT dispersion inside the CNT-NIPAM solution and CNT-pNIPAM hydrogel is confirmed by UV-VIS spectroscopy.

- The LCST temperature does not appear to be significantly influenced by the incorporation of SWNTs into the polymer hydrogels which means the phase transition properties is well preserved for the CNT-pNIPAM composites.
- The LDPE/CNT-pNIPAM bilayer actuator can reversibly fold and unfold which is controlled by the temperature of the water bath.
- The thermal response time is a function of the CNT concentration, the larger the CNT concentration, the faster the thermal response.
- Up to five times faster thermal response is observed for the CNT-pNIPAM hydrogel actuator compared to the pNIPAM actuator.
- The CNT-pNIPAM hydrogel begins to develop a black (i.e., opaque) spot where the laser beam is positioned within 2 seconds of exposure due to the shrinking of the hydrogel by the local heat generated from near-IR absorption of SWNTs. After the laser is turned off, the pNIPAM hydrogel exhibits an ultra-fast recovery to its original (transmissive) state within only 0.3 sec.
- The programmable material based on the thermal responsive hydrogel such as the 'cubes' and 'flowers' can reversibly fold and unfold which is controlled by the water bath temperature.

2.3 Nanowire connector integration

Several aspects of the nanowire connectors have been investigated as follows:

- Growth of NW connectors on flexible substrates.
- Integration of NW connectors into programmable matter fabrication process.
- Connector quality after integration.

2.3.1 Highlights

Nanowire arrays with a length of 10 μm and coated in 200 nm parylene can be grown on flexible Kapton substrates. They can then be easily integrated into programmable sheets by using a protective coating of water-soluble polyvinyl alcohol during processing.

2.3.2 Collaborations

Prof. Javey's group supplied the NW connectors, and Prof. Fearing's group integrated them into the flexure-based structures.

2.3.3 Approach

NWs are grown by chemical vapor deposition (CVD) on flexible Kapton (polyimide) substrates coated with 20 nm of silicon dioxide (see Figure 6). The flexible connectors can then be directly integrated into the programmable matter fabrication process because the Kapton substrate cuts well by laser. In order to protect the NWs from damage due to the laser ablation and lamination steps of fabrication, the NW arrays must first be coated with polyvinyl alcohol (PVA). Before processing, a solution of PVA dissolved in water is applied to the connector surface and allowed to dry. Then, after processing (Figure 7), the connectors are released by etching the PVA in water. The PVA is able to protect the connectors during lamination, where the temperature is 200°F. Because the PVA is easy to remove, it could also be left on the connectors until the entire patch is ready to use. This would prevent damage during transport.

2.3.4 Implementation

The NW connectors on flexible substrates are shown in Figure 6. This figure shows a connector being twisted by two tweezers. A strip of connectors was made by using the process outlined in Figure 7. This process allows the connectors to be precisely machined alongside the programmable matter structure. Because connectors do not have to be cut and placed by hand, the fabrication process is greatly accelerated. This also allows for the easy creation of more complex connector shapes.

Connectors were examined under SEM before and after integration to verify that the PVA is indeed protecting the NWs. Figure 8 shows that near the edges of the connectors, there is only minimal damage due to the UV laser ablation (355 nm). Within 10 μm of the edges, there is some slight damage likely as a result of melting the parylene coating. However, this represents a small percentage of the overall patch size, so its effects are likely small. Further from the edge, the processed and unprocessed samples are indistinguishable as shown in Figure 8. Therefore, the PVA is providing protection from mechanical deformation caused by lamination.

2.3.5 Findings

- NW connectors can be grown on flexible Kapton backing.
- NW connectors can be directly integrated into the programmable matter fabrication process.
- Polyvinyl alcohol (PVA) allows easy integration of NW connectors.
- PVA coating protects against mechanical deformation and thermal damage below 200°F.

2.4 Polymer microfiber connectors

Several aspects of the nanowire connectors have been investigated as follows:

- High-density polyethylene (HDPE) microfiber connectors.

2.4.1 Highlights

High-density polyethylene (HDPE) microfiber connectors show modest shear adhesion ($\sim 4\text{N}/\text{cm}^2$) compared to germanium nanowires, but they are much simpler to fabricate.

2.4.2 Approach

An alternative to germanium nanowire connectors are polymer microfiber connectors. These connectors show about a tenth of the performance of NW connectors, but they are much simpler to fabricate. Polymer microfiber arrays were made from high-density polyethylene (HDPE) which was thermally molded into polycarbonate filters using a laminator. The polycarbonate filter was then etched in methylene chloride. From start to finish, each sample only took about 15 minutes to make. Also, the filters come in a range of pore diameters (0.05 to $10\ \mu\text{m}$), and they are available as large sheets (8" x 12"). We tested the shear connection strength of a range of microfiber connectors between 2 to $0.6\ \mu\text{m}$, and lengths of 20 and $10\ \mu\text{m}$.

2.4.3 Implementation

Figure 9 shows the experimental set-up and results of the polymer microfiber connectors. The connectors were preloaded by hand, and then shear-loaded until failure. This was repeated on the same sample up to 3 times. All samples degraded with each trial because they were loaded until failure. At just over $4\ \text{N}/\text{cm}^2$, the highest performing sample was the $0.8\ \mu\text{m}$ diameter, $20\ \mu\text{m}$ long fibers. While the shear adhesion of this first round of microfiber connectors is much lower than that of the NW connectors, there may be some room for improvement by adding hierarchical structures, or adjusting the fiber densities and aspect ratios with various processing tricks.

2.4.4 Findings

- HDPE microfibers show mild shear adhesion of $\sim 4\text{N}/\text{cm}^2$, but are easy to make.

2.5 Magnetic metal spikes

Several aspects of the nanowire connectors have been investigated as follows:

- Fabrication of steel spike arrays.
- Shear force of steel spikes loaded with switchable magnets.

2.5.1 Highlights

Steel spike arrays increase shear force between switchable magnets by more than 9 times compared to smooth steel.

2.5.2 Collaborations

Prof. Fearing's group generated steel spike arrays and integrated them with switchable magnets provided by Prof. Rus' group.

2.5.3 Approach

As a solution for increasing the friction between the switchable magnets used for smart cubes, we explored steel spikes. The spikes are fabricated using a precision UV laser machining system. Steel spikes were chosen for their durability and conductivity. Also, spike arrays operate by mechanical interlocking since they are too stiff to develop the intimate contact needed for van der Waals interactions. Because they can not generate any adhesive force on their own, they need a constant preload to remain engaged. This means that when the magnet is switched off, the spikes can no longer support any shear force. This matches perfectly the requirements needed for connectors used in smart cubes.

The spikes are cut out of the surface of 1 mil steel shim by using a crosshatch pattern. The laser removes lines of material, leaving spikes in between. The minimum spacing of the spikes is dependent upon the spot size of the laser, which varies with power settings. The spot size also affects the spike diameter, but the spike diameter is mainly controlled by the line spacing. Figure 10 shows an SEM image of an array of metal spikes. These spikes are 5 μm in diameter at the tip, approximately 15 μm tall and 30 μm apart.

The performance of the steel spikes was determined using the set-up in Figure 11. Two 1 cm^2 samples are placed face-to-face and loaded with two switchable magnets made by Prof. Rus' group. Samples are attached to glass-fiber squares using double-sided tape. The glass-fiber squares have holes cut out so that the magnets can make direct contact with the back of the samples. During testing, one sample is fixed to an aluminum plate while the other is loaded with weight until failure. Smooth 1 mil steel was tested in addition to the spikes to provide a control.

2.5.4 Implementation

The results of shear tests performed on the steel spikes is shown in Figure 11. The plot shows that the steel spikes can hold 270 g on the first trial, which is almost 9 times more weight than the smooth steel can hold. However, this drops severely on the second trial and stays near an average of 74 g for the remaining tests. The reason for the sharp decline can be seen in Figure 12. This figure shows the spike tips before and after testing. After testing, many of the spikes are bent over, preventing future interlocking. Most of the damage is isolated in the areas directly between the poles of the magnets. This is presumably where the pressure

is the greatest. In the future, the damage can be mitigated by better distribution of the load, and by operating below failure thresholds.

2.5.5 Findings

- Steel spikes with 5 μm diameter tips can be fabricated by laser ablation.
- Steel spikes increase the shear force of the switchable magnets by 9 times over flat steel.
- Steel spikes allow electrical conductivity.

2.6 Microconnectors for reconfigurable millirobots

Several aspects of the microconnectors for reconfigurable millirobots have been investigated as follows:

- Design and fabrication of micromolded connectors.
- Modeling and analysis of micromolded connectors.
- Integration of micromolded connectors into programmable matter sub-units.
- Creep experiments over long time periods have been performed on the microconnectors.
- Sensitivity of the microconnector to environmental conditions has been investigated.
- Fabrication of micromolded connector from low melting point metal.
- Integration of metal microconnector with flexible copper clad kapton backing.

2.6.1 Highlights

We have developed a micromolded connector for applications such as folded millirobots where reusability, low engaged profile and rapid assembly are required. Using laser micromachining and micromolding techniques, the microconnector is formed with a manufacturing process that can be integrated with the rapid prototyping of the millirobots. The microconnector engages through shear in one direction while forming a strong connection in orthogonal directions, with an engaged thickness of 200 μm . We have developed a new force displacement apparatus that can be used to test the strength of connector patches on a size scale and with a precision not possible before. This allows for more detailed characterization of the connector and will give further insight into the connector functionality. The microconnector has an approximate shear strength of $42\text{N}/\text{cm}^2$ and a normal strength of $27\text{N}/\text{cm}^2$.

The microconnectors have also been successfully integrated into various millirobots for quick appendage changes, showing their applicability to millirobots. We have developed programmable matter sub-unit chassis with integrated microconnectors. The sub-units have been successfully combined to create a programmable matter robot chassis.

2.6.2 Approach

To be useful for the assembly of millimeter-scaled reconfigurable components, a connector with several properties is desired. The connector must form a strong connection between components through a distinct engage/disengage action. This engage/disengage action must require a minimal force to avoid damaging components, must not damage the connector to allow for repeated use and must be fast to allow for rapid assembly. The connector must also be robust to failure and external damage to allow the connector to be reused if the connection is forcefully broken. Also, the connector must be inexpensive and easy to manufacture so that it can be easily integrated with the rest of the components. Finally, for millirobots, the connector must have a sub-millimeter engaged thickness so that its size does not interfere with the function of the millimeter-scaled components.

The microconnector involves a repeating unit pattern that is connected by a shear action along the engaging direction. The repeating unit pattern is designed such that the connector on each surface can be identical, also known as an AA style connector. This is unlike a hook and loop connector which requires one side to be loops and the other to be hooks, in an AB style. The repeating unit involves two alternating L-shaped ridges that slide into contact parallel to the ridge length. The alternating L-shaped ridges are $125\ \mu\text{m}$ high, $70\ \mu\text{m}$ wide and $1.7\ \text{mm}$ long. The ridges are spaced $140\ \mu\text{m}$ apart and are arranged in a repeating pattern with a pitch of $680\ \mu\text{m}$. The connectors are engaged by positioning the opposing connector surfaces adjacent to each other, and then shearing the two surfaces, causing the ridges to interdigitate. At the end of each ridge is an alignment feature that guides the opposing surface into the proper orientation during engagement. Once connected, each row of ridges is interdigitated with the ridges on the opposing surface, forming an anisotropic connection. Since the position of the interdigitated ridges is constrained after engagement, the connector can be engaged with a repeatable alignment. The connection can also be reconnected with a discrete offset by shifting the connectors before engagement by one row laterally. The geometry of the ridges is arranged so that when engaged there is a slight interference fit between the ridges on the adjacent surfaces, causing them to bend slightly from their vertical rest position. This bending causes a normal force between the connected ridges which results in a friction resistance that helps the connectors stay in place.

To engage the connector, the two surfaces are brought into contact with a slight normal pressure, with the connector area on each surface adjacent to each other. The surfaces are then slid in shear until the alignment ridges make contact, ensuring that the ridges on each surface are parallel and interlock properly. When the two patterns have aligned, the two surfaces are slid in the shear direction parallel to the ridges, causing the ridges on one surface to interdigitate with the ridges on the opposing surface. This forms a mechanical interlock between the two surfaces. The interlocking ridges form a connection that is very strong in shear applied perpendicular to the ridges and in the normal direction, but can be easily disconnected when shear is applied parallel to the ridges. Since the connection causes very little strain in the components, the connector can be used repeatedly without a loss in performance. The geometry of the ridges is also arranged so that when engaged, there is a slight interference fit between the ridges on the adjacent surfaces, causing them to bend

from their vertical rest position. This bending causes a normal force between the connected ridges. This normal force results in a friction resistance that helps the connectors stay in place.

A new primitive element has also been developed. Previous designs lacked the ability to ambulate, making self construction of individual elements into larger functional objects difficult. We developed a design for a new primitive that is able to actuate, making locomotion and shape change possible. By allowing each element the ability to change shape and locomote, elements are able to move and combine into interesting functional devices, as seen in Figure 13.

To be useful for connecting units together, the microconnectors previously reported must be able to connect strongly to other units over long periods of time without creeping. A low creep rate in the connection will ensure that shapes can be held without large deformations over long time periods. We have set out to measure the creep rate of the microconnector using a stress relaxation test. In the stress relaxation test, the microconnector is rigidly clamped between each side of the force displacement tester. The stage is then displaced by $100\ \mu\text{m}$ to induce a stress in the connector. As time passes, creep in the connector causes the stress to decrease. By measuring this drop in stress, we can identify the creep performance of the connector.

The microconnectors have been shown to be useful as mechanical connectors between the programmable matter subunits. However, if the connectors could be made to be conductive, then they could also be used as electrical connectors, making it possible to transmit power and information between the subunits. One possible way to make the units conductive would be to make them out of metal, or add a metal coating to the connectors. Making the connector out of metal may also have the added benefit of making the mechanical connection stronger.

2.6.3 Implementation

The design of the micro connector includes alternating L shaped ridges that are $125\ \mu\text{m}$ high, and $1.7\ \text{mm}$ long. The ridges are spaced $140\ \mu\text{m}$ apart, and are arranged in a 2 ridge repeating pattern with a pitch of $680\ \mu\text{m}$. The repeating unit pattern is designed such that the connector pattern on each surface can be identical, also known as an A-A style connector. At the end of each pair of L shaped ridges is an arrow shaped alignment feature. These alignment features ensure that the connector is always engaged in the proper orientation. See Figure 14 for details.

The micro connector is formed by hot embossing with a rubber mold onto a thin polymer film. The creation of the rubber mold is described in figure 15. The master pattern is created using a mold fabricated with laser ablation micromachining techniques into a PC film. The polycarbonate film can now act as a mold to form the microconnector ridges. The polycarbonate mold is removed from the gelpack and placed face down on a glass slide. A $50\ \mu\text{m}$ thick polyethylene film is then placed on the polycarbonate mold, and the entire stack is placed in a hot press at $150\ \text{C}$ for 200 seconds. The stack is then cooled, removed from the glass slide and put in a methylene chloride etching solution that dissolves

the polycarbonate film, leaving the formed micro connector shape in the polyethylene. High temperature resistant silicone rubber (Dow Corning 3120, Shore 60A) is then cast over the polyethylene master pattern. Once cured, the master pattern is peeled off the rubber, leaving a negative of the micro connector pattern in the rubber. This rubber mold can then be used as a stamp to create the micro connector pattern on thin thermoplastic films.

This molding process can be implemented as a roll-to-roll manufacturing setup which is extremely cost effective. This process can also be directly integrated with the robot rapid manufacturing process already established in our lab. In this manner, it is possible to create the modular robots with the micro connectors in parallel.

The microconnectors were integrated with the newly proposed programmable matter primitive mentioned above. Various orientations and connections of the subunits were experimented with in order to test the feasibility and effectiveness of the new design. The new programmable matter primitive will consist of 2 dimensional "printed" robot tiles, containing several actuated flexure joints that will allow the tile to emulate a kinematic chain, making possible a wide variety of shape changes, as well as locomotion and steering. Several connector surfaces were integrated into the surface of the tile, allowing it to attach to surrounding surfaces as well as other elements.

Experiments were performed on a custom built force displacement apparatus. The custom force displacement apparatus consists of two custom fabricated acrylic platforms to which samples can be mounted with a clamp and screws. The first acrylic platform is mounted on a 6 axis force torque sensor (ATI AI Nano 43 F/T sensor) attached to two manual rotation stages (Newport RSP-2) and two linear slides (Newport 423 slide) and mounted onto an air table (Newport VH series). The second acrylic platform is mounted on two perpendicular stepper motor controlled linear stages (Zaber T-LSR 150B) that are attached to the same air table. The acrylic platforms attached to the faces of the linear stages and force sensor can be adjusted with the rotation stages to be planar. The linear slides mounted to force sensor are each parallel with one axis of travel of the motor controlled stages, and are held in equilibrium with two opposing springs. This allows compliance of the platform in the testing directions that gives a larger range of displacements over which data can be taken. This increases the precision of the strength measurements by extending the time over which the test occurs, negating impulse forces that would arise from a rigid platform (Figure 16).

The micro connectors were tested for ultimate strength in 4 directions perpendicular to the ridges as shown in figure 17. Samples were prepared by molding a $5 \times 5\text{mm}$ sized microconnector pattern with high density polyethylene films (HDPE) that are $50\mu\text{m}$ thick, with an elastic modulus of 0.4GPa and a yield strength of 16MPa . The films are molded directly onto $380\mu\text{m}$ thick posterboard tabs measuring $10 \times 40\text{mm}$. The poster board tabs were clamped to the acrylic platforms, with the poster board overhanging the platform by approximately 10mm . The connectors were engaged by hand with one surface mounted to the force sensor and the other to the linear stages. The linear stage was then moved away from the force platform at a specified speed of 1mm/s and pull-off angles of 0° , 30° , 60° and 90° . Data was collected from the force sensor until failure of the connector was observed. The results found in figure 17 show that the connector has an approximate shear strength

of $42N/cm^2$. As the pull-off angle is increased, the strength of the connector decreases, with a normal pull-off strength of approximately $27N/cm^2$.

The results found in figure 18 show trend lines of samples repeatedly tested to failure at a given pull-off angle. Samples tested to failure in pure shear lost on average 30% of their initial strength after 10 cycles, while samples tested to failure in the normal direction lost 45% of their initial strength after 10 cycles. This suggests that some permanent deformation of the microconnector occurs during failure, but the majority of the strength is maintained, indicating that failure can be mostly attributed to elastic deformation of the ridges.

To measure stress relaxation of the microconnector, samples were fabricated as stated previously, and then clamped to each side of the acrylic stages in our force displacement tester. One stage was then displaced to a fixed distance, and the induced stress was measured for 30,000 seconds. The experiment was also repeated for posterboard and CA adhesive and PSA for 600s. The results suggest that the microconnector has a very low creep rate, and that the majority of the relaxation occurs within 1000 seconds of loading. This indicates that the microconnector can hold a stable connection over long periods of time without failing.

Forces were measured during engagement and disengagement by mounting one side of the microconnector to the force sensor and then engaging it with another sample. During engagement, a normal force of approximately $1.5N$ and a shear force of $1N$ was required to engage the $0.25cm^2$ sample, and a shear force of $1N$ was required to disengage the sample.

Using the SCM process previously developed in the lab, programmable matter sub-units were created in parallel with the microconnectors. The microconnectors can be molded directly onto the surface of the programmable matter sub-units, which allows for rapid manufacturing of many sub-units. The sub-units were then connected into a small crawling robot chassis that shows how one might combine the sub-units into a larger functional object. The subunits and the programmable matter robot can be found in figure 20.

We chose to make the microconnector conductive by fabricating with a low melting point metal alloy. The process starts by coating the low melting point metal onto a copper-clad polyimide film. This film is then placed on a PDMS mold of the microconnector pattern, with the low melting point metal in contact with the mold. A weight is used to hold the film flat while the stack is heated to 300F in a vacuum oven at 27 in Hg. Once the metal melts, it flows into the PDMS mold and forms the microconnector features. After cooling, the connector can be peeled out of the mold (Fig 21,22).

2.6.4 Findings

- Polymer microconnector can withstand an initial shear stress of $13.7 N/cm^2$.
- Polymer microconnector exhibit a repeatable shear stress, even when loaded to failure.
- Polymer microconnector can be fabricated using rubber molds in a scalable matter which greatly increases micro connector production and integration.
- Polymer microconnectors design has been improved to increase its strength and aid in ease of engagement.

- The microconnector has an approximate shear strength of $42N/cm^2$ and a normal strength of $27N/cm^2$.
- The $0.25cm^2$ microconnector can be engaged with a normal force of $1.5N$ and shear of $1N$.
- The microconnector maintains 70% of its initial strength after being run to failure 10 times in the normal direction.
- Microconnectors can be successfully integrated into programmable matter subunits and allow for units to combine into functionally useful objects.
- Microconnectors can be held in tension for long periods of time with only about 20% creep.
- Posterboard used in the construction of the programmable matter subunits is sensitive to environmental conditions, and can change stiffness by 20% with a 20% change in %RH.
- Microconnectors can be successfully made from low melting point metal, making them potentially useful as electrical connectors as well as mechanical connectors.

2.7 Low-Stiffness Conformal Backing

Several aspects of the low stiffness conformal backing has been investigated as follows:

- Fabrication of flexible backing layer for future adaptable microconnectors
- Analysis of hinge backing for flexible microconnector
- Imaging of flexible backing

2.7.1 Highlights

We have worked to develop a backing that will allow connection to macroscopically rough surfaces, while also allowing for connection between programmable matter units when not perfectly aligned. This is currently being done using an island/flexure system modeled after keypads.

We have calculated the theoretical ability for our flexure backing to contact a sphere. We have successfully calculated the effective modulus of our backing and theoretical contact width using C Majidi's work.

2.7.2 Approach

To engage with a surface, connectors must come into contact with said surface. If the two surfaces are nonplanar or improperly aligned, the backing must deflect for contact to be made (or no engagement can occur). As the backing deflects from its natural state, elastic energy is stored in the material that desires to bend the backing to its original shape. This energy is in direct conflict with the adhesion or engagement energy of the connectors. In order for engagement of curved surfaces or misaligned connectors to occur, this bending of the backing must be minimized (or the adhesion energy must be maximized, not discussed here). In order to minimize the elastic energy, we aimed to create a flexible backing that minimizes this bending energy while allowing for the deformation outlined above.

The engineered backing features an array of square plates connected by V shaped hinge flexures designed for deformation in multiple directions. This "V" shaped joint allows for movement in tension or compression. Furthermore, it is not as thick in the z-direction as the blocks (.5mm compared to bulk thickness of 1.5mm), which encourages a moment by decreasing the beam thickness against bending. This should allow the system to bend, elongate and compress in multiple direction to contour to a natural surface and makeup for misalignment. Here one can see how the hinge system enables the backing to drape over the sphere with only gravity as surface forces as compared to the control.

Previously, C Majidi (Adhesion of an Elastic Plate to a Sphere, Proc Roy Soc, 464: 2008) created an analysis to calculate the theoretical adhesion width of an elastic plate to a sphere. This analysis has been shown to accurately predict the width of the contact zone. Using this analysis, we used an effective modulus of our backing in combination with Majidi's work to calculate the theoretical width of contact for our hinged backings.

To determine the mechanical properties of a flexible backing support structure, a method for mounting and imaging contact area must be determined. The measured contact area will allow comparison with a non-engineered backing and allow us to gauge the performance of various structures.

2.7.3 Implementation

Using the UV and IR lasers available, we have created various backing prototypes to maximize conformation to surfaces with compound curvature and passive alignment of the islands. The islands act as the carrier of the adhesive system, while flexures allow for the movements described here. Overall this system aims to decrease the energy of deformation of the backing into adhesive contact. This will allow for programmable matter to adhere to surfaces of varying shape, while also connecting with misaligned neighboring pieces of programmable matter.

This structure was originally created in cardboard models and eventually kapton films. Figure 22 shows the kapton "draping" over a hemispherical shape. This kapton sheet of 50 μm thickness has curved flexures 30 μm in width with islands measuring 100 μm x 100 μm . These films show very good "drape-ability" which is comprised of in and out of plane deformation with low stress. This system does however show significant plastic deformation

through testing and warping due to laser cutting. This has urged us to look for molding techniques of softer polymers that will be less susceptible to plastic deformation and thermal warping due to laser cutting.

Using IR lasers, molds were cut out of acrylic on top of wax and a glass slide. The mold is cut in such a way that the flexure is thinner than the 1.5mm thick islands, and approximately .5mm. Smooth-on Body Double PDMS cures in the mold, and the scum layer is squeegeed off of the top. This creates a sample of 4mm x 4mm x 1.5mm islands with hinge shaped flexures, figure 23. This sample has a footprint of 17mm x 17mm (square mold size).

The contact area was measured using an LED light ring and a series of light blocking sheets to obtain the right lighting conditions. The lighting conditions result in the contact area being viewable by total internal reflection at the backing-lens interface. Images were taken with a digital camera that can be post-processed to determine the exact contact area.
2011-05-11

2.7.4 Findings

- Robust samples of PDMS with little scum layer can be successfully made with our technique.
- We were able to successfully approximate the contact width of the modified elastic backing
- The effective modulus, 4.42 MPa, of a patterned PDMS backing is about half of the control bulk modulus
- This apparent modulus is essentially independent of t and L values within reason
- The theoretical width of adhesion of a $500\mu m$ sheet of PDMS on a sphere with a radius of $10mm$ is $7.89mm$ according to Majidi's equations
- Using effective modulus for the same material and thickness, we found a critical width of about $9.51mm$
- Method for measurement of contact area between lens and engineered backing was determined.

2.8 Magnetic Connectors and Smart Sand

The main participants in this part of the project are Kyle Gilpin, and Daniela Rus. We have been working on the smart pebbles system prototype as follows

- Continuing our work to build and demonstrate a testbed of smart pebble system.
- Develop communication algorithms for smart pebbles.

2.8.1 Collaborations

We are working with the Harvard group on fabrication.

2.8.2 Highlights

We have developed a system of 27 Pebbles and demonstrated shape formation by disassembly using this system.

2.8.3 Approach

Subtraction has one distinct advantage over existing self-assembly technique. Subtraction does not rely on complicated attachment mechanisms that require precise alignment or careful planning. Subtraction excels at shape formation because it is relatively easy, quick and robust. The drawback associated with subtraction is that the initial mass of material must be pre-assembled. While we do this by hand for our experiments, it could be automated. Our modules, due to symmetry in their magnet-endowed faces, are rotation invariant within the plane, so an inclined vibration table should be able to rapidly assemble large, regular sheets of modules. In the future we envision deploying modules such as spheres which naturally pack 3D spaces in an efficient manner.

Shape formation by subtraction proceeds through five basic stages: *neighbor discovery*; *localization*; *virtual sculpting*; *shape distribution*; and *disassembly*. In the first stage, *neighbor discovery*, modules are connected to form the initial structure. During this phase, modules detect when they are supplied with power and then attempt to communicate with and latch to their new neighbors. As the structure grows, modules keep track of with which neighbors they are able to communicate.

After the initial structure has been assembled, the *localization* stage commences. One arbitrary module, (typically the module connected to a PC), is assigned an absolute set of coordinates, for example (0,0). We call this module the root. Using the root as a starting point, all other modules in the structure exchange local messages to determine their positions with respect the root. All modules in the structure are able to determine their relative coordinates without any concept of the structure as a whole. Each module then sends a reflection message containing its position back to the root. The root forwards these reflection messages to a GUI running on the PC, and the GUI builds a virtual model representing the initial arrangement of modules in the physical structure.

Using this GUI model, the user drives the *virtual sculpting* stage by selecting which modules should be included in the final shape. After this sculpting process is complete, the program generates a sequence of inclusion messages.

During the fourth stage, *shape distribution*, the GUI transmits the inclusion messages to a the root module. The root then propagates these inclusion messages to their proper destinations. As with the localization process, the inclusion messages do not contain a complete representation of the final structure. To conserve space and save time, they only contain local information.

The final phase is *disassembly*. During the disassembly phase, the modules not designated to be in the final structure disconnect from their neighbors to reveal the shape the user sculpted previously. Each of the phases of self-disassembly is dependent on a distributed, localized message passing algorithm executing on each module. Since the algorithms are communication intensive, the main optimization point is to minimize the size and number of required messages for each phase of the disassembly process.

We have developed the Smart Pebble system, a modular distributed robot system consisting of 27 modules. The modules are 12mm cubes and they are capable of autonomously communicating with and latching to four neighboring cubes in the same plane to form 2D structures. Each completed module weighs 4.0g. The major functional components of each cube are power regulation circuitry, a microprocessor, and four EP magnets, which are responsible for latching, power transfer, and communication. The four faces containing EP magnets are all symmetric which allows for modules to be oriented arbitrarily during the assembly process.

Each module is formed by wrapping the flexible circuit around the brass frame labeled. The flex circuit is a two layer design, and the entire stack-up including solder masks is 0.127mm (5mils) thick. The flexible circuit is stiffened with 0.254mm (10mils) of Kapton in the six square areas corresponding to the six faces of the cube. The flex circuit is secured to the brass frame using a set of holes in the unstiffened portions of the flex circuit that mate with nubs on the edges of the frame. These holes and nubs align the flex circuit to the frame, and by soldering the flex circuit to the frame at these points, we form a secure bond between the circuit and the frame. This scheme allows for quick and easy disassembly of a module for service or debugging.

The mechanism that enables programmed connections, communication, and power transfer between the Pebbles is an *electropermanent magnet*. Each EP magnet consists of rods of two different types of permanent magnet materials, with soft-iron poles, and with a copper coil wrapped around both magnets. One of the permanent magnets is Neodymium-Iron-Boron, and the other is Alnico V. Both of these materials have essentially the same remnant magnetization, about 1.2 Tesla, but very different coercivity; it takes about 100 times less applied magnetic field to switch the Alnico magnet than the Neodymium magnet. A current pulse through the coil in the positive direction switches the polarization of the Alnico magnet so it is aligned with the polarization of the Neodymium magnet. In this case, magnetic flux from both flows through the soft iron poles and to the other magnetic, or any ferromagnetic target object, attracting it. The attraction continues after the current in the coil is returned to zero. We call this the "On" state of the connector. A current pulse through the coil in the negative direction switches the polarization of the Alnico magnet so it is opposite the polarization of the Neodymium magnet. The polarization of the neodymium magnet is unchanged because it has a much larger coercivity — a much larger current pulse than is used would be required to switch its polarization. With the two magnets having opposite polarization, magnetic flux circulates inside the device but does not leave the poles, and thus does not exert force on the other connector or external ferromagnetic objects. Once again, this flux pattern continues after the current is returned to zero. We call this the "Off" state

of the connector.

The electropermanent magnets used here are low average power but high peak power devices. Our system uses a 20V, 5A, 100 μ s pulse to switch, provided by a 100 μ F power-supply decoupling capacitor in each cube. (Power is not transmitted between cubes at anywhere near this level, because switching is infrequent, only once every several seconds at most.) The time-averaged power devoted to magnetic attraction is many orders of magnitude lower than would be required using equivalent electromagnets, which, although they would require lower peak power, require the continuous application of power. For more information about the EP magnets in this system, including a detailed design guidelines and an electro-mechanical model.

The magnetic rods and pole pieces were custom-fabricated by BJA Magnetics Inc. (Rutland, MA) The magnetic rods are Grade N40SH Neodymium-Iron-Boron, and Cast Alnico 5, both 1.587mm diameter and 3.175mm long, magnetized through their length. The magnetic rods were fabricated by cylindrical grinding. The magnetic rods were coated with a 5 μ m Parylene by the Vitek Research Corporation. (Derby, CT) The pole pieces were are 3.175mm by 2.54mm by 1.27mm blocks of Grade ASTM-A848 soft magnetic iron, with a diagonal notch cut off to allow clearance when four are placed inside the cube. The pole pieces were fabricated by wire EDM, and chromate coated to slow corrosion and facilitate solderability. The rods and pole pieces were assembled with tweezers under magnification, using a mounting plate with slots to hold the pole pieces and a center support to hold the magnetic rods. The rods and glued to the pole pieces, and the spaces between the magnets filled, using Loctite Hysol E-60HP 60-minute work time epoxy (Henkel Corporation, Dusseldorf, Germany). After assembly, the pole faces are flattened by rubbing the assembly against a 320 Grit aluminum-oxide oil-filled abrasive file (McMaster-Carr, Princeton, NJ). An 80-turn coil is wound around the magnetic rods using #40 AWG magnet wire with 390 $^{\circ}$ C solder-strippable insulation, (MWS Wire Industries, Westlake Village, CA) using a custom-made clamp and a Model 1201 Bobbin Winder (Adams-Maxwell Winding System, Los Angeles, CA).

The four electro-permanent magnets in each cube are driven by a set of 2mm square MOSFETs which are capable of handling the 4–5 Amps required to switch the EP magnets (Fairchild Semiconductor FDMA2002NZ and FDMA1027P). In order to reduce the component count, we avoided driving each EP magnet coil with its own full H-bridge. Instead, each EP magnet has one dedicated half bridge connected to one side of its coil. We call these the “face-specific” drivers. The other sides of the four coils are tied together and serviced by a single “common” half-bridge. Using this configuration, we are able to pass current in both directions through each of the EP magnet coils, but we cannot control each of the coils independently. In practice, the software only ever drives one coil at a time. The two control lines for the common half-bridge are driven by the microcontroller’s timer output compare pins. Using the output compare pins we can precisely control the duration and spacing of the current pulses flowing through the EP magnet coils.

Each module is controlled by an Atmel ATmega328 processor which offers 32KB of program memory and 2KB of RAM in a 5mm square package. To minimize the external com-

ponent count, we employ the processor’s internal 8MHz RC oscillator as the processor’s primary clock source. We use the processor’s SPI interface to communicate with the outside world. Specifically, the processor in each cube is able to act as an SPI bus master while another Atmel processor in a test fixture acts as a slave. This slave processor translates the SPI data to a traditional UART bit stream at 19.2Kbps and vice versa. The four electrical connections required by the SPI bus are made through pads on the bottom (outside) of each flex circuit (cube). The SPI interface was chosen because the same interface can be used to program the processor. This eliminated the need to route more of the microprocessor’s pins to the outside of the cube. The ATmega328 was also chosen in part because it includes support for Atmel’s one wire in-circuit debugging protocol, debugWire. This again reduces the number of pins, traces, and external pads that must be used when developing and using the system.

The EP magnets form an inductive communication channel between neighboring modules. In short, when two EP magnets are in contact, they behave just like a 1:1 isolation transformer. We utilize this fact to transfer data between modules without affecting their ability to latch together. All inter-cube communication occurs at 9600bps using a series of $1/\mu s$ magnetic pulses induced by the coil of one EP magnet and sensed by the coil of the neighboring EP magnet assembly. The presence of a single $1\mu s$ pulse during a bit period signifies a logical ‘1’ while the lack of any pulse signals a ‘0’. Neighboring modules transfer data using pulses of the same polarity as the longer pulses used to latch the EP magnets. As a result, there is no risk of the latching strength decreasing over time during intensive communication. Communication may have a slight positive effect on latching strength.

The modules in our programmable matter system do not contain their own power sources. Instead, electrical power is distributed from one, (or several), centralized sources and then transferred from one cube to the next. Power is transferred between units via ohmic conduction of DC power through the soft magnetic poles of the connectors. Within each cube, the EP magnets are mounted to the flex circuit, which serves as an elastic mount, allowing slight bending and translation as needed for the two magnetic connectors to achieve intimate contact. When one magnet is turned on, it attracts any nearby neighbor; intimate contact is achieved; the adjacent cube receives power, starts its program; and the two cubes communicate to drive a single, synchronized pulse through their magnets to bond more strongly. All of the magnetic materials used in the connector are good conductors of electricity, so it was necessary to coat the rods of Alnico and Neodymium-Iron-Boron separating the two poles with 5 microns of Parylene to electrically isolate the two poles.

Each module contains a $100\mu F$ low equivalent series resistance, (low ESR), reservoir capacitor. These capacitors are responsible for sourcing the high-current demands of the EP magnets when they are switching on or off. These capacitors fill the interior of each cube and can only be installed once the flex circuit is partially folded around the brass frame. Instead of being mounted as a traditional surface mount capacitor would, the storage capacitor is soldered by its ends to the bottoms of two tabs. Because the tabs are flexible, the capacitor has some freedom to move around inside of the closed module.

In order to achieve the self-assembly functionality we developed two high-level algorithms.

The first algorithm allows us to form large shapes (that would otherwise be impossible to achieve) in a post-disassembly re-assembly process. The algorithm works by partitioning the shape to be formed into multiple subcomponents, each of which is sized such that it can be formed through self-disassembly from the initial block of host material. Once this self-disassembly is completed, the user manually arranges the subcomponents to resemble the initial goal shape. As the subcomponents come into contact with each other, they bond together once aligned. By exchanging information, the subcomponents ensure that they only bond in the configuration which will result in the desired goal shape. This approach to forming large shapes does not allow us to form shapes with more modules than we have available in the initial block of material, but it does allow the formation of shapes with abnormal aspect ratios that would otherwise require a very specific configuration of the initial block of host material. We have also begun to plan how to implement this algorithm in the Smart Pebble hardware. In particular, we will use the modules' on-board non-volatile EEPROM memory to record information identifying each subcomponent. Therefore, even though the subcomponents will lose power as the user is rearranging them to form the goal shape, they will still be able to tell with which other sub-assemblies they should bond.

The second algorithm is a routing algorithm that allows messages to travel between arbitrary modules in a structure of Smart Pebbles. Currently, no such mechanism exists. The algorithm is based on the traditional bug algorithm developed for mobile robots. We use it because it requires minimal knowledge of the structure and can be implemented in a distributed manner. Each message is treated as a bug that follows the most direct path from source module to destination until it encounters an obstacle. When it does, the message traverses the outside of the obstacle until it again intersects the imaginary line from source to destination. There are several challenges associated with implementing this routing algorithm in a discrete setting, but we are working to solve these. Once complete, this routing algorithm will form the basis of a sensing algorithm that will allow an initial block of modules to detect and replicate a concavity. If this concavity is formed by a passive object, the system will be able to replicate or magnify that object. The routing algorithm will also allow the system to better handle real-time changes in the network topology. If the bond between two modules is unintentionally broken during the self-disassembly process, the system should now be robust enough to still form the desired shape.

2.8.4 Findings

- The Pebbles simulator has a good model for communication failures. It can be used to implement a wide range of applications including shape molding.
- The Pebbles provide a robust and light-weight modular platform for self-assembly by disassembly
- Electropermanent magnets can be used for programmed connections, communication, and power transfer between adjacent modules in a Pebble system.

2.9 Algorithms

The main participants in this part of the project include Erik Demaine, Daniela Rus, ByoungKwon An, and Kyle Gilpin.

Our main goals in this part of the program have been to develop algorithms that achieve shapes by automatically folding a smart sheet with embedded actuation and supporting electronics.

2.9.1 Highlights

We have are in the process of finishing our algorithms and will have highlights once this is done.

2.9.2 Collaborations

We are working with the Harvard group to identify new objects for the hardware experiments.

2.9.3 Approach

Self-folding sheets form a new approach to reconfigurable robotics and programmable matter developed as part of this project. Their body fabrication is described earlier in this report. In brief, a self-folding sheet is a flat piece of material with integrated sensing, actuation, communication, computation, and connectors capable of autonomously folding into desired shapes. It is similar to a piece of paper that can be folded by humans into origami structures, except that the sheet *folds itself* into shape. The self-folding sheet is constructed with a built-in structure of bends that can be actuated individually, or with parallel group actuation, to achieve a desired deformation of the sheet that is consistent with the physical constraints of its folding structure. Controlled by either on-board or external computation, the sheet acts on itself internally to transform at will into a desired shape. Each sheet can achieve multiple shapes. For example, the sheet could fold itself into a table, and once the table is no longer needed, the sheet could become flat for re-use at a later time, for example as a chair or a bookshelf, according to the user's needs.

The sheet approach has two advantages over unit-modular self-reconfiguring robot systems. Unlike the usual reconfigurable modular robots, a self-folding sheet is a single morphable robot, simplifying robot construction and assembly by avoiding the need for complex connectors and more than one power source. Furthermore, unlike most robots in general, a self-folding sheet is a thin two-dimensional object, making it relatively easy to manufacture using standard tools for 2D rapid prototyping.

In this project we developed an algorithmic theory for how to design and control self-folding sheets, minimizing parameters such as number of actuators. While a mathematically ideal self-folding sheet can actuate any of the infinitely many possible crease lines by any amount at any time, building such a general sheet would be inefficient if not impossible. In this paper, we develop algorithms to design an efficient construction of a self-folding sheet that can fold into any shape belonging to a desired set of foldings. By specifying the target

shapes in this way, we show how to optimize the design to use few actuators and re-use shared components among foldings.

How do we choose foldings that can share many components? A powerful class of origami achieving this goal is *box pleating*, where all creases of a rectangular sheet lie along a square grid with alternating diagonals. In mathematics, this grid is called the *tetrakis tiling*. The $n \times n$ box-pleat pattern was recently shown to be *universal* in that crease patterns formed by subsets of the hinges fold into all possible orthogonal shapes made out of $O(n)$ cubes. Therefore, exponentially many shapes can be made from different subsets of one common hinge pattern, forcing this collection of foldings to share many creases. We focused on box pleating because of its uniformity and versatility for both practical and algorithmic origami design, although our techniques apply more generally to any straight-line hinge pattern.

Given k target shapes, we have developed a planning and control system for the self-folding sheet to folding itself into each of the k shapes. More precisely, the input consists of k origami designs—valid foldings of the box-pleated sheet—that come from either human origami designers or automated design algorithms. The output from our planning algorithms consists of both a physical design and plans for controlling the actuators for the sheet to reach the target origami designs. The physical design consists of the locations and interconnections of the actuators required to realize the design target shapes. Each plan consists of a sequence of discrete *phases*, where several edges fold simultaneously during each phase. We have found this type of plan to be both flexible—most origami cannot be achieved without folding many creases simultaneously—and practical—often many creases can be actuated together (reducing the number of phases and the intrinsically high number of degrees of freedom). Plans assume that the sheet starts unfolded.

Each *single origami planner* converts an origami design into a plan for folding the design via a sequence of discrete phases, where each phase consists of one or more creases folding simultaneously to an angle achievable by an actuator (multiple of 90°). The *multiple origami planner* combines multiple plans, each produced by the single origami planner, into a single design for a self-folding sheet robot, along with a plan for how to fold the sheet into each of the original origami designs. The multiple origami planner specifies the edge actuators and their electrical connectivity, so it is in fact needed even for designing self-folding sheets that make only a single shape. The goal of the multiple origami planner is to write each phase in each single-origami plan as a union of groups. A *group* consists of one or more edge actuators that can be permanently electrically connected because they always fold together. More precisely, if two folds (including both the hinge and the fold angle) always appear together in each phase of the single origami plans, then they can belong to a common group. Our algorithm essentially maximally packs folds into groups. The planner requires that the crease patterns for the different origami designs are all subsets of a common hinge pattern, e.g., an $x \times y$ box-pleat pattern.

2.9.4 Findings

- The single origami planner is provably correct.

- The multi-origami planner is provably correct and generates plans that can be executed on the self-folding devices we have built.

2.10 Simulation and Task Specification

The following people participated in this part of the project: Vijay Kumar, Mark Yim, Steven Gray, Paul White, Jun Seo, Nora Ayanian, Nathan Zeichner.

Several aspects of programmable matter have been investigated as follows in date order:

- Static analysis of right angle tetrahedron chains for mechanical functionality (Sep 2009).
- A toolchain for simulating foldable programmable matter (Sep 2009).
- A multi-vertex origami model for constructing two-dimensional polyominoes. (Dec 2009).
- Incorporating strength analysis functionality into the Programmable Matter Editor (Jan 2010).
- Developing a mechanical strength model of programmable matter (May 2010).
- Improving right angle tetrahedron chain programmable matter system (Aug 2010).
- Reconfiguring chain-type programmable matter based on the Carpenter's Rule Theorem (Sep 2010).
- Developing a general stiffness model for programmable matter (Mar 2011).

2.10.1 Highlights

The major achievements from this period continue our work on motion planning for foldable programmable matter and build on the contributions from other groups within this other groups outside this project but within the programmable matter program. The joint programmable matter meetings made it clear that the material strength (e.g. stiffness) of programmable matter is a critical problem area to enable the usefulness of programmable matter as a tool for many militarily relevant scenarios. Is it possible to make programmable matter that can form not only different shapes but also one shaped like a wrench that can actually turn a bolt? This is especially evident when one considers an wrench folded from a flat sheet.

One of the ideas expressed by other teammembers in the programmable matter program was that chains of modules, permanently bonded and hinged, can still approximate any 3D shape. The permanent bond is likely to be stronger than any temporary bond, so material strength of the conglomerate is likely to be stronger as well. How do we calculate this strength? How do we exploit this anisotropy in a full system? Finite element methods are

analogous to a modular structure however either too simple to adequately model the stiffness or too slow to be useful as a design tool.

In this work we have linked folding sheets with folding chains. Developed strength analysis tools for programmable matter in general. Developed automatic folding in 2D using carpenter’s rule including a decentralized method and a tool chain that links all of this together as a design tool for programmable matter.

2.10.2 Collaborations

Our work was done as a deep collaboration between Vijay Kumar, with input from Daniela Rus, Erik Demaine, and Rob Wood.

2.10.3 Approach

A key insight linking our work on foldable sheet programmable matter to the chain work is that a chain is a one dimensional subset of two dimensional sheet folding. Indeed, part of the output of this phase work, we develop an automatic method for generating linked chain of polyhedron from a flat sheet, including right angle tetrahedrons and chains of cubes.

To these ends we completed a simulation toolchain for foldable programmable matter. Any motion planning algorithm can be incorporated into this toolchain. We also developed motion planning algorithms for foldable programmable matter based on the Carpenter’s Rule Theorem that was both centralized and decentralized.

Part of this toolchain included design optimization algorithms for the static analysis of identical modules with anisotropic bonds using six degree-of-freedom elastic elements and a 6x6 stiffness matrix model. We constructed a second generation of externally actuated right angle tetrahedron chains and demonstrated 20 successful trials of folding. The six degree-of-freedom stiffness model method was verified by using experimental data from three different systems under various static load conditions.

2.10.4 Implementation

- The Programmable Matter Editor was coded in C++ and has two XML schemas called PMML and CMML. The Programmable Matter Markup Language (PMML) is designed to hold the geometric information of foldable programmable matter and the Controllable Matter Markup Language (CMML) is designed to hold sequences of fold events. Physics, Graphics, and interface design are handled using PhysX, OpenGL, and FLTK, respectively. Any motion planning algorithm for foldable programmable matter can be simulated if the output complies to the CMML format and the PMML document precisely describes the geometry of the given foldable programmable matter (Jan 2010).
- Reconfiguring chain-type modular robots has been considered a difficult problem scaling poorly with increasing numbers of modules. We addressed the reconfiguration problem for robots in 2D by presenting centralized and decentralized algorithms based

on the Carpenters Rule Theorem. The theorem guarantees the existence of instantaneous collision-free unfolding motions which monotonically increase the distance between all joint pairs until an open chain is straightened or a closed chain is convexified. The motions can be found by solving a convex program. Compared to the centralized version, the decentralized algorithm utilizes local proximity sensing and limited communications between subsets of nearby modules. Because the decentralized version reduces the number of joint pairs considered in each convex optimization, it is a practical solution for large number of modules.

- In addition to the external shape of a module configuration, the internal arrangement of modules and bonds between them can greatly impact functionally relevant mechanical properties such as load bearing ability. A fast method to evaluate the mechanical property aides the search for an arrangement of modules achieving a desired mechanical property as the space of possible configurations grows combinatorially. We developed a fast approximate method where the bonds between modules are represented with stiffness matrices that are general enough to represent a wide variety of systems and follows the natural modular decomposition of the system. The method includes non-linear modeling such as anisotropic bonds and properties that vary as components flex. We showed that the arrangement of two types of bonds within programmable matter systems enables programming the apparent elasticity of the structure. We also developed a method to experimentally determine the stiffness matrix for chain style reconfigurable robots. The efficacy of applying the method is demonstrated on the CKBot modular robot and two programmable matter systems: the Rubik’s snake folding chain toy and a right angle tetrahedron chain called RATChET7mm. By allowing the design space to be rapidly explored we opened the door to optimizing modular structures for desired mechanical properties such as enhanced load bearing and robustness.

2.10.5 Findings

- We investigated if multi-vertex rigid origami can approximate any two or three-dimensional goal shapes. Our first result is that any two-dimensional polyomino with nonzero thickness can be folded from a chain of 5×3 box-pleating patterns (Dec 2009).
- We developed a toolchain integrating an efficient shape editor for foldable programmable matter, a stable dynamic simulator for visualizing motion plans, and a reliable static analysis method for evaluating required mechanical functionalities (Jan 2010).
- We performed hardware experiments to figure out the stiffness of an individual module. We then used the module stiffness to predict the displacement of several connected modules under external loads in six degrees-of-freedom. (Mar 2010).
- We developed a motion planning algorithm for chain-type programmable matter based on the Carpenters Rule Theorem. The constraints in the theorem can be relaxed into a decentralized form by introducing hybrid-type control rules (Jul 2010).

- We developed a next generation right angle tetrahedron chain programmable matter system. Modules bond using low melting point alloy enabling further miniaturization and easier module fabrication (Aug 2010).
- We presented a fast method to evaluate the mechanical properties of programmable matter based on stiffness matrices. The stiffness matrices are general enough to represent a wide variety of systems. The method can also cover nonlinear modeling such as anisotropic bonds and properties that vary as components flex. We showed that the arrangement of two types of bonds within a programmable matter systems enables programming the apparent elasticity of the structure (Feb 2011).
- We developed a stiffness model using general six degree-of-freedom springs tailored to programmable matter and modular robot structures. Automatically filling out a 6x6 stiffness matrix from measured data turns out to be difficult given errors in sensing and maintaining a positive definite matrix that has reasonable fidelity. (Mar 2011).

2.11 Papers

The following publications resulted as part of this project.

- B. An, N. Benbernou, E. Demaine, and D. Rus, “Planning to Fold Multiple Objects from a Single Self-Folding Sheet” *Robotica*, pp 87-102, 2011.
- J. Paik, B. An, D. Rus, and R.J. Wood, “Robotic origamis: self-morphing modular robots”, to appear: Proc. 2nd Int. Conf. on Morphological Computation, Venice, Italy, Sept., 2011.
- J. Paik, R. Kramer, and R.J. Wood, “Stretchable Circuits and Sensors for Robotic Origami” , to appear: IEEE/RSJ Int. Conference on Intelligent Robots and Systems, San Francisco, CA, Sept. 2011.
- J. Paik, E. Hawkes, and R.J. Wood, “A Novel Low-Profile Shape Memory Alloy Torsional Actuator,” to appear: *Smart Materials and Structures*, 2010.
- E. Hawkes, B. An, N. Benbernou, H. Tanaka, S. Kim, E.D. Demaine, D. Rus, and R.J. Wood, “Programmable matter by folding,” *Proc. Nat. Acad. Sci.*, 107 (28), pp. 12441-12445, 2010.
- E. Torres-Jara, K. Gilpin, J. Karges, R. Wood, and D. Rus, “Composable Felxibe Small Actuators Made for Thin Shape Memory Alloy Sheets” in *IEEE Robotics and Automation Magazine* vol 17 no 4, pp 78-87, December 2010
- Cagdas Denizel Onal, Robert Wood, Daniela Rus, “Towards Printable Robotics: Origami-Inspired Planar Fabrication of Three-Dimensional Mechanisms”, In *Proceedings of the 2011 International Conference on Robotics and Automation*, May 2011

- Kyle Gilpin, Kent Koyanagi, Daniela Rus, “Making Self-Disassembling Objects with Multiple Components in the Robot Pebbles System”, In Proceedings of the 2011 International Conference on Robotics and Automation, May 2011
- Byoungkwon An, Daniela Rus, “Making Shapes from Modules by Magnification”, in Proceedings of the 2010 International Symposium on Intelligent Robot Systems (IROS), October 2010
- Kyle Gilpin, Ara Knaian, Daniela Rus, “Robot Pebbles: One Centimeter Modules for Programmable Matter through Self-Disassembly”, in Proceedings of the 2010 International Conference on Robotics and Automation, May 2010
- Xiaobo Zhang, Cary L. Pint, Min Hyung Lee, Bryan Edward Schubert, Arash Jamshidi, Kuniharu Takei, Hyunhyub Ko, Andrew Gillies, Rizia Bardhan, Jeffrey J. Urban, Ming Wu, Ronald Fearing, Ali Javey, “Optically- and Thermally-Responsive Programmable Materials Based on Carbon Nanotube-Hydrogel Polymer Composites ,” *Nano Letters* Article ASAP 2011.
- A.G. Gillies and R.S. Fearing, “A micromolded connector for reconfigurable millirobots,” *J. Micromech. Microeng.* 20 (2010) 105011.
- H. Ko, Z. Zhang, Y.-L. Chueh, E. Saiz, A. Javey, “Thermoresponsive Chemical Connectors Based on Hybrid Nanowire Forests”, *Angew. Chem. Int. Ed.*, 49, 616-619, 2010.
- H. Ko, Z. Zhang, J. C. Ho, K. Takei, R. Kapadia, Y.-L. Chueh, W. Cao, B. A. Cruden, A. Javey. “Flexible Carbon Nanofiber Connectors with Anisotropic Adhesion Properties”, *Small*, 6, 22-26, 2010.
- H. Ko, Z. Zhang, Y.-L. Chueh, J.C. Ho, R.S. Fearing, and A. Javey, “Wet and Dry Adhesion Properties of Self-Selective Nanowire Connectors,” *Advanced Functional Materials*, DOI:10.1002/adfm.200901178, 25 August 2009.
- P. J. White, S. Revzen, C. E. Thorne, and M. Yim. A general stiffness model for programmable matter and modular robotic structures. *Robotica*, 29(Special Issue 01):103-121, 2011.
- J. Seo, S. R. Gray, V. Kumar, and M. Yim. Reconfiguring chain-type modular robots based on the carpenters rule theorem. In *The Ninth International Workshop on the Algorithmic Foundations of Robotics (WAFR)*, 2010.
- P. J. White, M. L. Posner, and M. Yim. Strength analysis of miniature folded right angle tetrahedron chain programmable matter. In *Proceedings of IEEE International Conference on Robotics and Automation*, pages 2785-2790, Anchorage, AK, 2010.
- P. J. White, S. Revzen, C. E. Thorne, and M. Yim. A general stiffness model for programmable matter and modular robotic structures. *Robotica*, 2010.

- S. R. Gray, J. Seo, P. J. White, N. J. Zeichner, M. Yim, and V. Kumar. A toolchain for the design and simulation of foldable programmable matter. In *Proceedings of IDETC/CIE*, Montreal, Canada, 2010.
- P. J. White, C. E. Thorne, and M. Yim. Right Angle Tetrahedron Chain Externally- actuated Testbed (RATCHET): A Shape Changing System. In *Proceedings of IDETC/CIE*, San Diego, CA, USA, 2009.

Programmable Matter

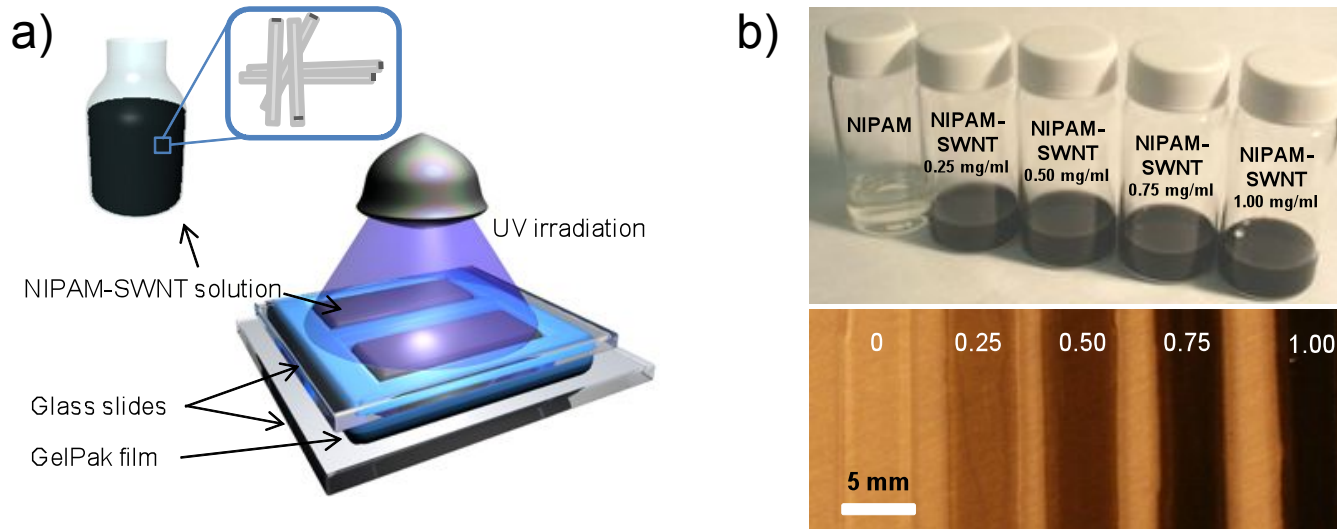
Final Project Report Figures

Team MIT, Berkeley, Harvard, Penn

PI: Daniela Rus

Fig. 1 Programmable matter based on SWNT-pNIPAM actuators

Fabrication Scheme for making SWNT-pNIPAM hydrogels



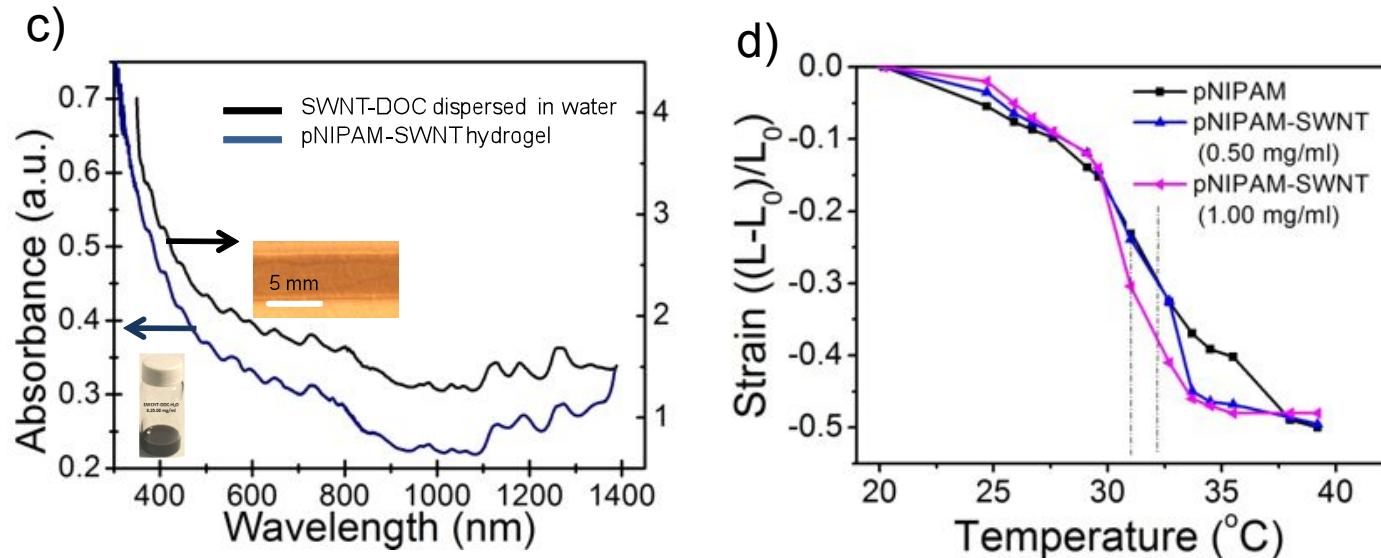
- a) Polymerization scheme for making SWNT-pNIPAM hydrogels using Gel-Pak confinement channels and UV curing.
- b) Polymer strips with different SWNT concentrations made using the method shown in part

A simple approach is utilized to fabricate reversible, thermally- and optically-responsive actuators utilizing composites of poly N-isopropylacrylamide (pNIPAM) loaded with single-walled carbon nanotubes.

Fig. 1 Programmable matter based on SWNT-pNIPAM actuators

UV-VIS and LCST characterization of SWNT-pNIPAM hydrogels

Figure 1

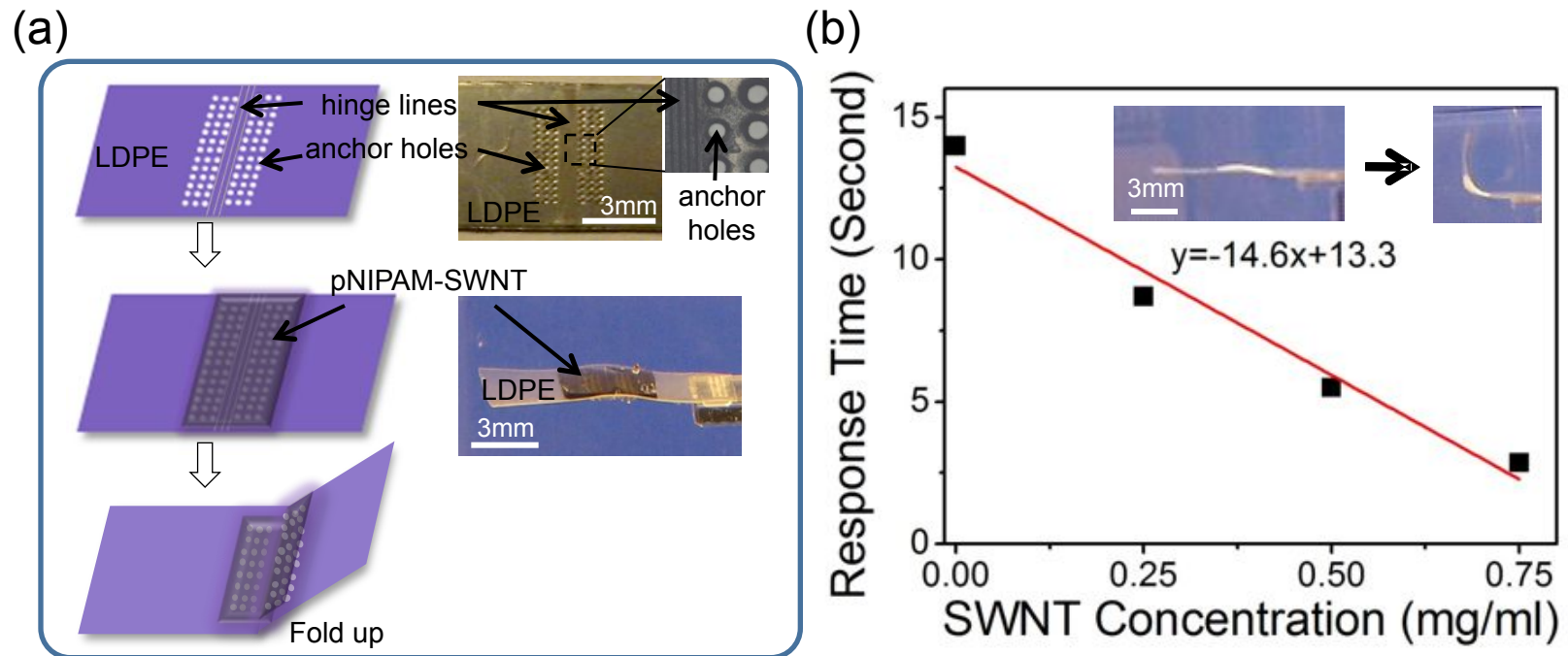


- c) UV-Vis-nIR absorption spectra of aqueous SWNT-DOC solution (blue) and a SWNT-pNIPAM hydrogel strip (SWNT concentration, 0.5 mg/ml) after polymerization (black).
- d) LCST characterization for the polymer strips with different SWNT concentrations.

Good SWNT dispersion is confirmed using UV-VIS;
SWNT-pNIPAM hydrogel shows well-defined Lower Critical Solution Temperature

Fig. 2 Programmable matter based on SWNT-pNIPAM actuators

Fabrication scheme for making thermally responsive actuators and response time measurement.



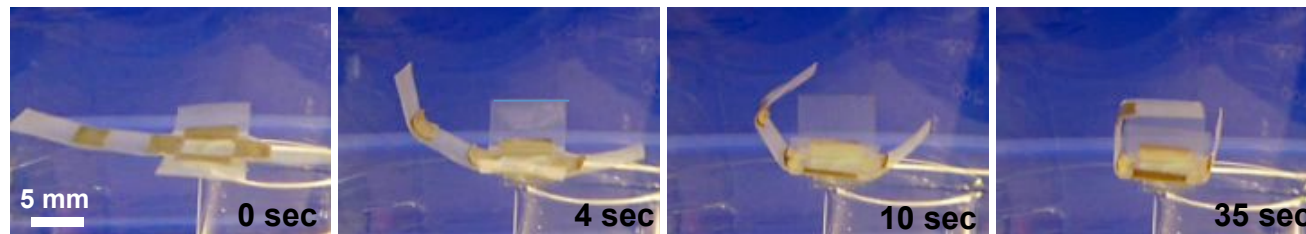
- a) Fabrication scheme for making SWNT-pNIPAM/LDPE bilayer actuators and the corresponding optical images.
- b) Response time measurement by measuring the time for the actuator to reach 90° folding angle. The inset shows an optical image of a pNIPAM/LDPE actuator before (left) and right (after) folding.

Fig. 3. Programmable Cubes – a folding cube based on thermal responsive actuators.

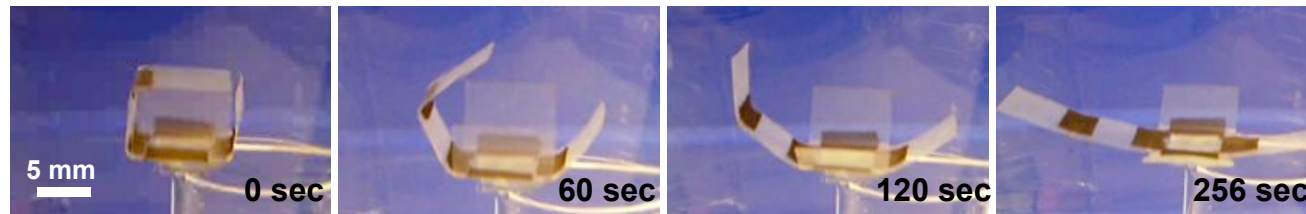
(a) Fabrication scheme for folding cube



(b) Cube folding at 48°C in water

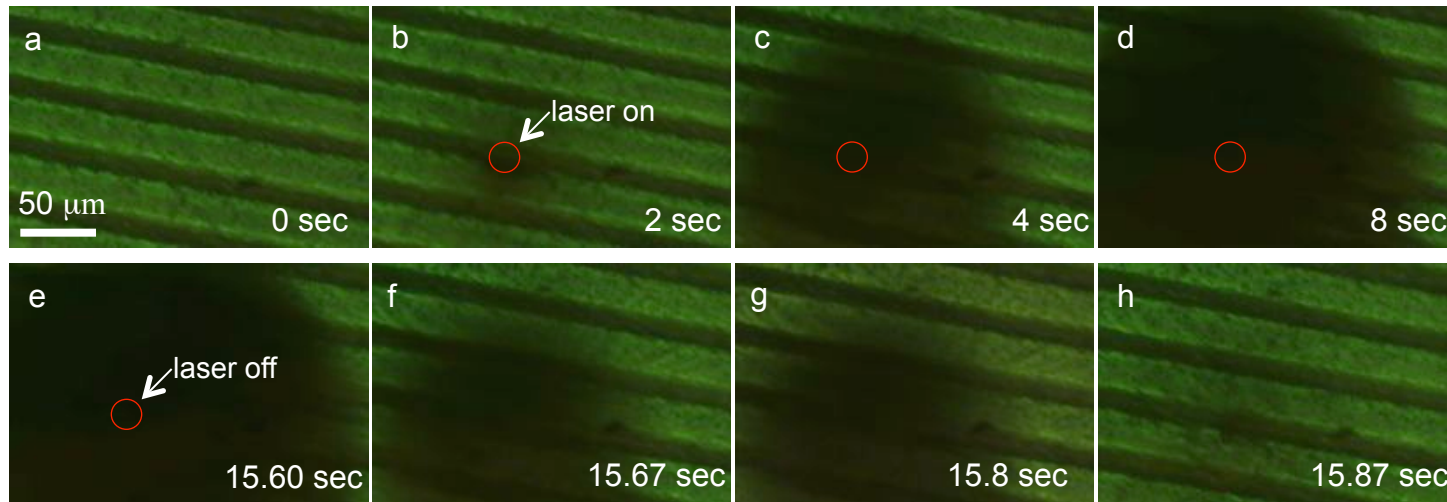


(c) Cube unfolding upon cooling down



- Fabrication scheme for folding cubes based on SWNT-pNIPAM/LDPE bilayer actuators.
- Cube folding by thermal actuation in 48°C water.
- Cube reversibly unfolds by cooling down the water bath in which cube is immersed.

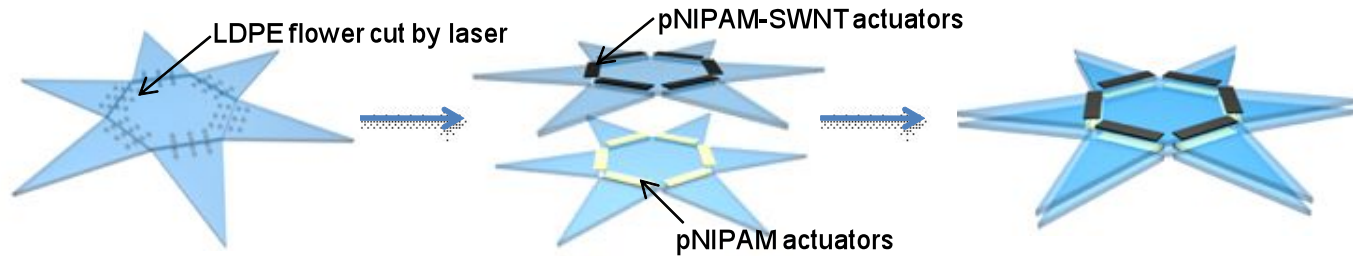
Fig. 4. Near-IR optical response measurement for SWNT-pNIPAM hydrogels



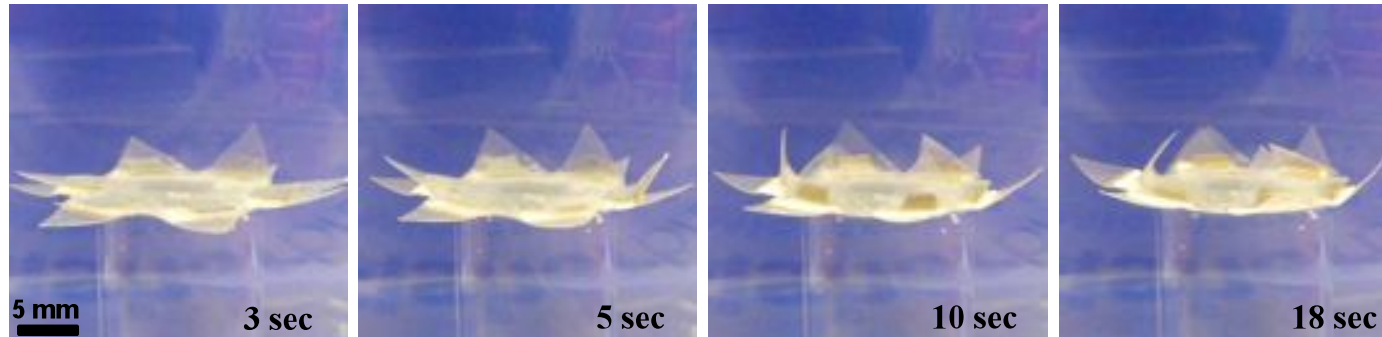
- a) SWNT-pNIPAM/LDPE bilayer actuator (note: the background features are the hinge lines).
- b)-d) SWNT-pNIPAM hydrogel turns opaque (i.e., black) after illuminated by the near-IR laser beam from the top due to the shrinking of the SWNT-pNIPAM layer.
- e)-h) SWNT-pNIPAM hydrogel turns transparent after the laser beam is turned off which indicates the transition of the hydrogel back to a swelled state

Fig. 5. Programmable “flower” made by heterogeneous integration of pNIPAM and SWNT-pNIPAM bilayer actuators

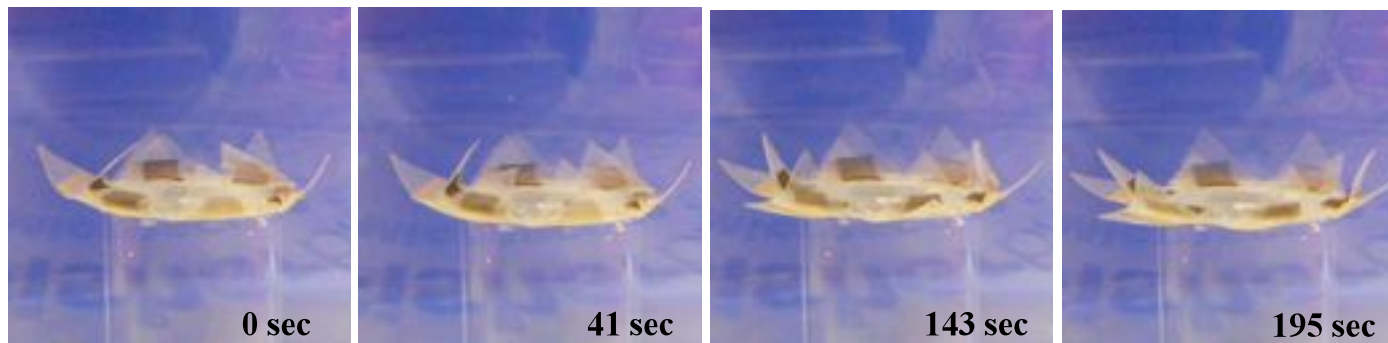
(a) Flower fabrication scheme



(b) Flower folding up upon heating up in 50°C water

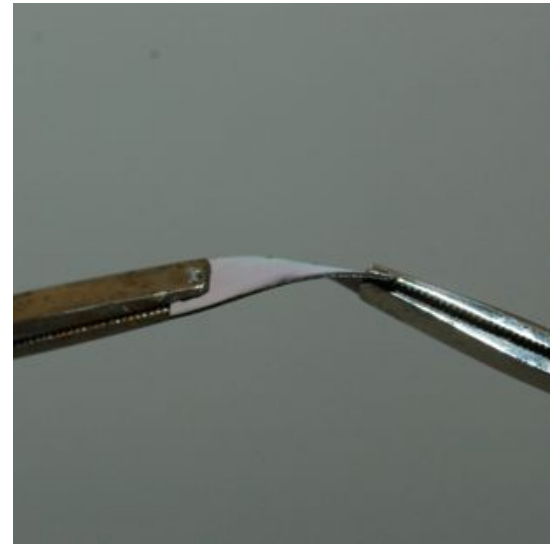
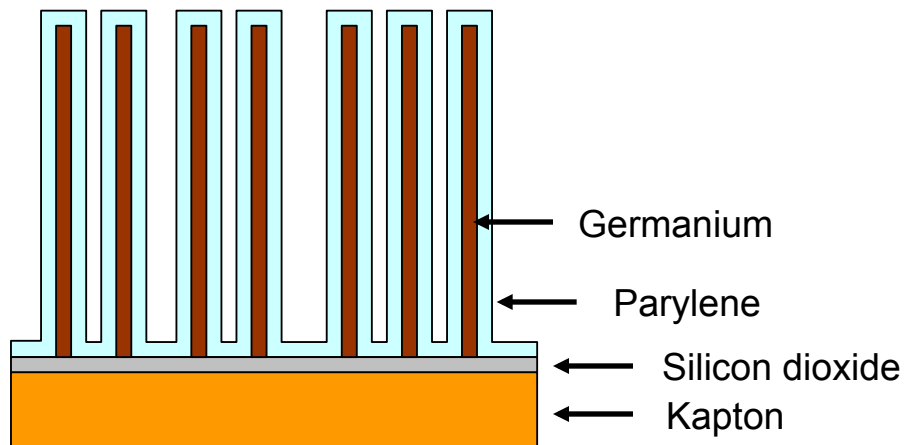


(c) Flower blooming upon cooling down



A programmable flower consisting of two layers of actuators folds (i.e., closes) when heated up and blooms when cooled down

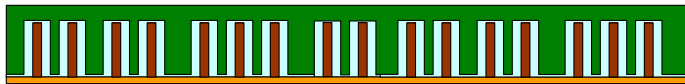
Figure 6. NW connectors on flexible substrate



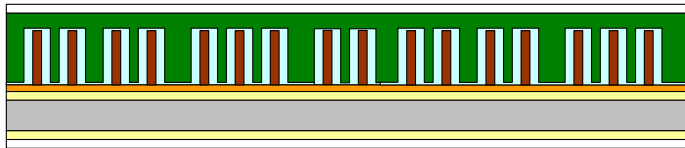
Demonstration of flexibility of Parylene-coated, Germanium NWs grown on Silicon-dioxide-coated Kapton

Figure 7. Integration of NWs into Programmable Matter

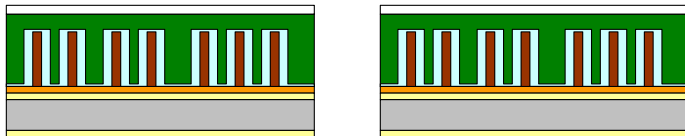
1) Coat NWs with PVA



2) Laminate to Glass fiber

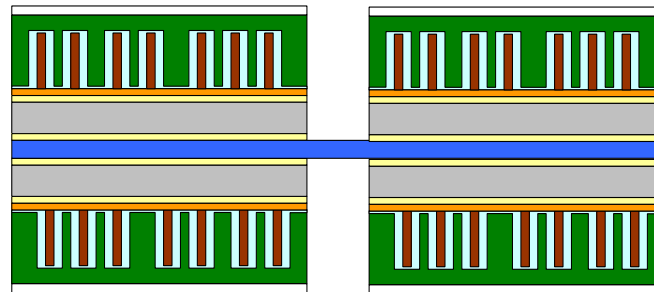


3) Laser cut flexures and fold lines



Wax paper	Kapton (25 μm)
PVA	Thermal Adhesive
Parylene	Glass fiber (125 μm)
Germanium NW	Polyester (12 μm)

4) Fold and laminate polyester flexure layer



5) Rinse off PVA in water

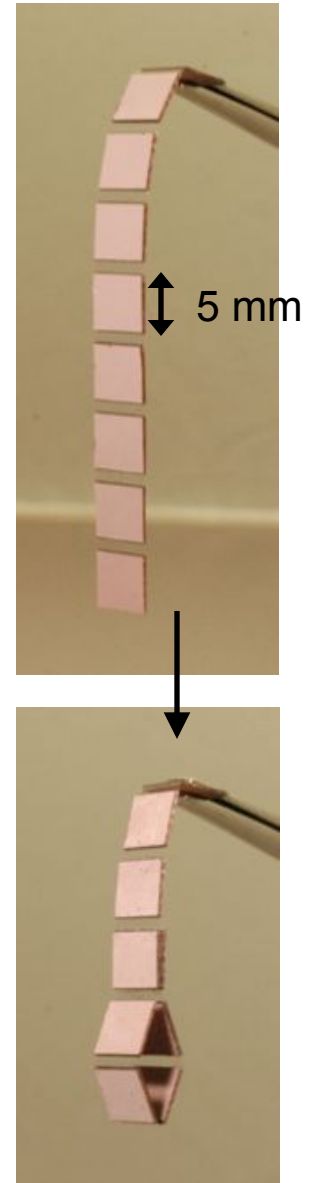
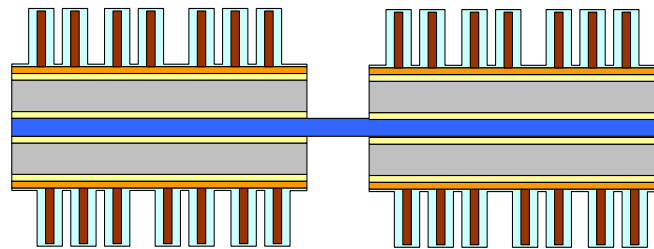


Figure 8. NW connectors before and after integration.

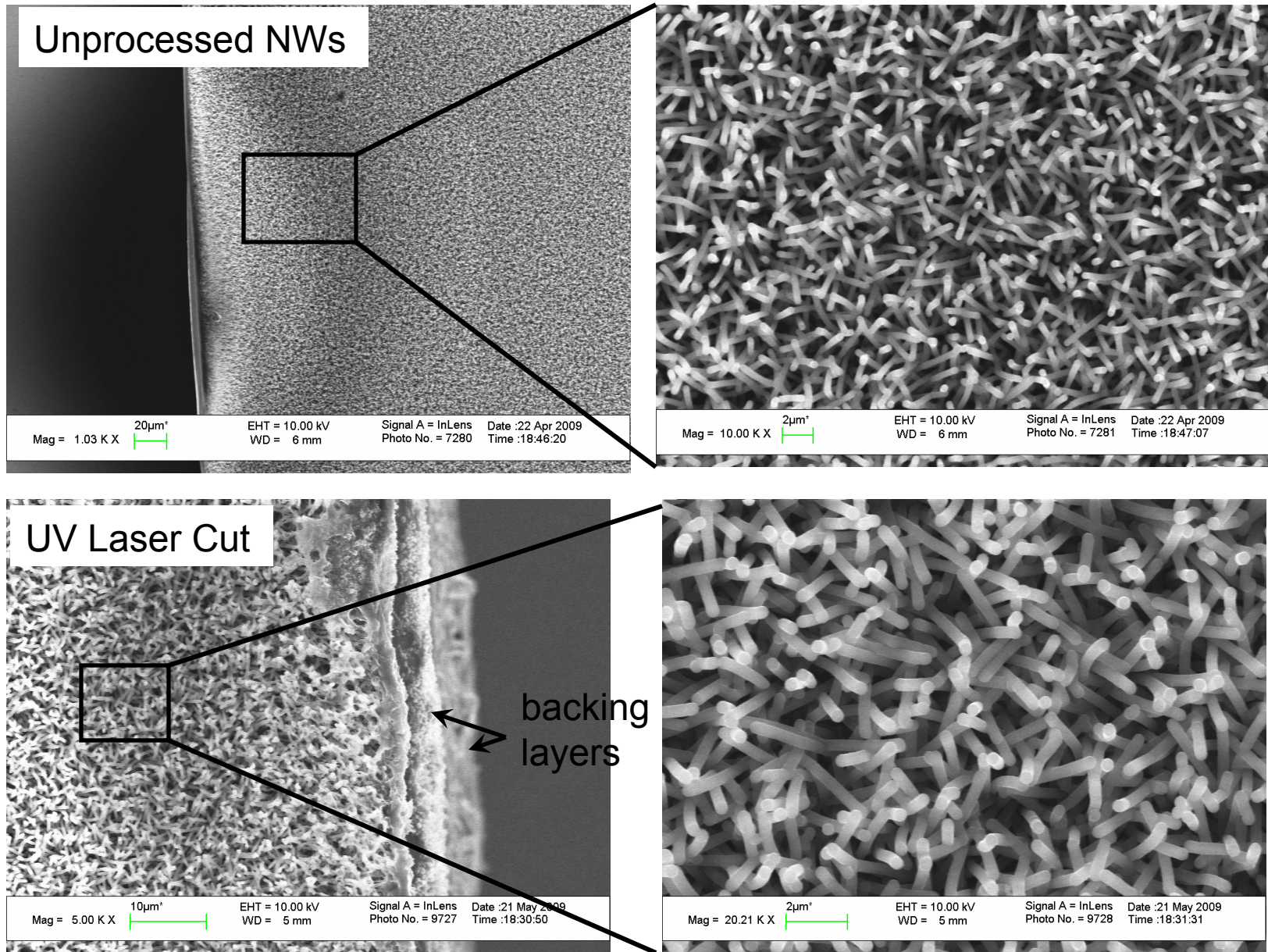
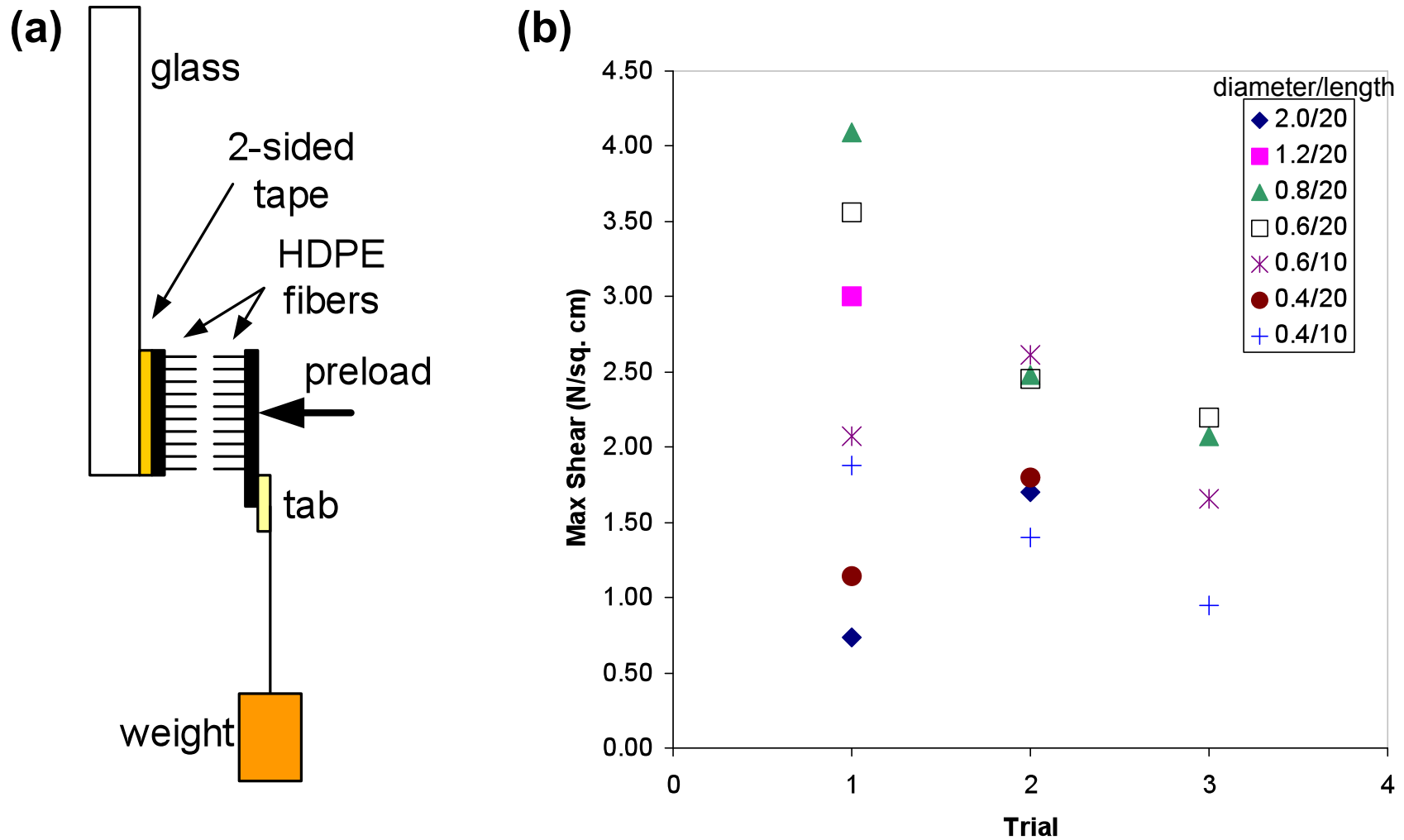
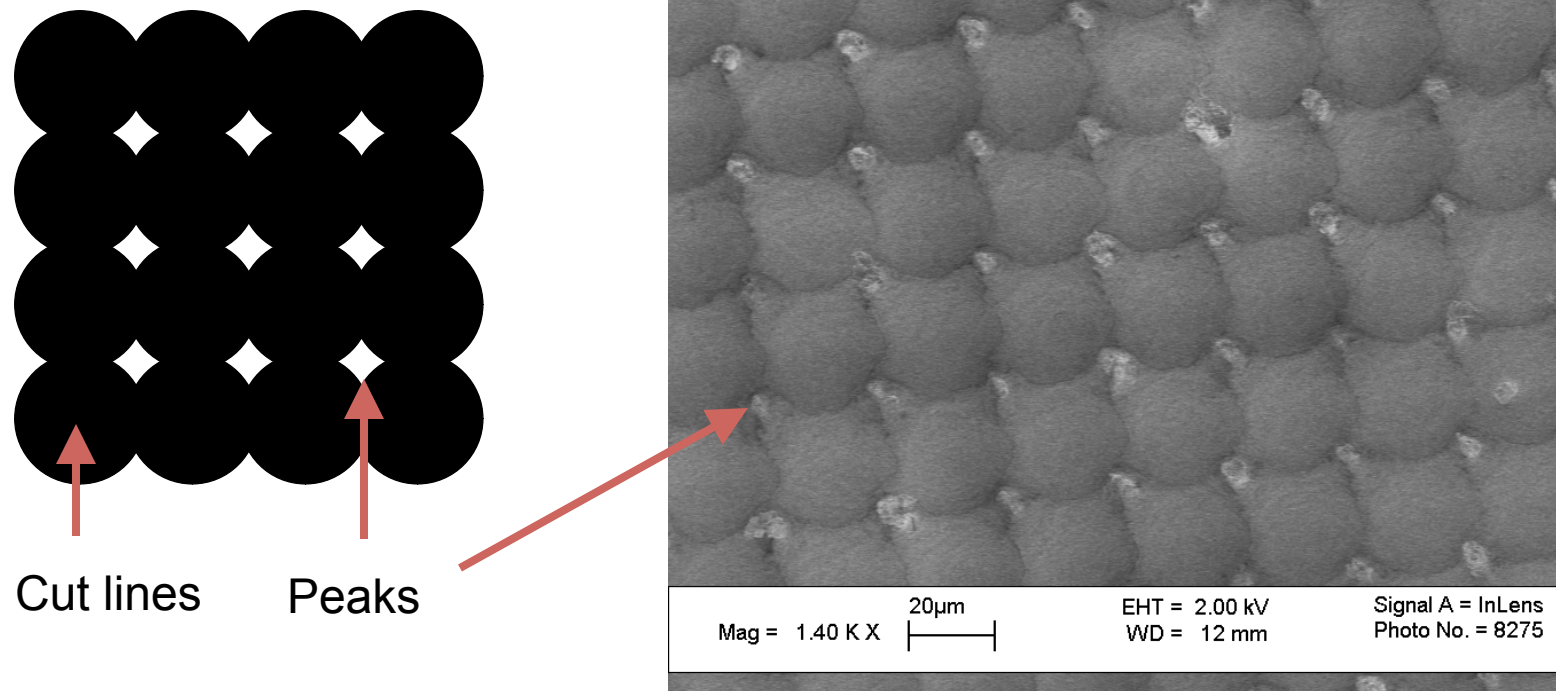


Figure 9. Polymer microfiber connectors.



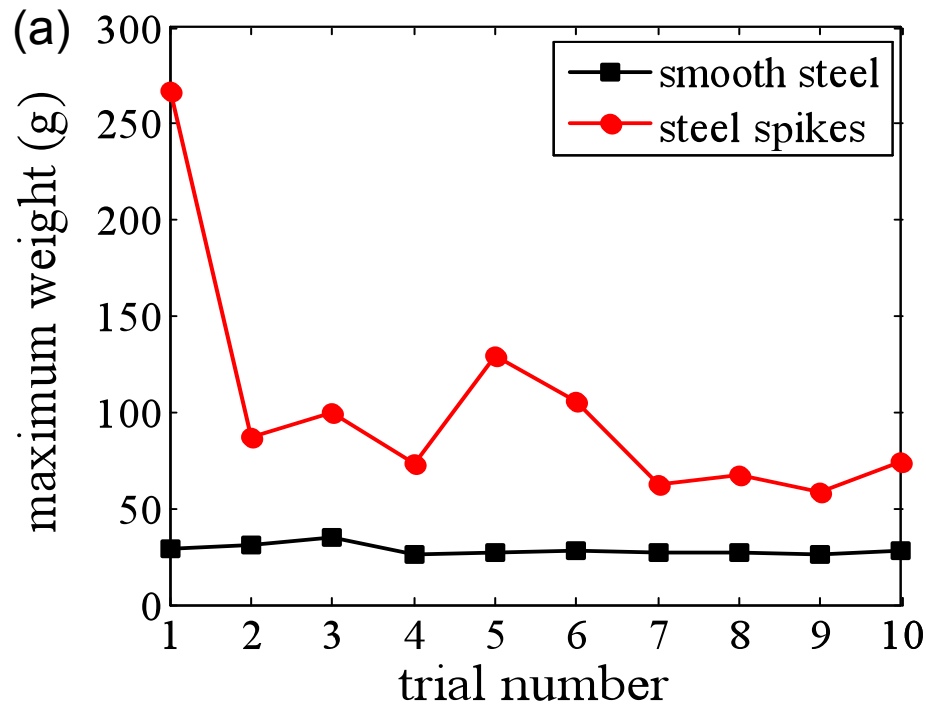
(a) Shear adhesion test of HDPE connectors. (b) Shear adhesion of HDPE connectors as a function of fiber diameters (μm), lengths (μm) and trial number. Samples preloaded by hand.

Figure 10. Laser patterning of steel spikes.



Steel spikes can be created using laser ablation to remove the material in crosses lines, leaving a spike. Spike size and spacing can be controlled by line spacing and laser power. SEM image is from the top with a slight tilt. Tip diameter is $\sim 5 \mu\text{m}$ with a spacing of $30 \mu\text{m}$ and peak to valley height of $\sim 15 \mu\text{m}$.

Figure 11. Shear testing of steel spikes.



(a) Shear tests with switchable magnetic loading shows that spike-on-spike increases the shear force considerably over smooth steel-on-steel. (b) The shear test set-up consists of two samples attached with tape to a glass fiber plate that holds the magnets. The two samples are placed face to face and loaded in shear.

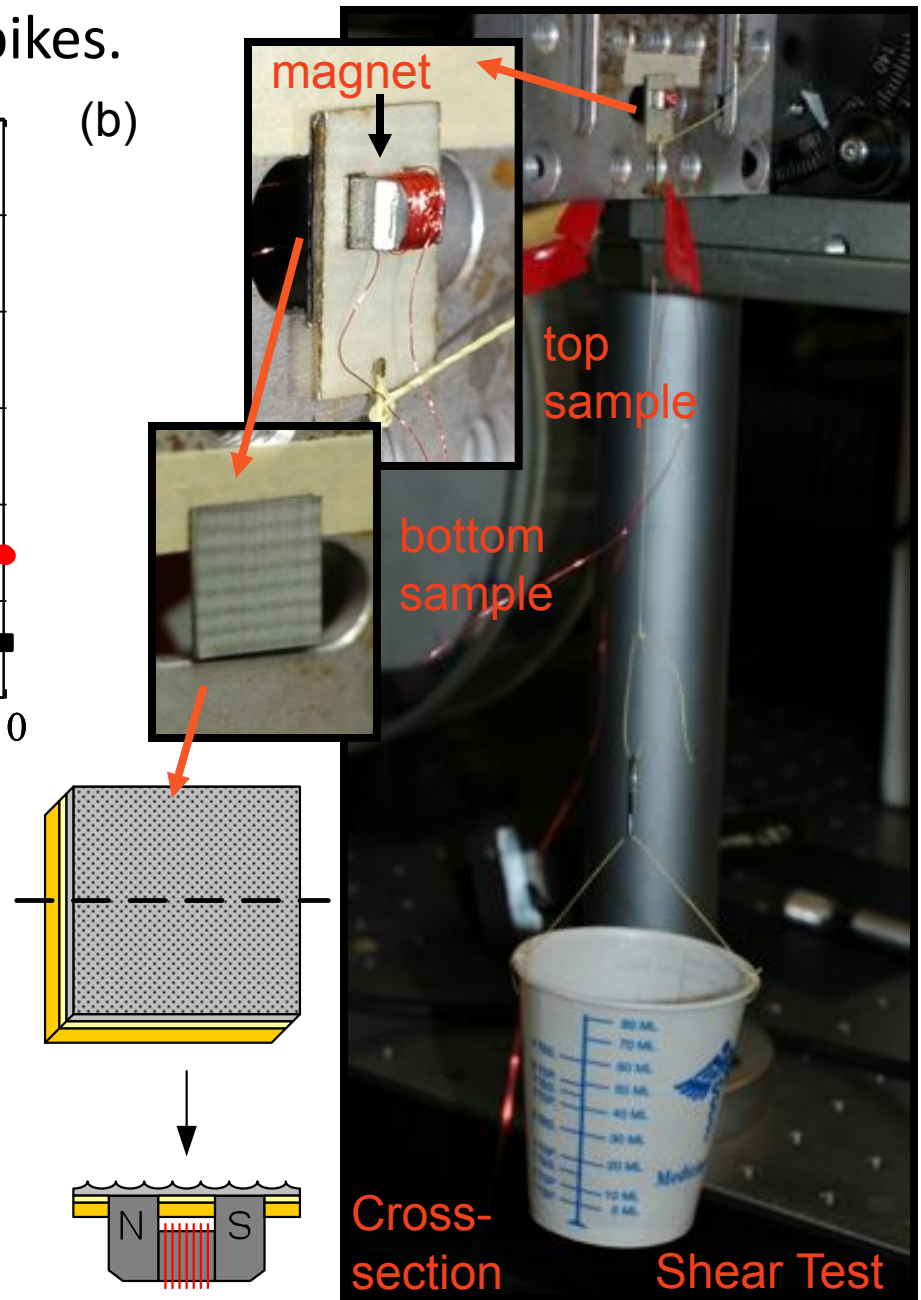
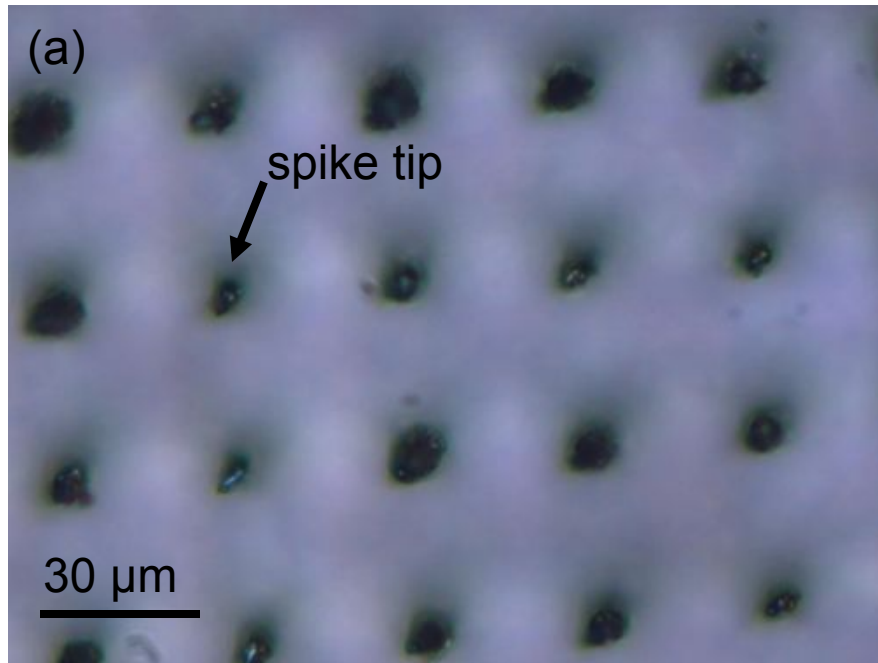


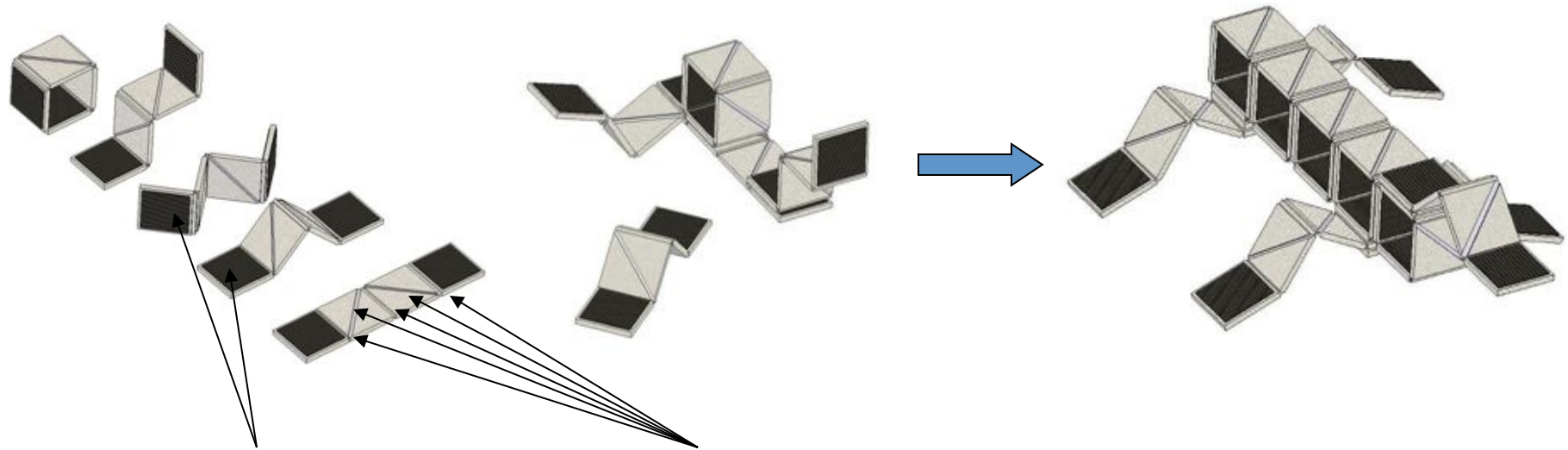
Figure 12. Steel spike failure.



When loaded to failure, the metal spikes experience considerable deformation. (a) Spike array prior to testing. (b) Spike array after testing. Many spikes are bent over onto their sides.

Fig. 13. New Primitive Design

- Primitive is a tile capable of actuation
- Able to change shape and combine to form interesting functional devices.
- Connectors and actuators allow tiles to ambulate across varied terrain and to connect to other tiles.

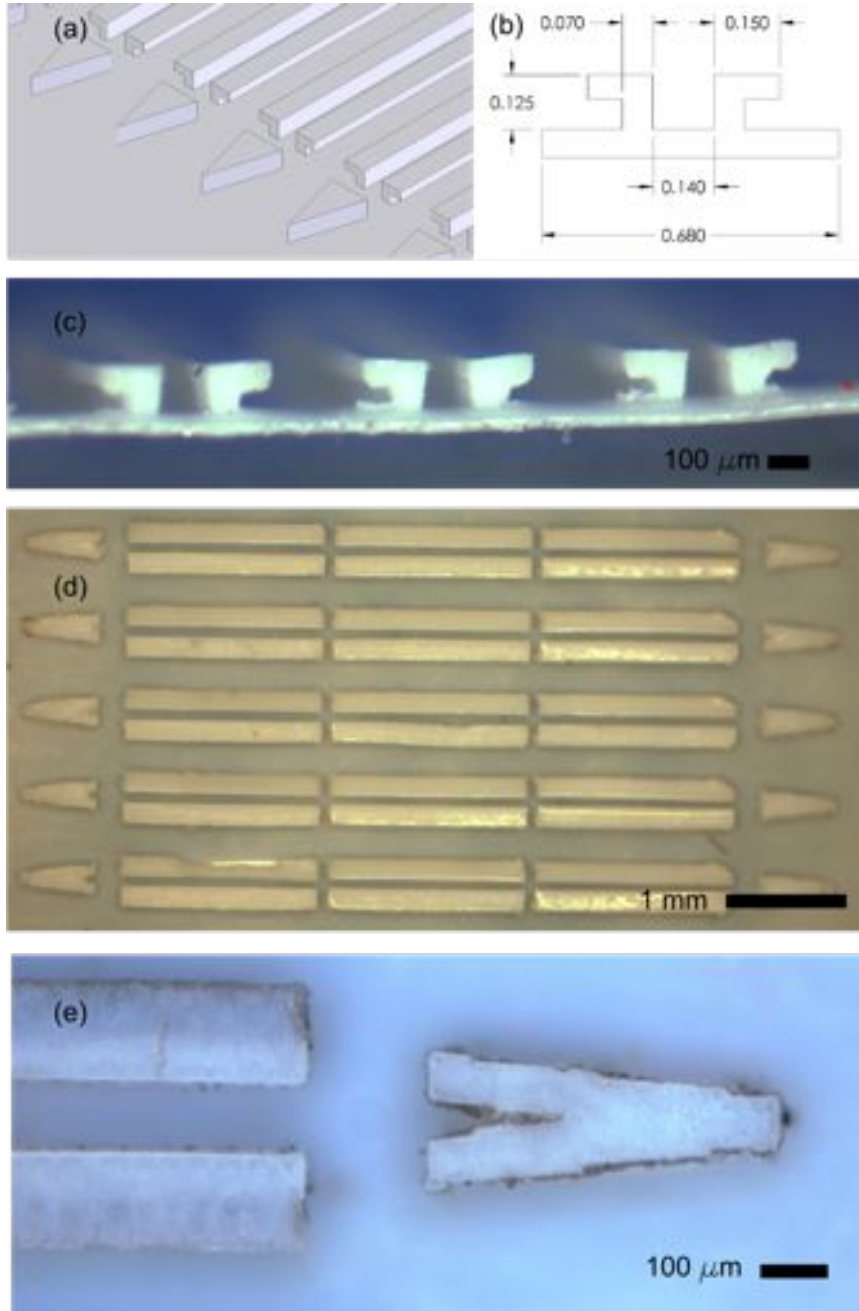


Tiles have connectors on both sides to enable connecting to surfaces and other tiles

Tile primitive capable of actuating 5 joints to emulate a general kinematic chain

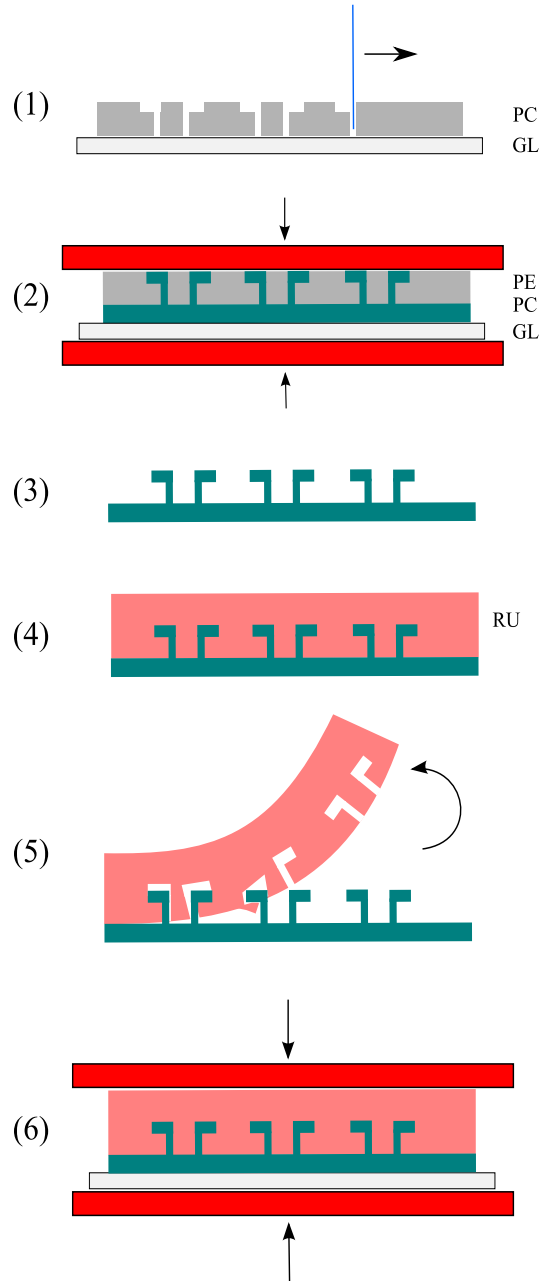
Tiles can crawl and connect to form larger functional structures

Figure 14: New design for micro connector



- New design of micro connector:**
- (a)** 3D schematic of design showing alignment features and L shaped ridges
 - (b)** Drawing of ridge cross section showing dimensions in mm
 - (c)** Cross section of fabricated micro connector
 - (d)** Top view of micro connector fabricated with stamping process
 - (e)** Close up view of alignment feature

Figure 15: Mass Manufacturing of PE Micro Connectors



New fabrication method for micro connector:

- (1) Cut negative in polycarbonate (PC) film while mounted on glass (GL)
- (2) Fill with polyethylene (PE) in hot press
- (3) Etch PC
- (4) Cast high temperature resistant rubber (RU)
- (5) Peel rubber off master
- (6) Mold PE film into rubber using hot press

Figure 16: Force displacement apparatus

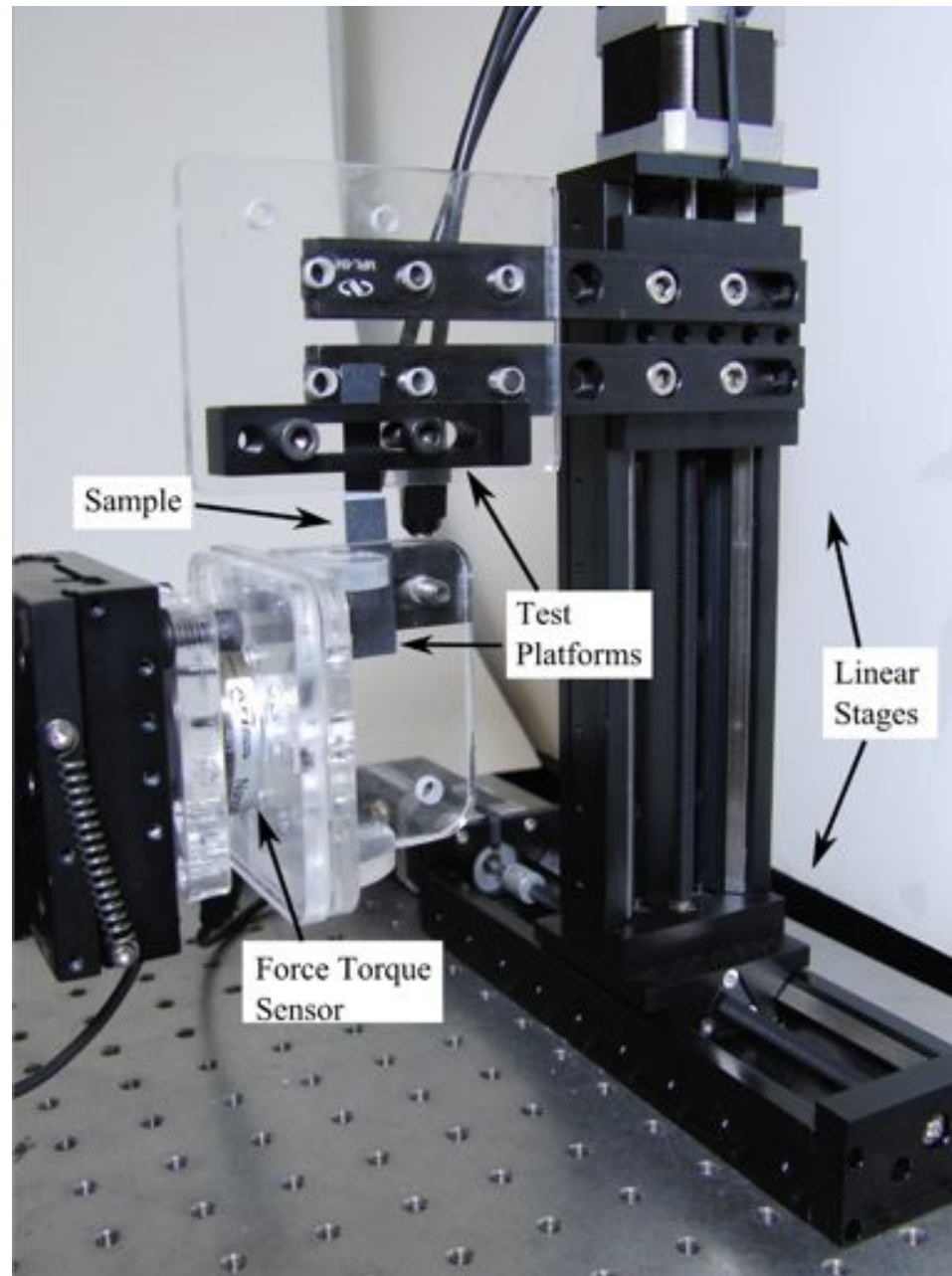


Figure 17: Microconnector Failure Strength

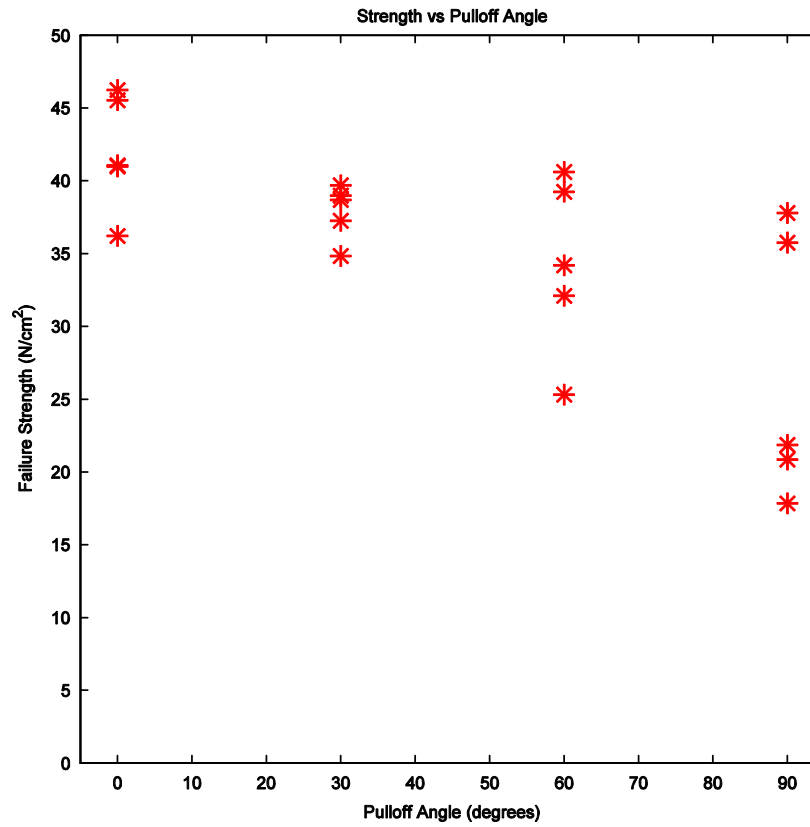
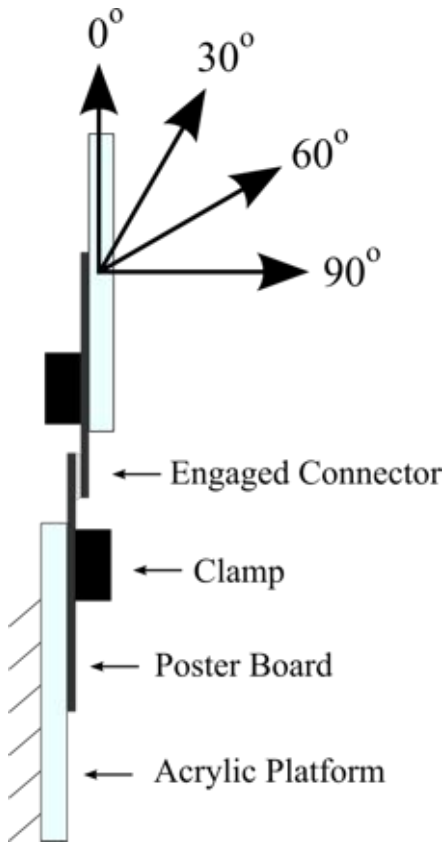
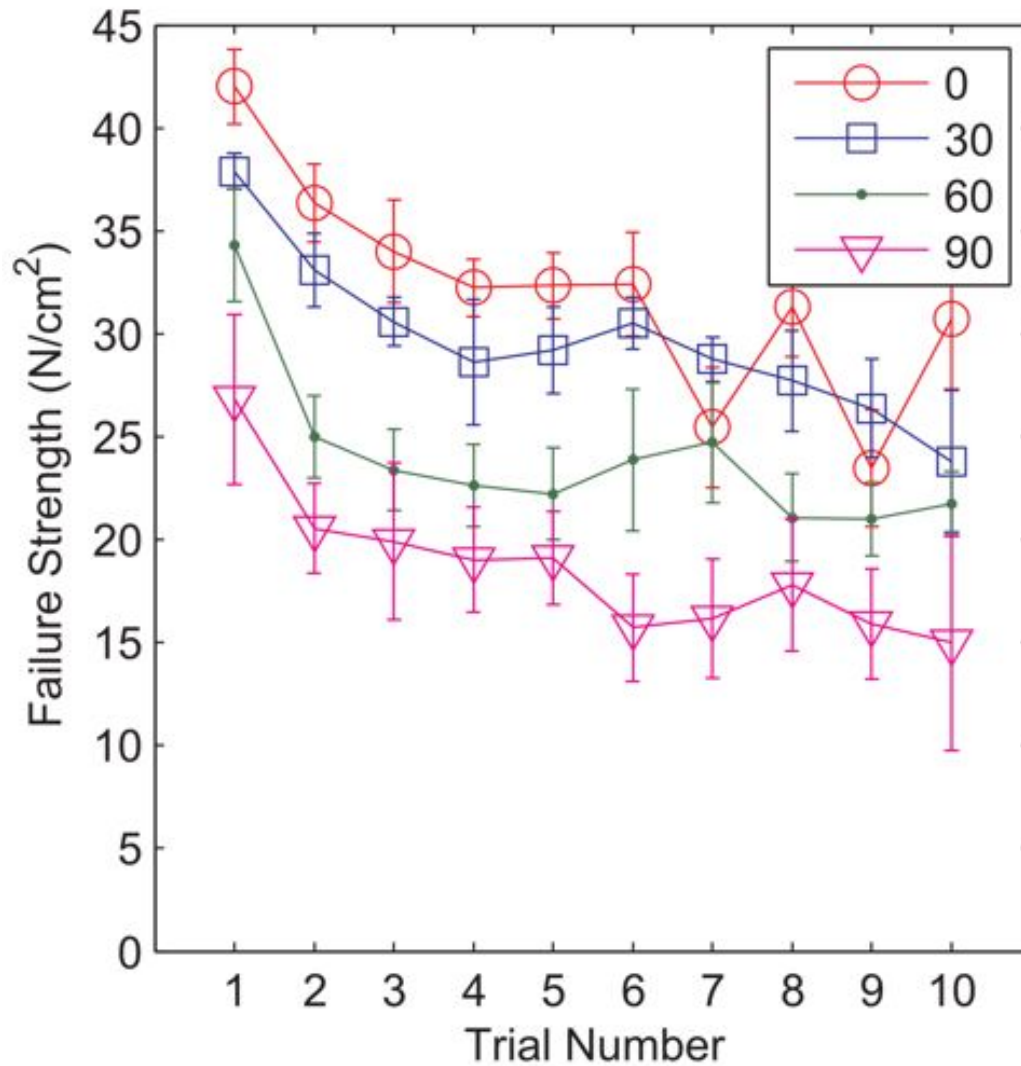
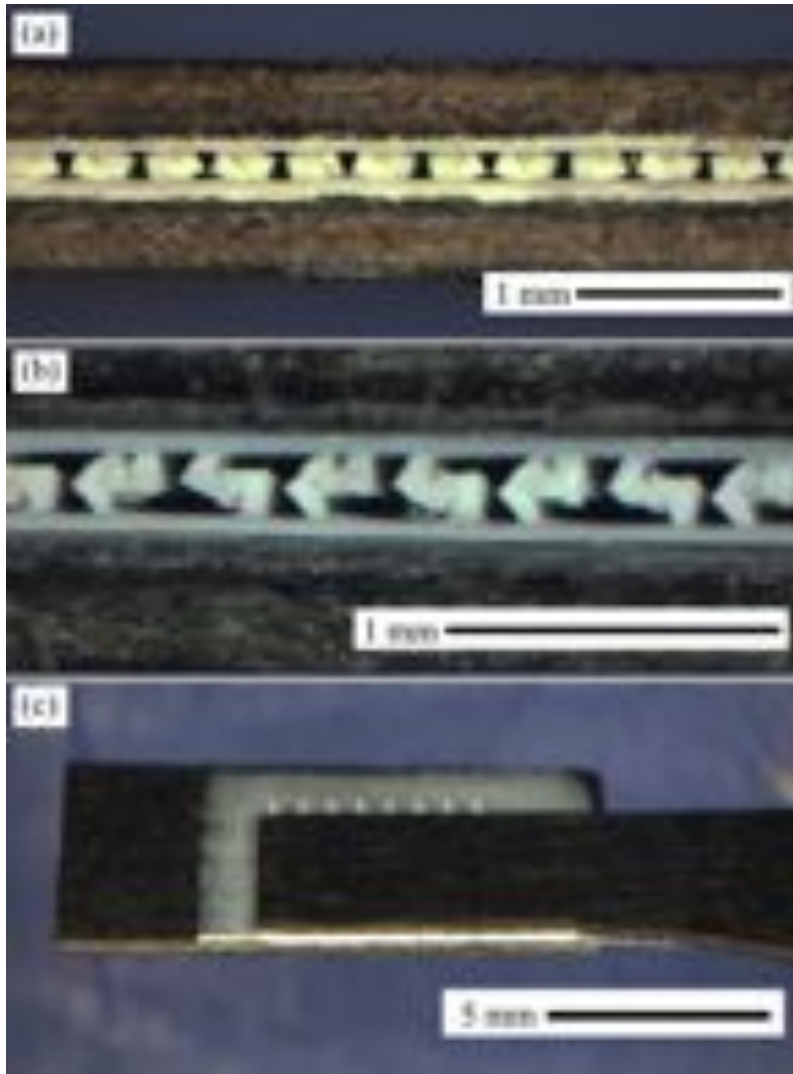


Figure 18: Microconnector Reusability



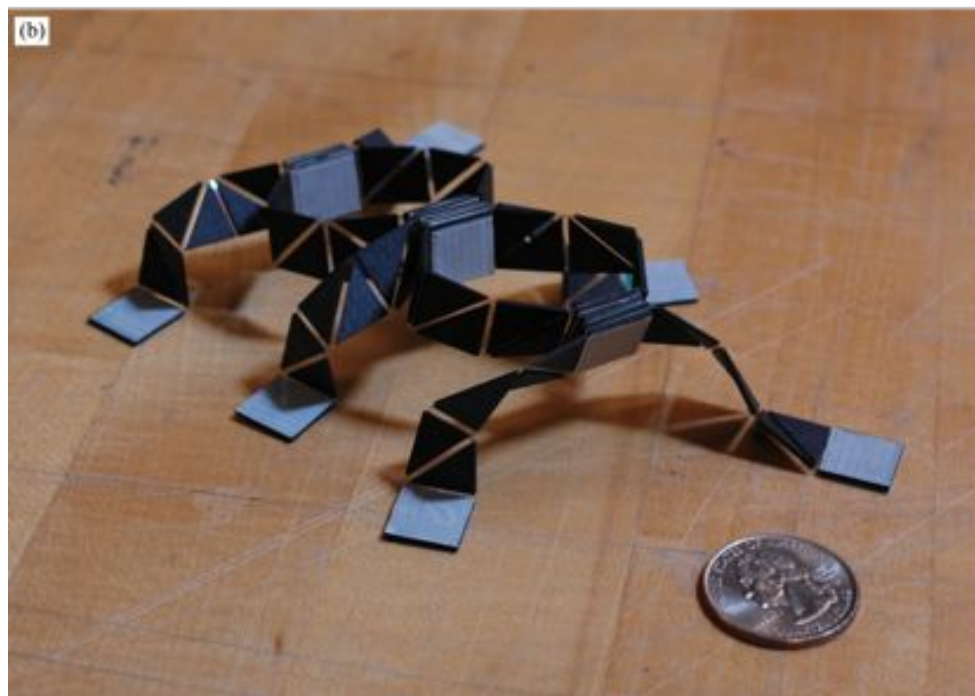
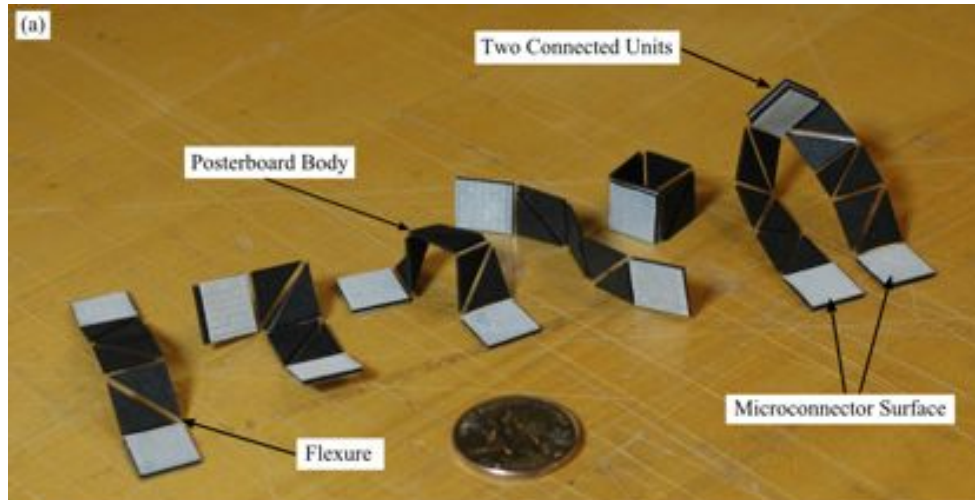
Samples tested to failure 10 times at pull-off angles of 0,30,60 and 90 degrees show they can maintain 70%-55% of their strength depending on pull-off direction.

Figure 19: Engaged microconnectors



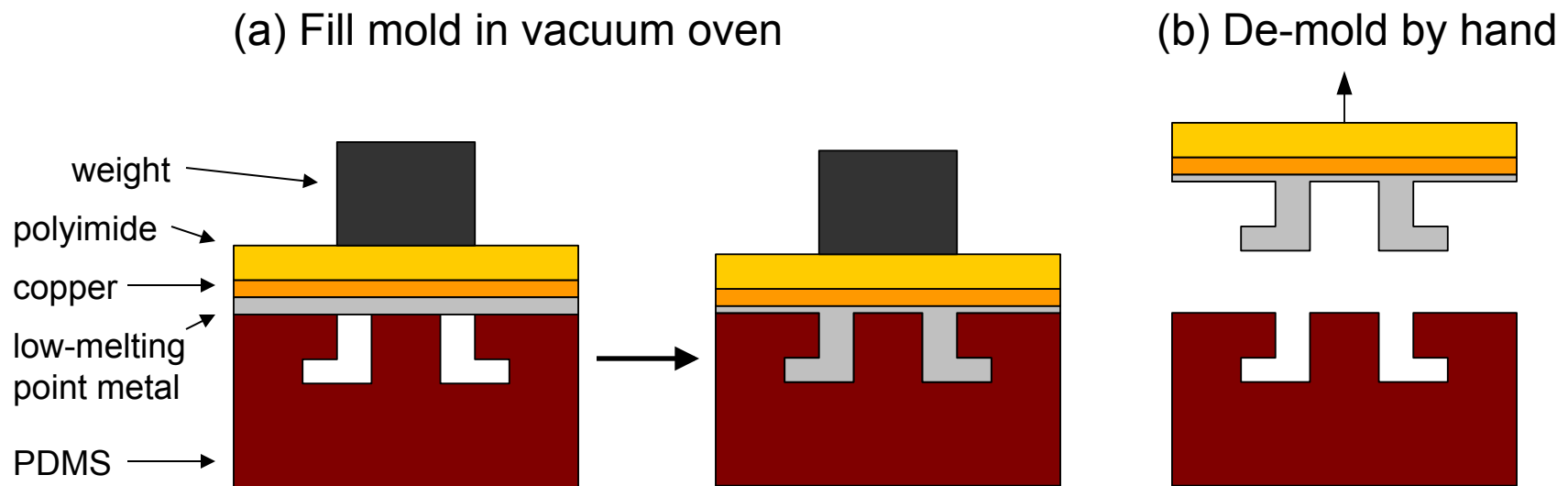
- (a) Cross section of an engaged connector
Engaged connector after being tested to failure 10 times
Oblique view of engaged connector

Fig. 20. Programmable matter chassis



(a) Microconnectors integrated into the surface of possible programmable matter units modeled after the robots presented by Koh and Cho (b) A modular robot frame built out of programmable matter units.

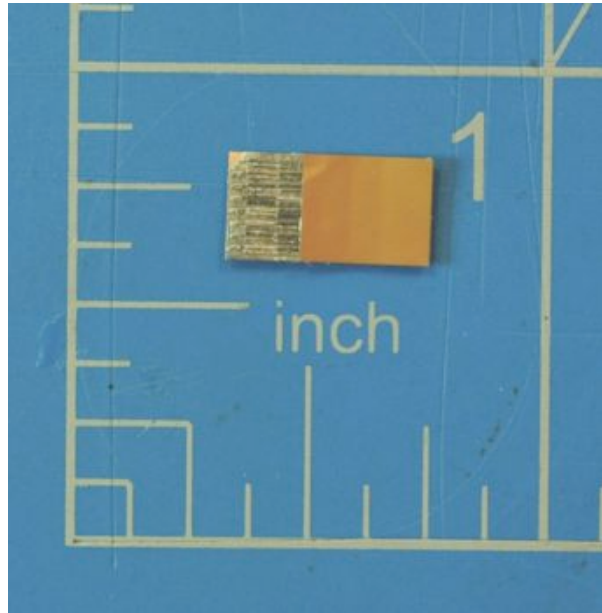
Fig. 21. Conductive Connector



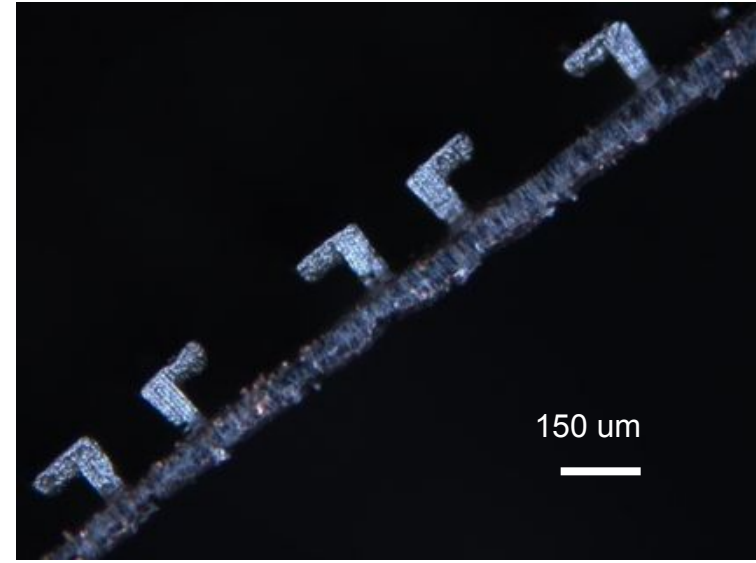
(a) Copper-clad polyimide that is coated with a thin layer of low melting point metal (Cerrosheet) is placed against the PDMS mold. A weight is used to hold the film flat while the stack is heated to 300°F in a vacuum oven at 27 inHg. (b) After cooling, the connector can be peeled out of the mold.

Fig. 22. Conductive Connector

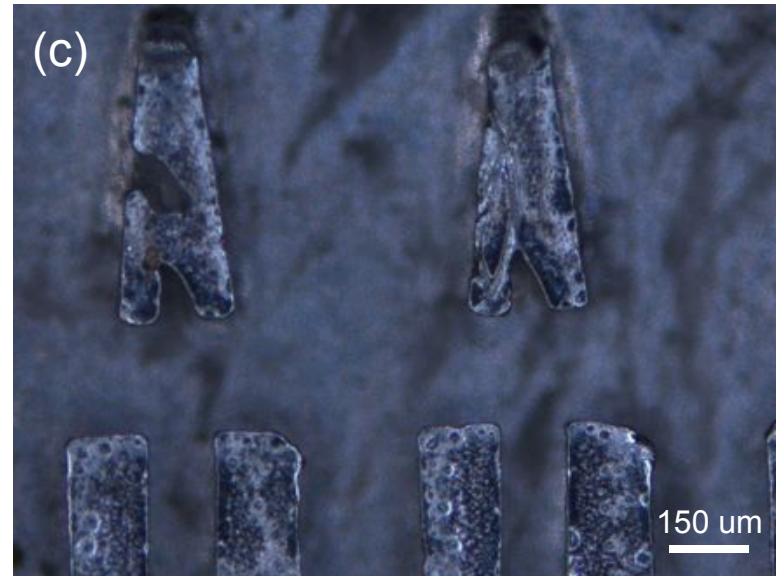
(a)



(b)

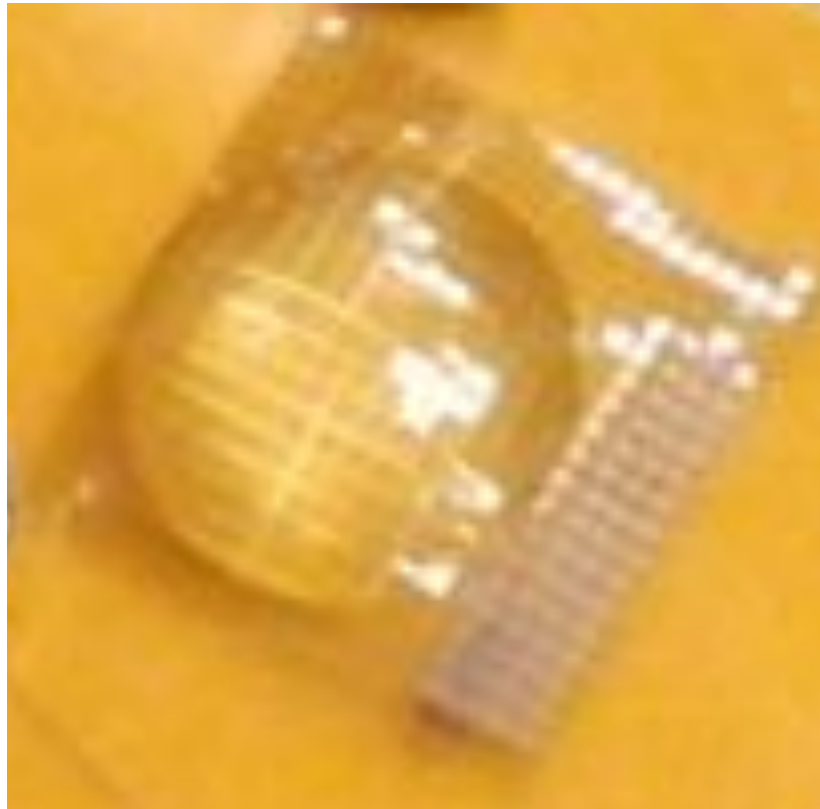


(c)



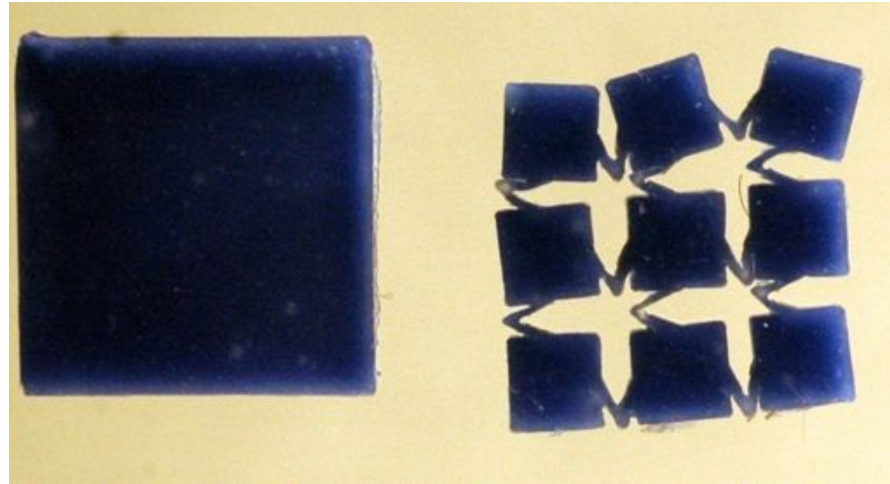
(a) Two electrical connectors partially engaged. (b) Cross-section of electrical connectors. (c) Top view of connectors showing alignment features.

Fig. 23. Conformal backing for connector



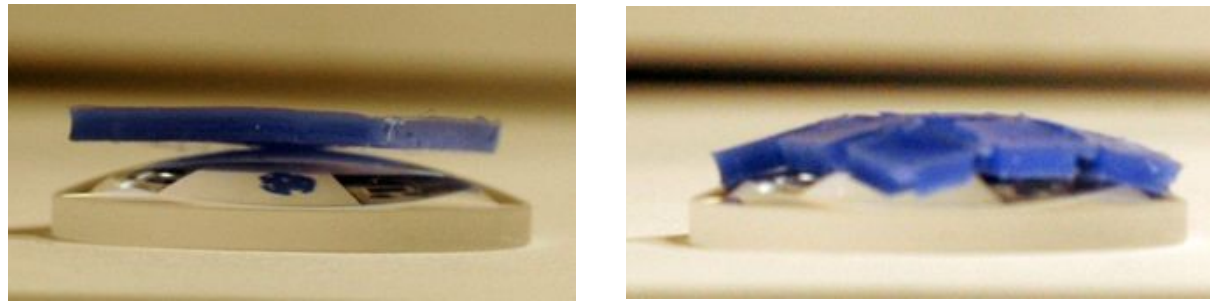
Kapton sheet laser cut in UV Laser pressed over hemisphere lens.

Fig. 24. Island/Flexure Backing Connector System



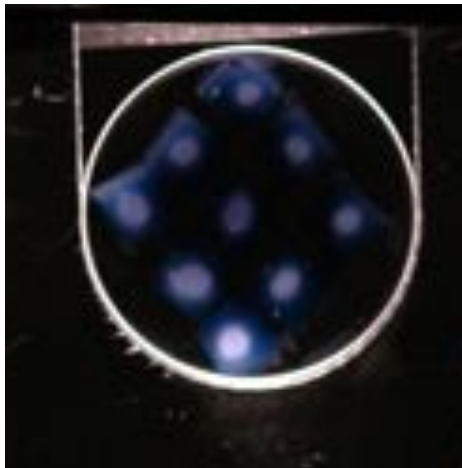
a) Control (left) of 17mm x 17mm PDMS; Engineered Backing (right) with “V” hinge flexures of same square dimensions

Fig. 24. Island/Flexure Backing Connector System



b) 1.5 mm thick control (left) and engineered backing (right) resting on optical sphere with a radius of 31.01mm

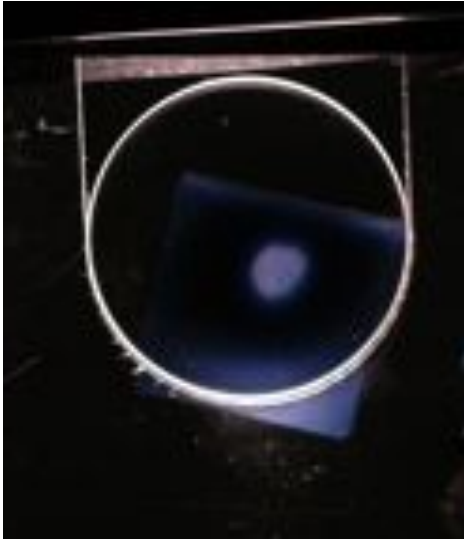
Fig. 25. Island/Flexure Backing Connector System



a): Vertical hang test on sphere radius 31.01mm for engineered backing. Contact area assumed as bright purple spots.

Table 1	Trial 1 (seen above)	Trial 2
Pixels	14375	14320
Percentage (of total curved area)	10.24%	10.2045%

Fig. 25. Control



b): Vertical hang test on sphere radius 31.01mm for control. Contact area assumed as bright purple spot.

Table 2	Trial 1	Trial 2 (seen above)	Trial 3
Pixels	4061	6360	2463
Percentage (of total curved area)	2.89%	4.53%	1.76%

Fig. 25. Engineered backing in various states of contact with the lens

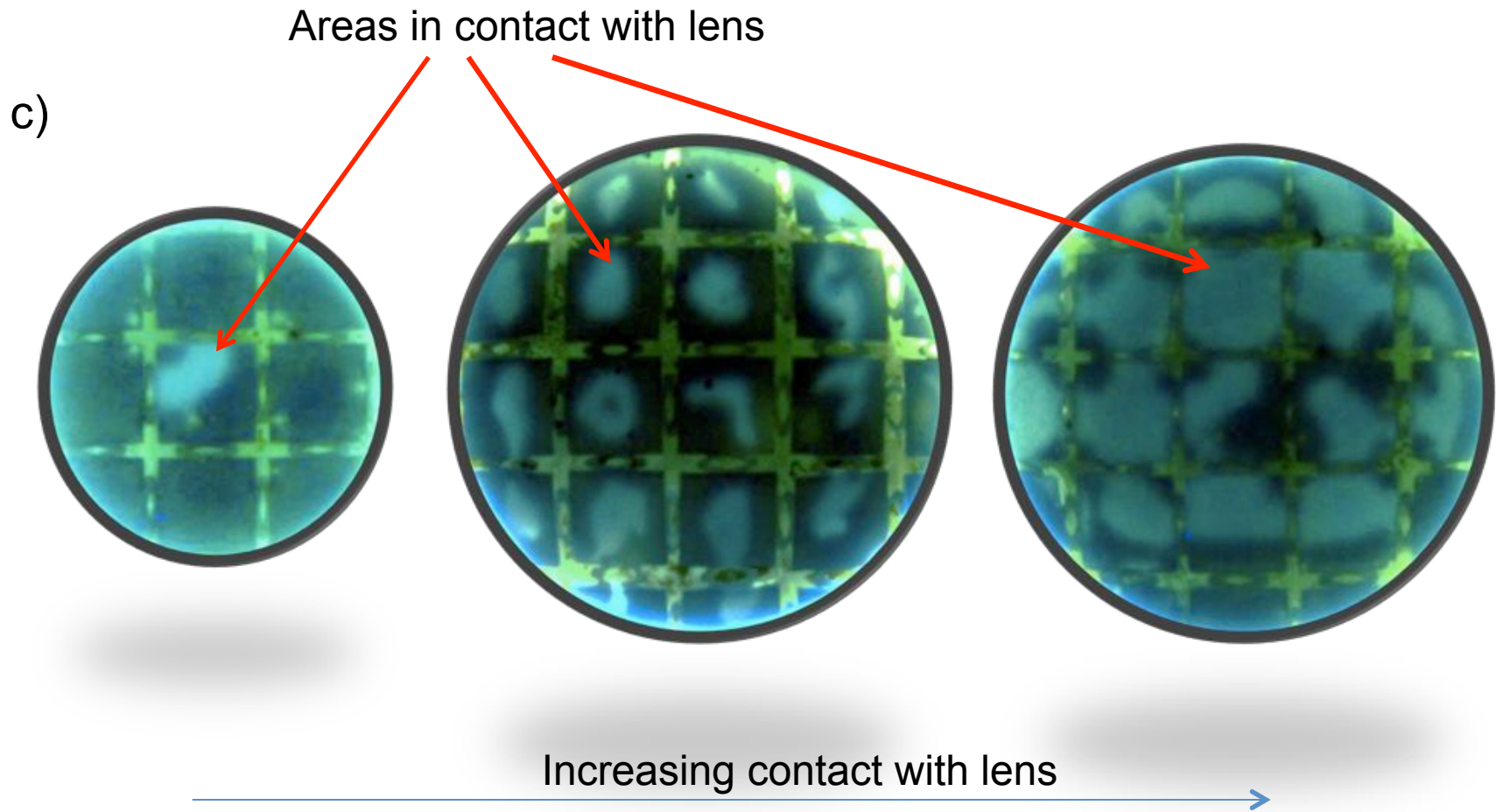


Fig 26 Self-folding Sheet

a)



b)



A 4x4 Sheet self-folded
As two shapes

c)



d)



An 8x8 sheet self-folded
As two shapes

Fig 27 The Architecture of a Self-Folding Sheet

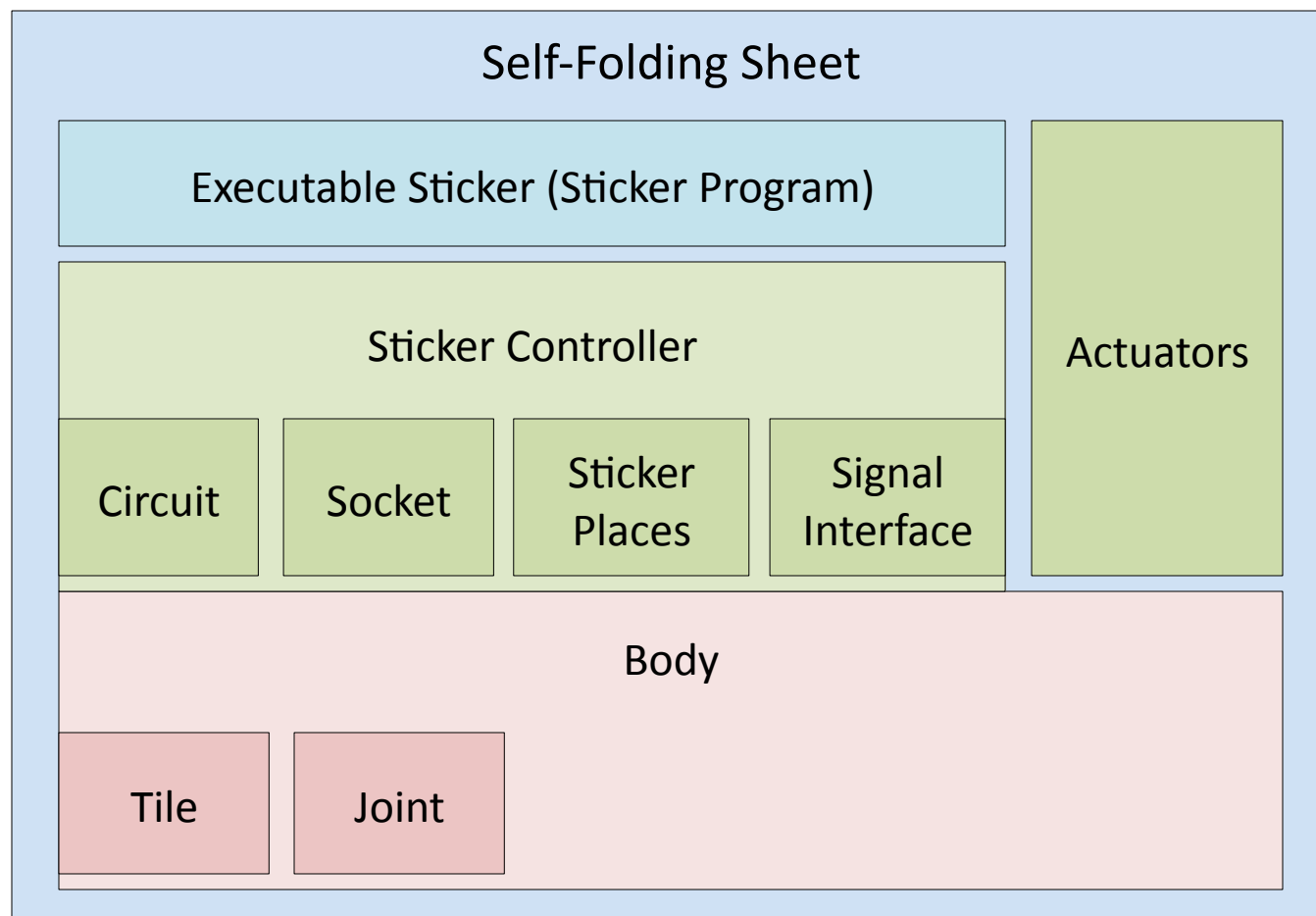
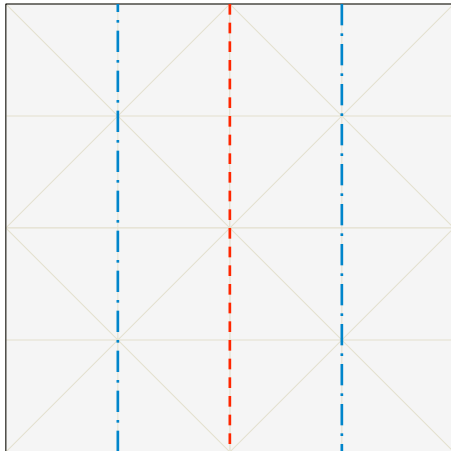


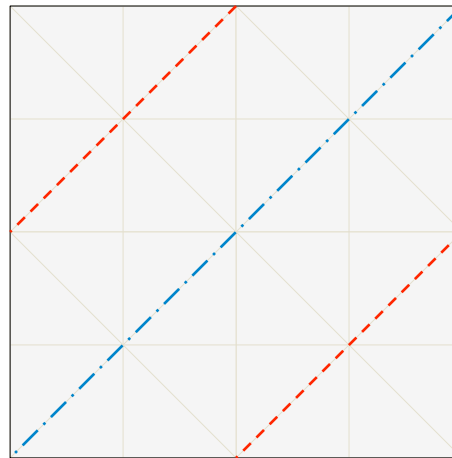
Fig 28 The Creases Required for Folding the Shape in

Fig 26s

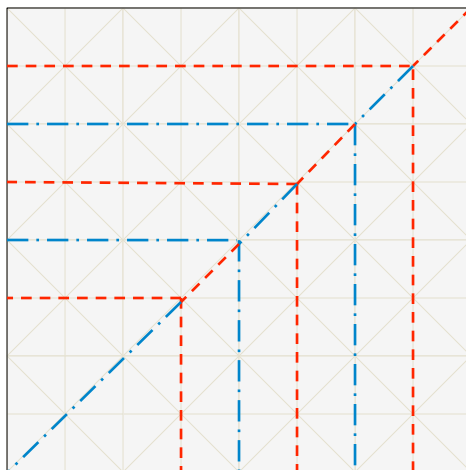
a)



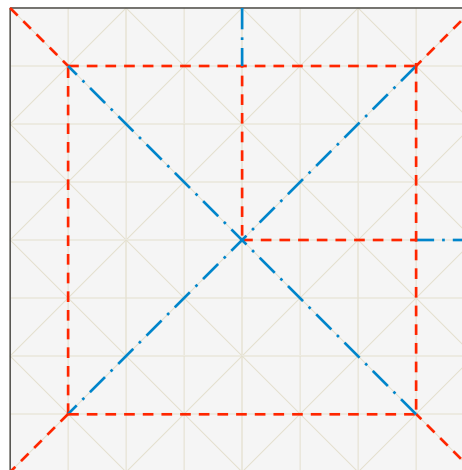
b)



c)



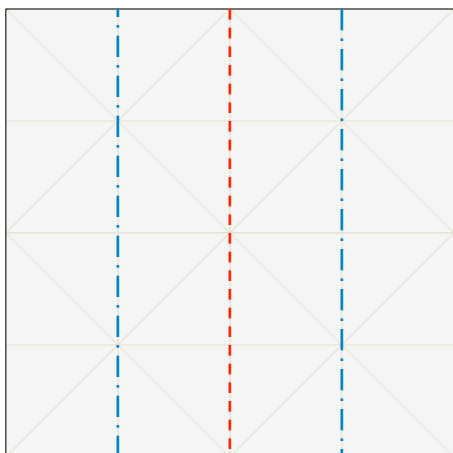
d)



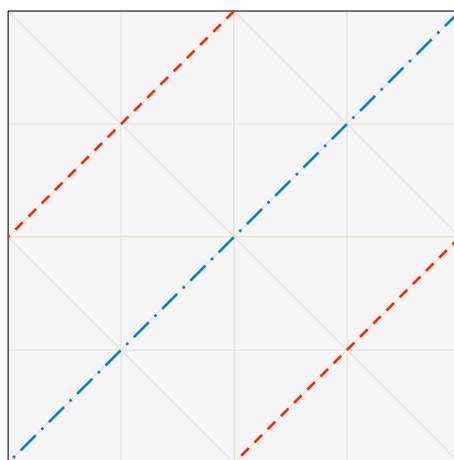
Line	Angle
	0
	+180
	+90
	-90
	-180

Fig 29: Details of folding the 4x4 Sheet

a)



b)



Line	Angle
	0
- - - -	+180
.....	+90
- . - . -	-90
- . - . -	-180

c)



d)

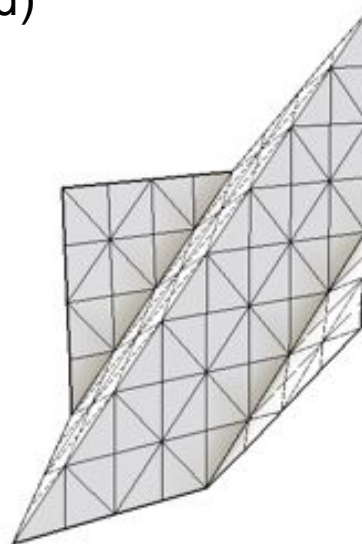
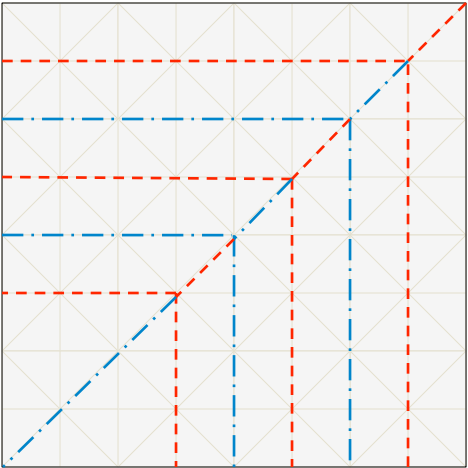
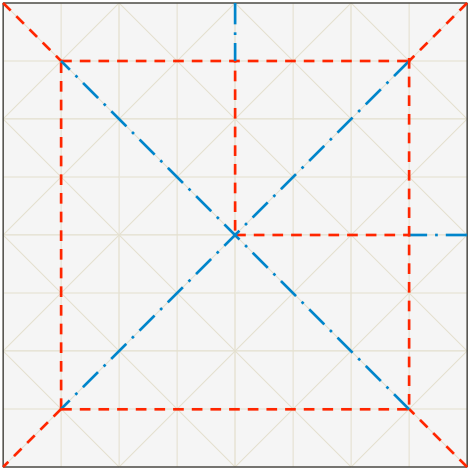


Fig 29. Details of Folding the 8x8 Sheet

a)

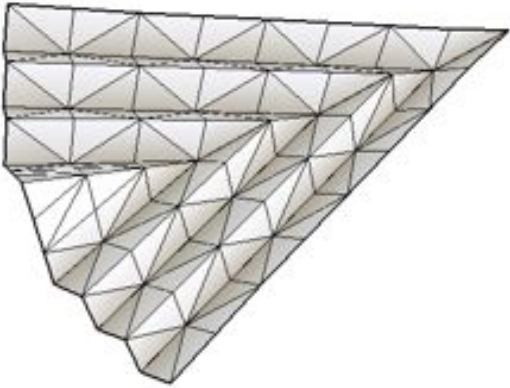


b)



Line	Angle
	0
- - - -	+180
.....	+90
- . - . -	-90
- . - . -	-180

c)



d)

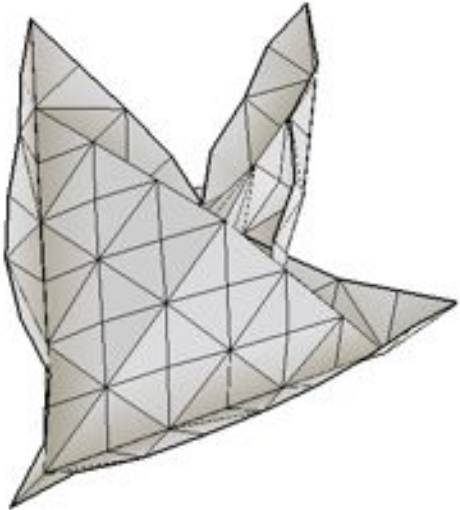
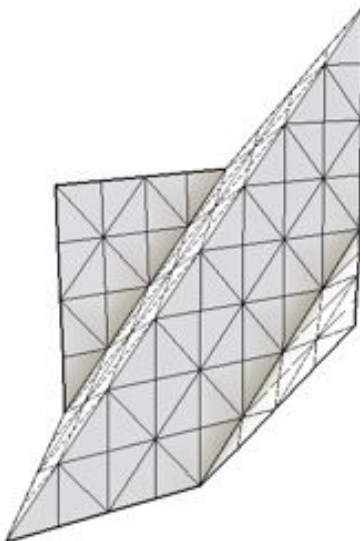


Fig 30. Snapshots from Self-Folding Simulations

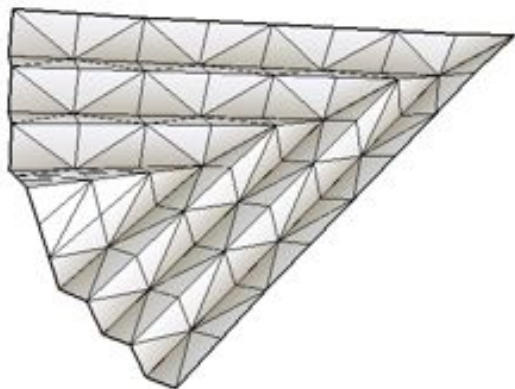
a)



b)



c)



d)

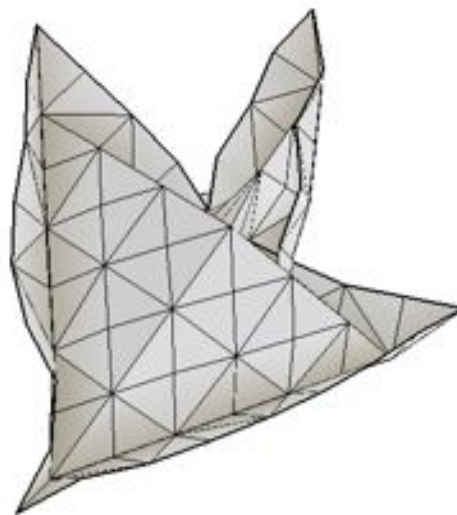


Fig 31 The Body of the 8x8 Sheet

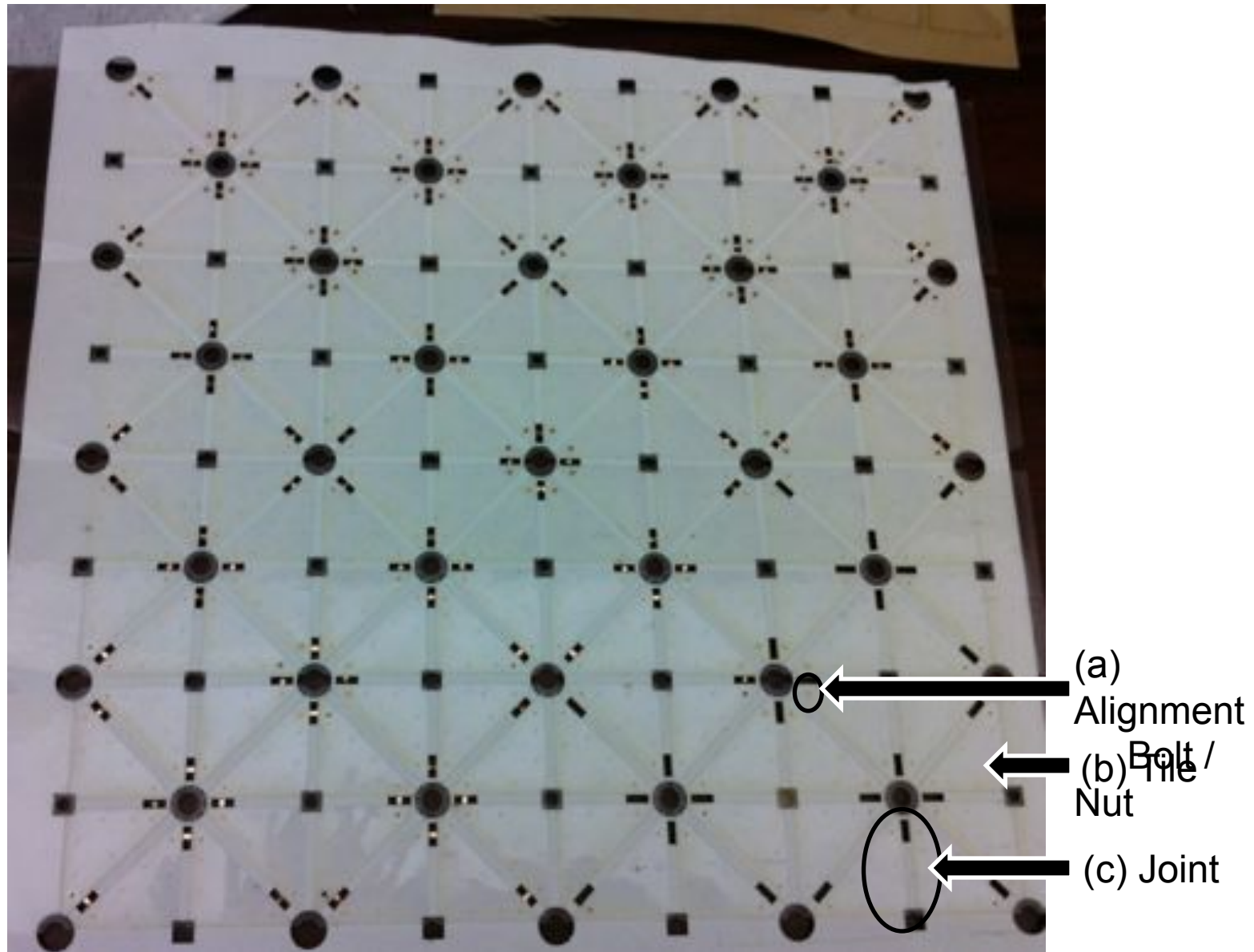


Fig 32: The Actuators Used in for Folding



Fig 33: 4x4 Sheet with Actuators

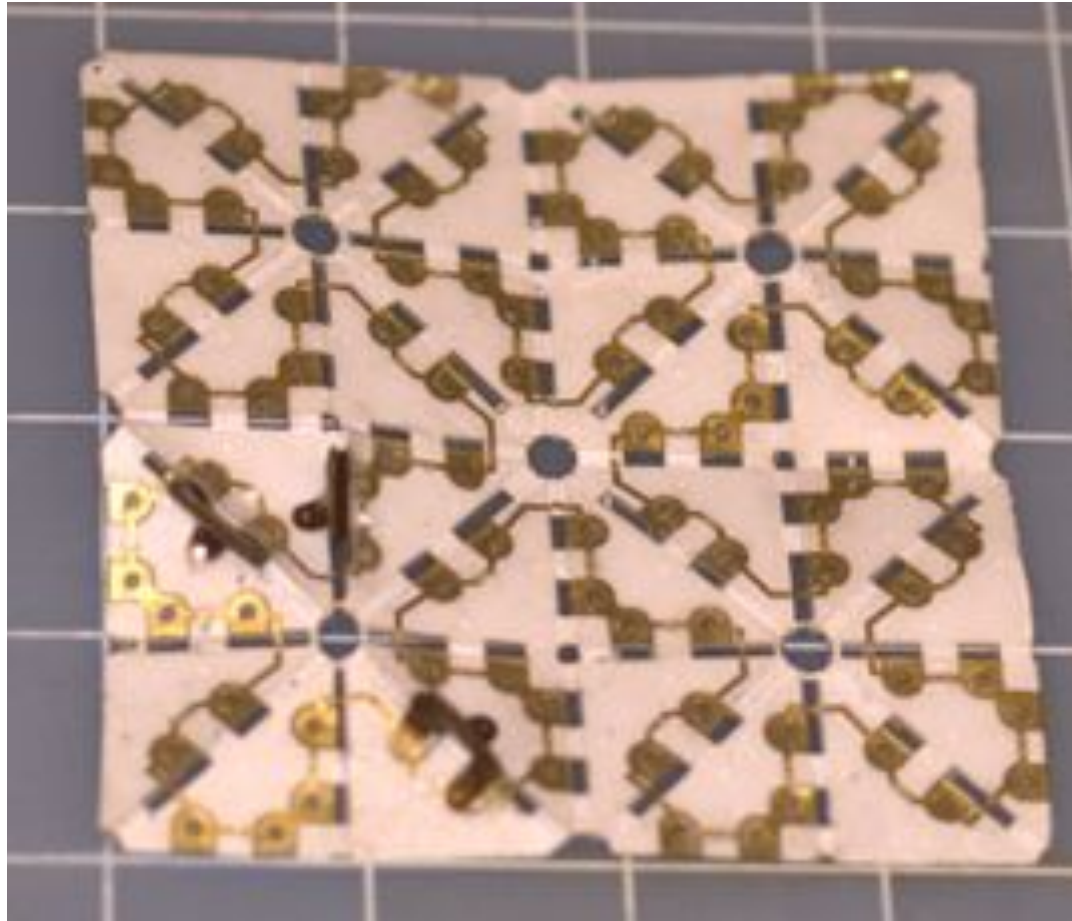


Fig 34: Details of the 4x4 Sheet with Actuators (Front)

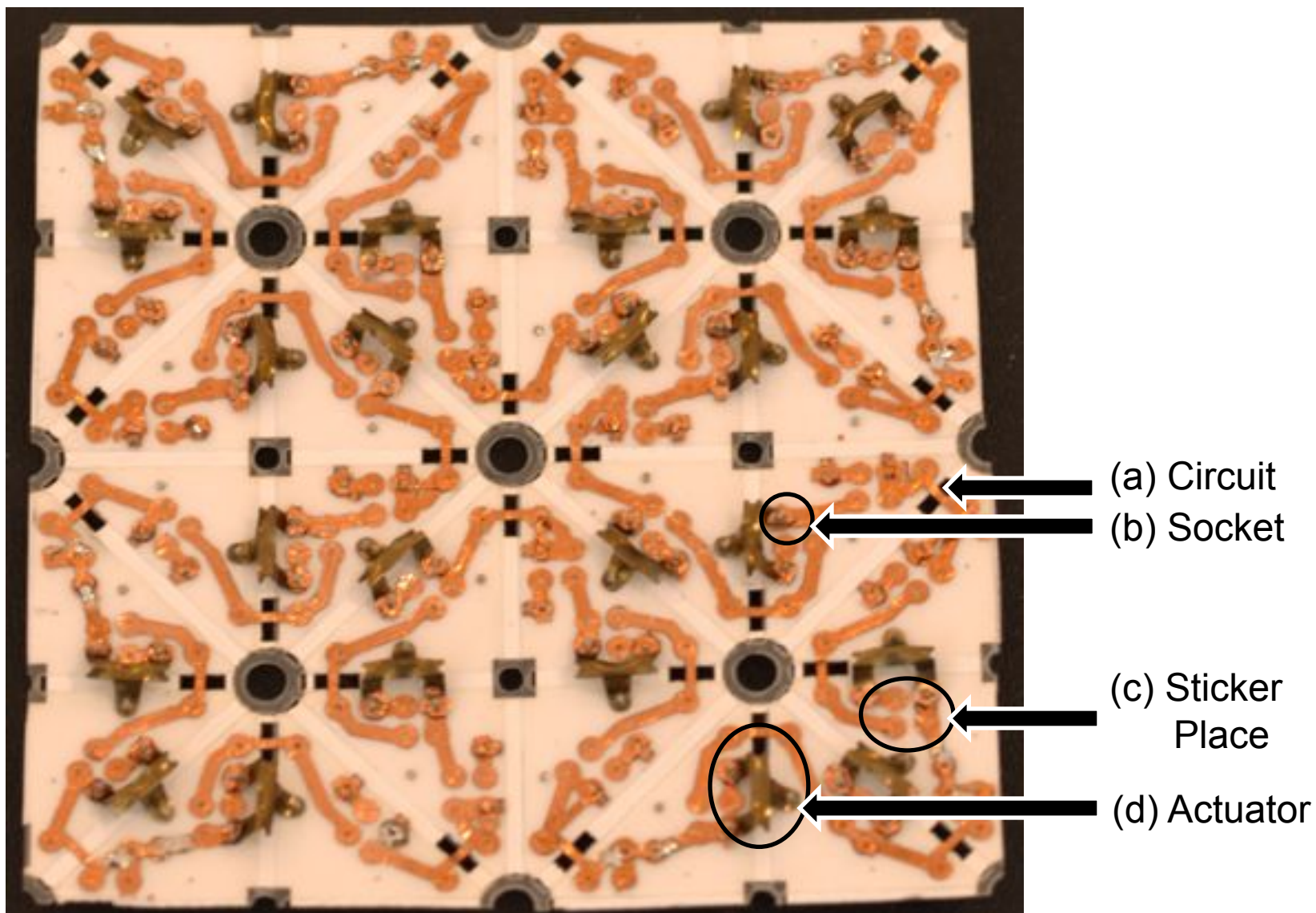


Fig 35. Details of the 4x4 Sheet with Actuators (Back)

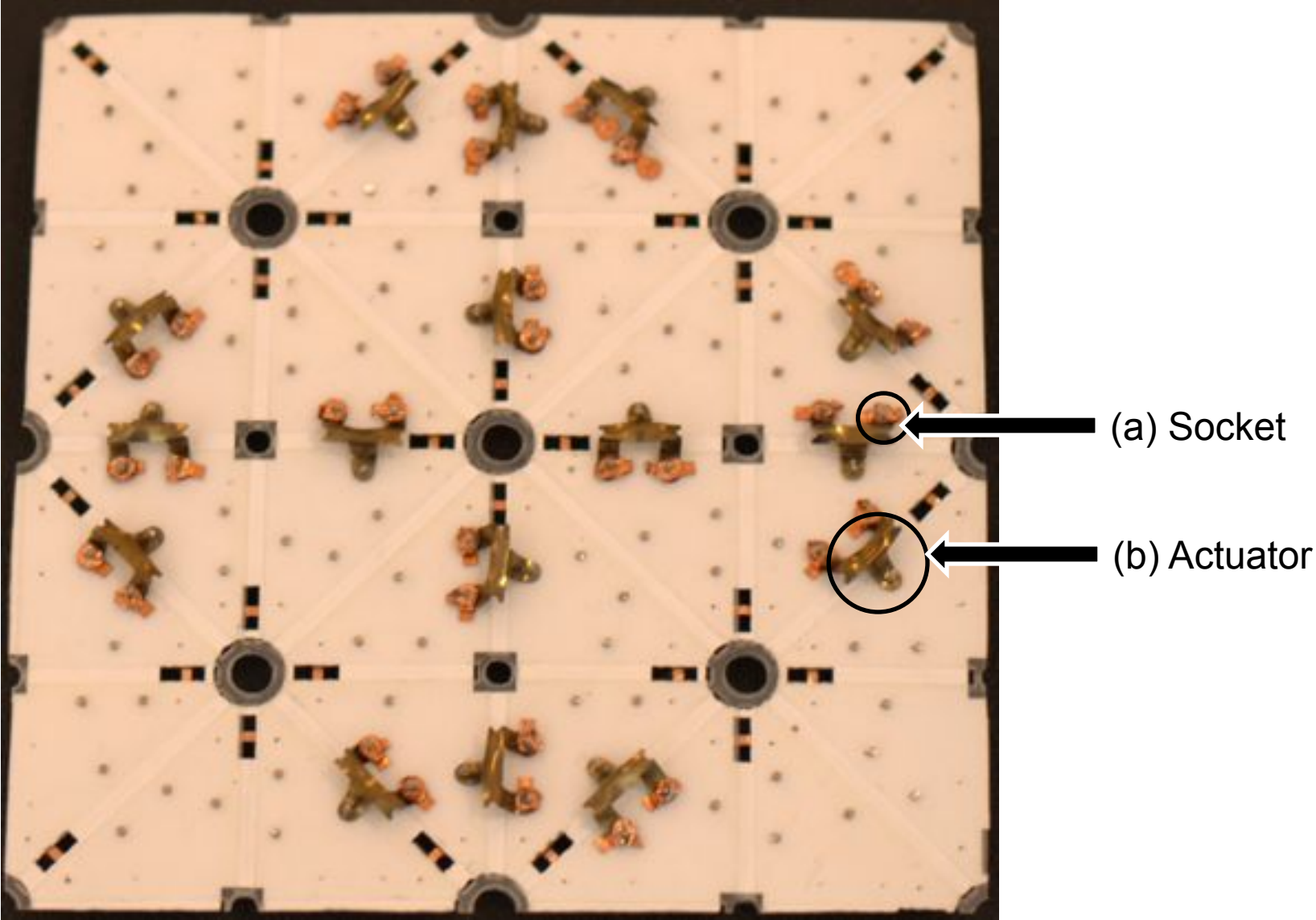
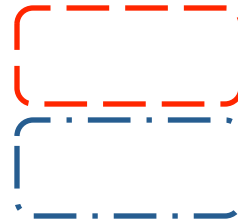
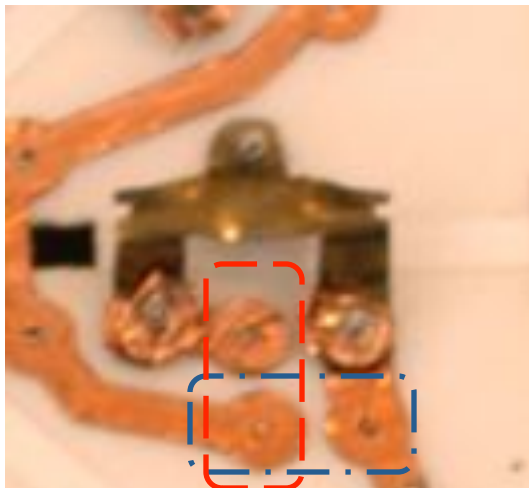


Fig 36. Details of 4x4 Sheet with Sticker Places



Enabling Actuator

Disabling Actuator

Fig 37. Completed 4x4 Sheet with Supporting Electronics for Actuators and Stickers

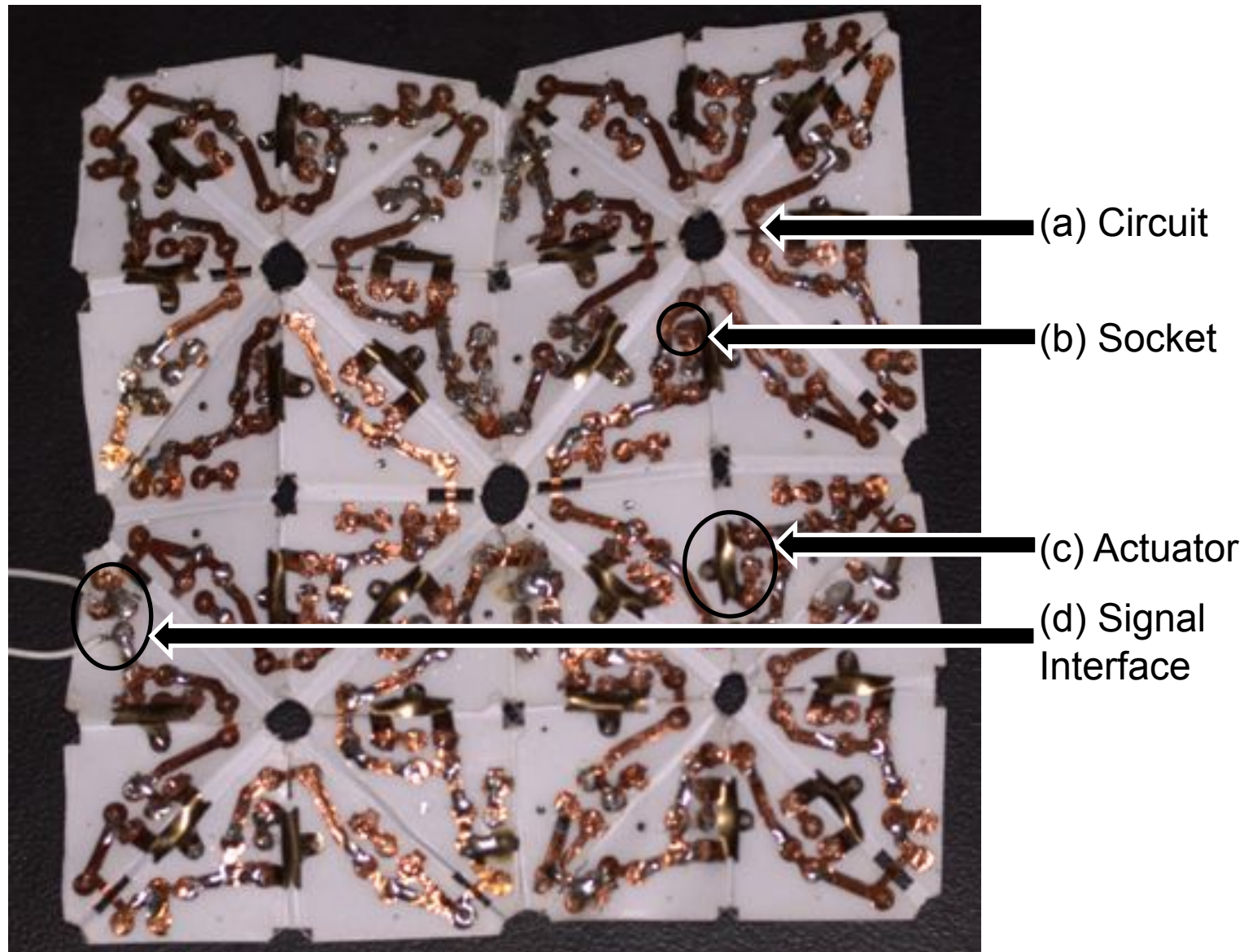


Fig. 38: Circuit Before Attachment to the Body

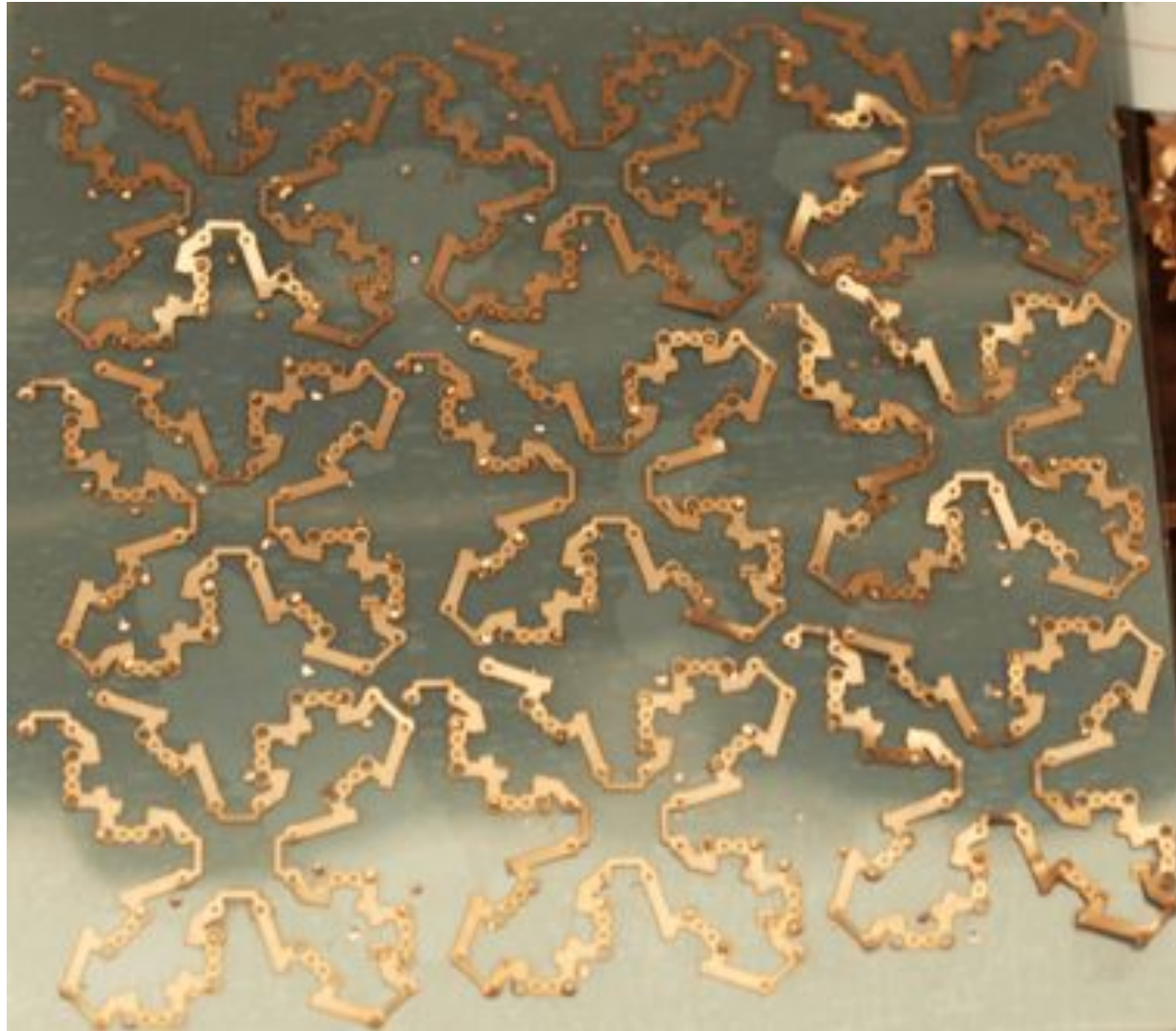
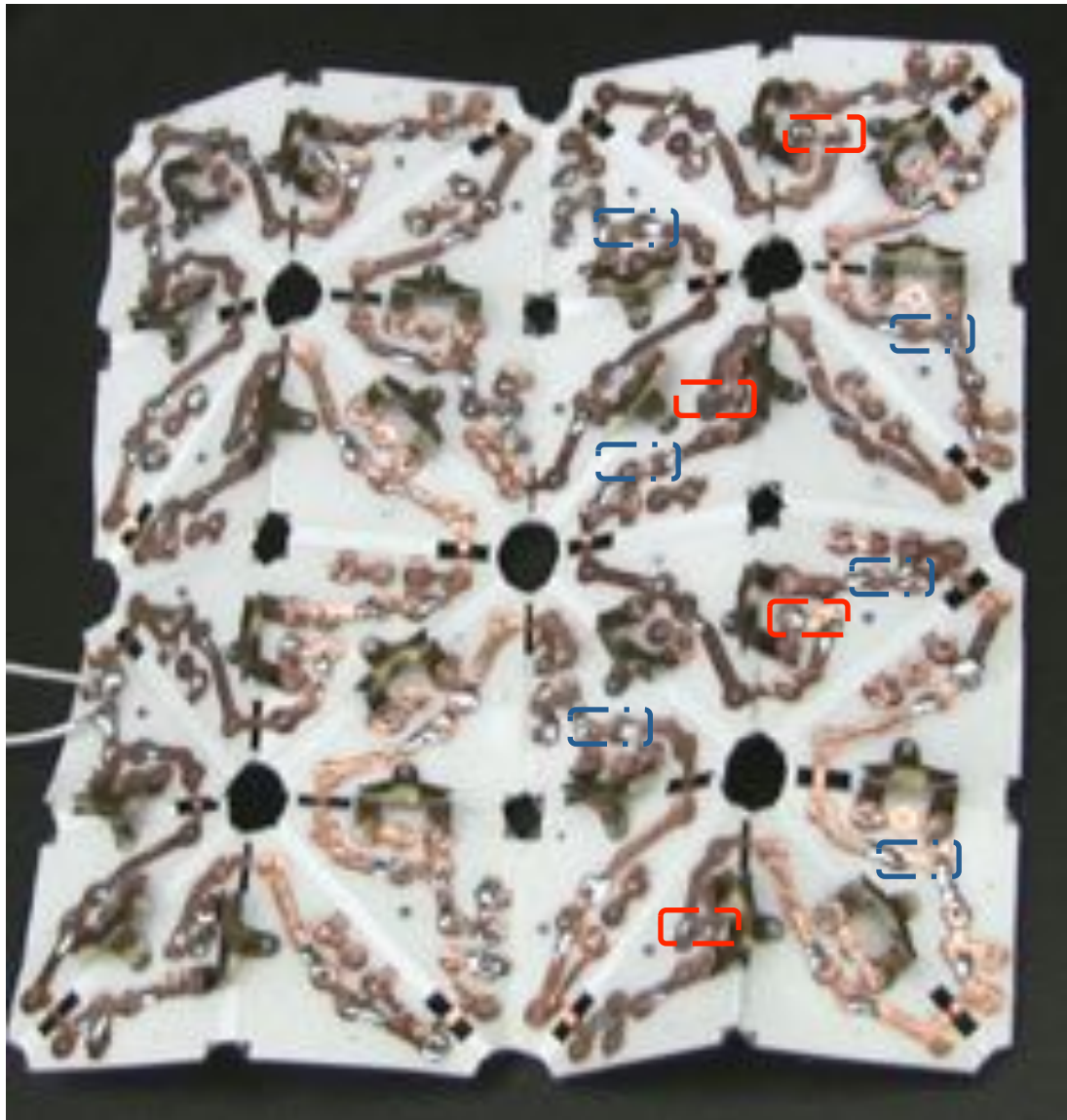


Fig. 39: 4x4 Sheet with Stickers



 Small Sticker for
Disabling Actuator

 Small Sticker for
Enabling Actuator

Fig 40. 8x8 Sheet without Actuators

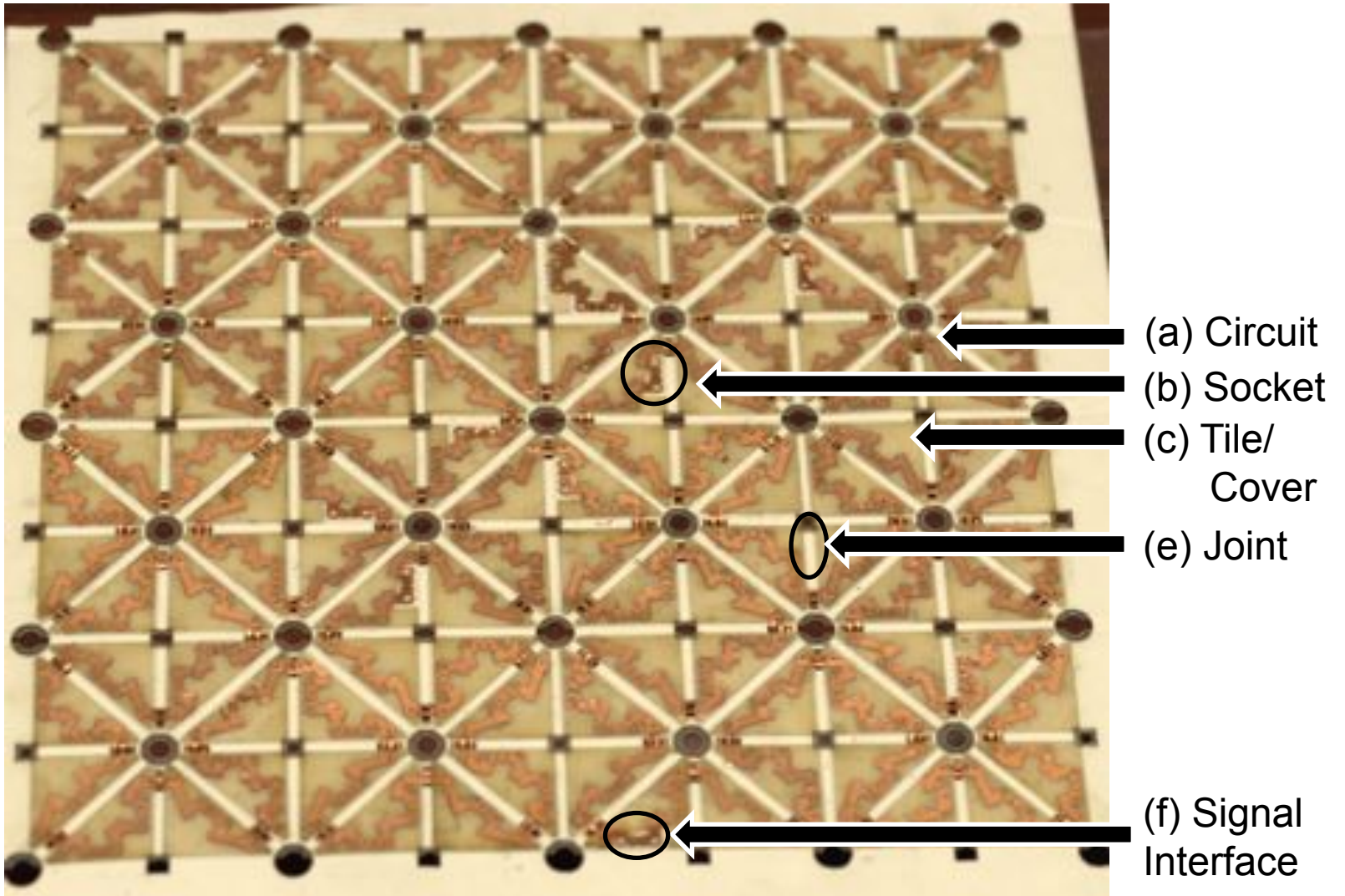


Fig 41. 8x8 Sheet with Actuators

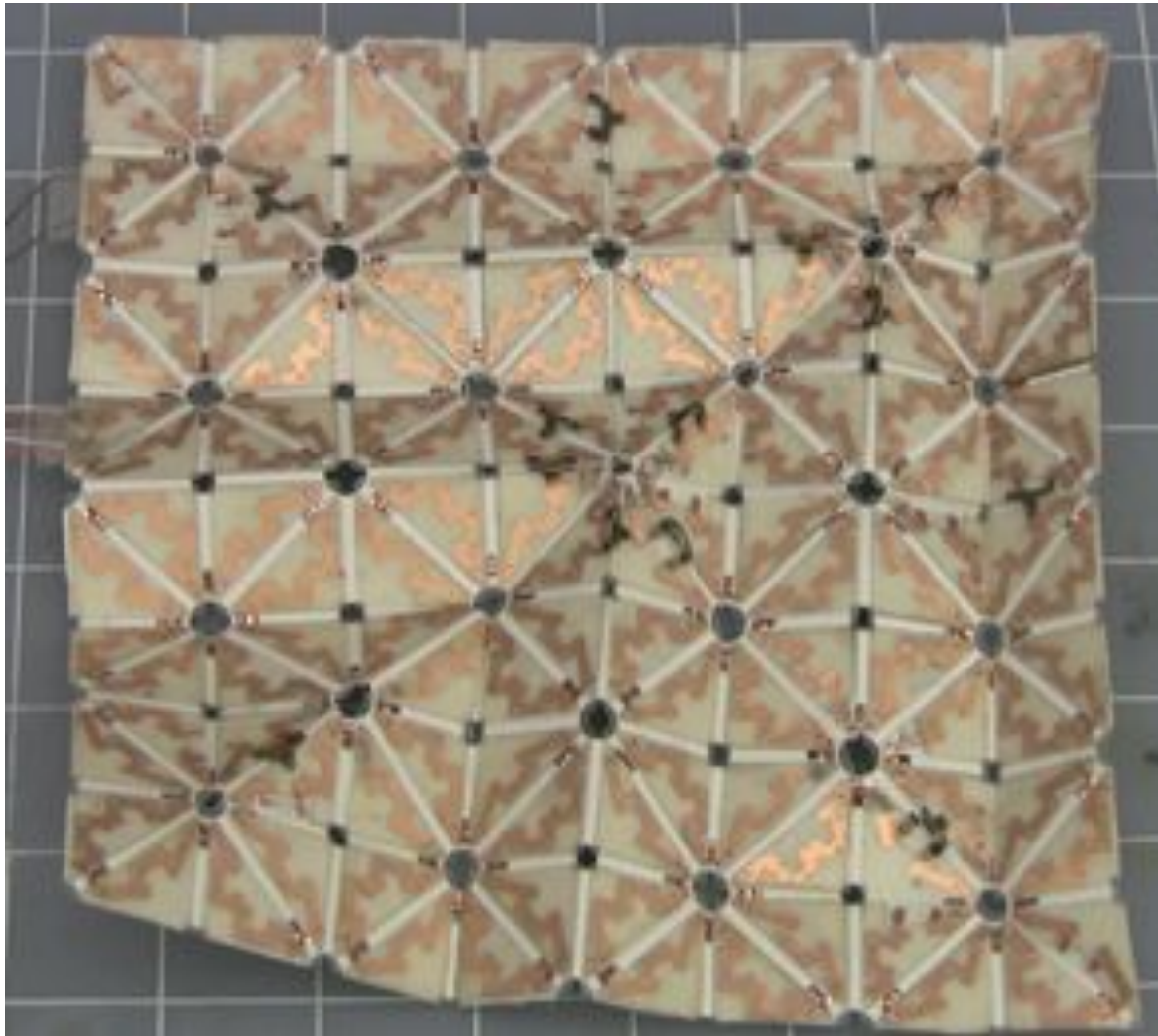
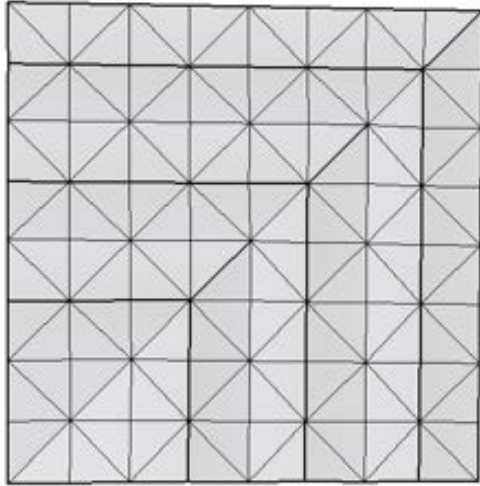
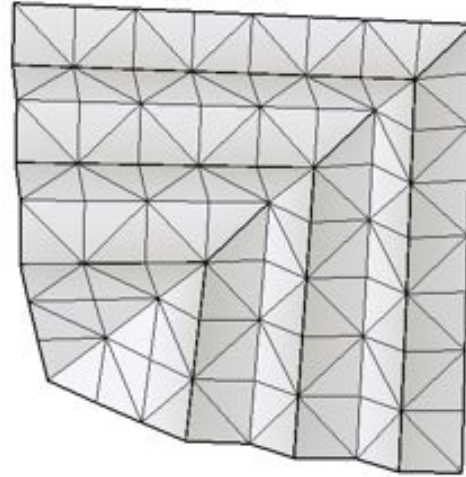


Fig. 42. Simulation Snapshots for 8x8 Sheet Folding itself into the Space Shuttle Shape

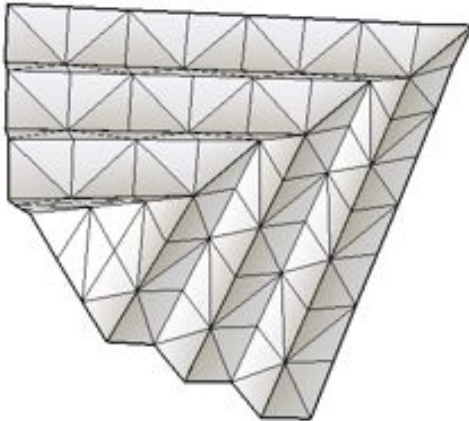
a)



b)



c)



d)

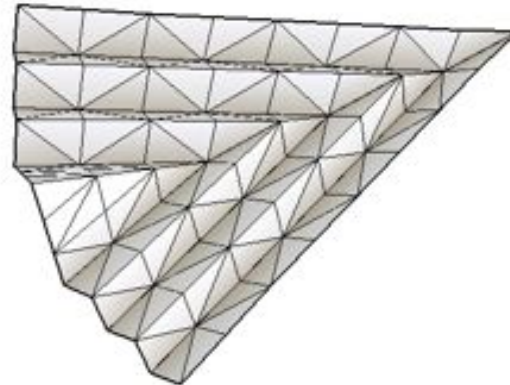


Fig. 43: Snapshots from 8x8 Experiment

00:00



00:02



00:04



00:06



Fig. 44. Simulation Snapshots from 8x8 Sheet
Folding into a Hat

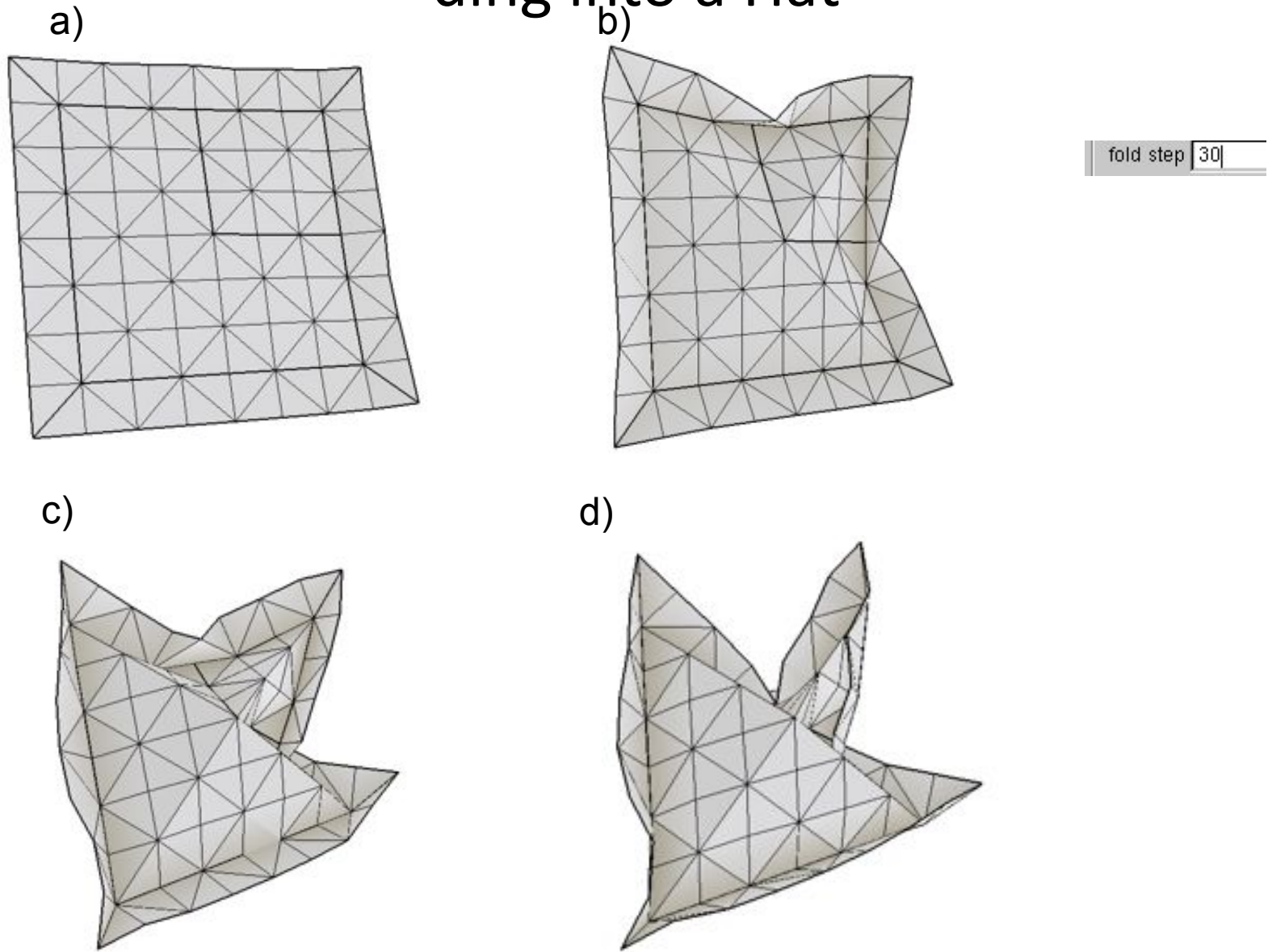


Fig 45. Experiment with 8x8 Sheet Folding Hat Shape

00:00



00:01



00:02

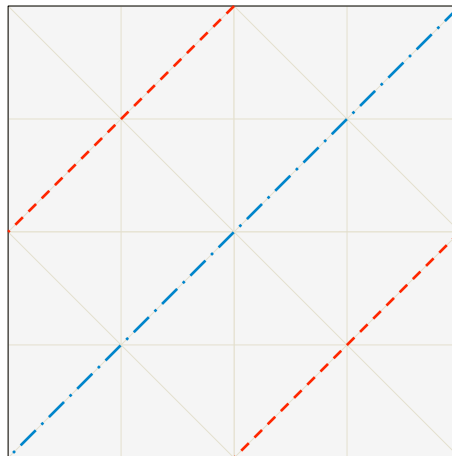
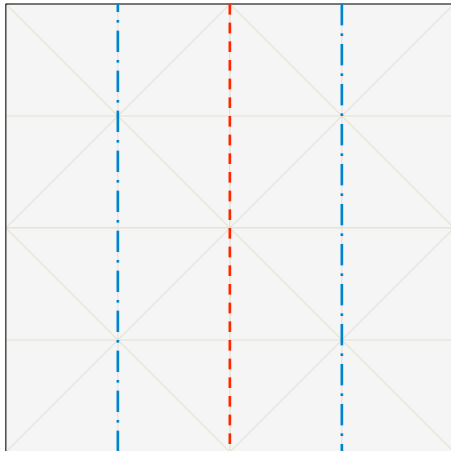


00:03



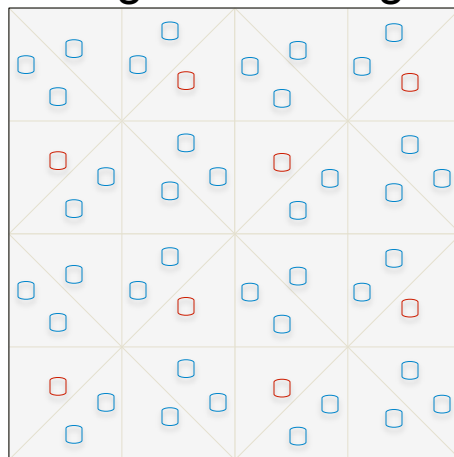
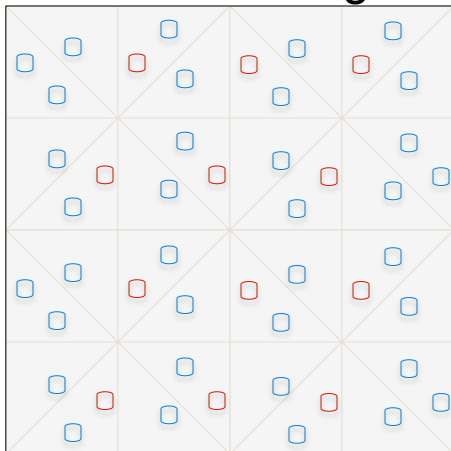
Fig. 46. Sticker Placement for 4x4 Sheet

a) Vertical Folding Shape b) Diagonal Folding Shape



Line	Angle
	0
- - - - -	+180
.....	+90
- . - . -	-90
- . - . -	-180

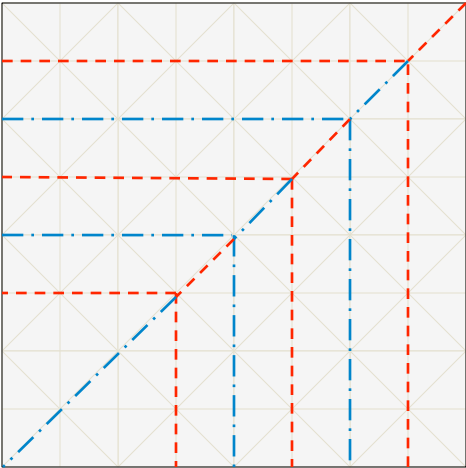
c) Executable Sticker Design for Vertical Folding Shape d) Executable Sticker Design for Diagonal Folding Shape



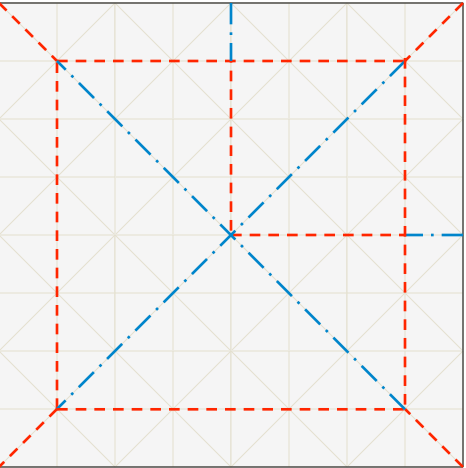
- ◻ Small Sticker for Enable Actuator
- ◻ Small Sticker for Disable Actuator

Fig 47. Folding Plans

a) Target Shape
Space Shuttle Shape

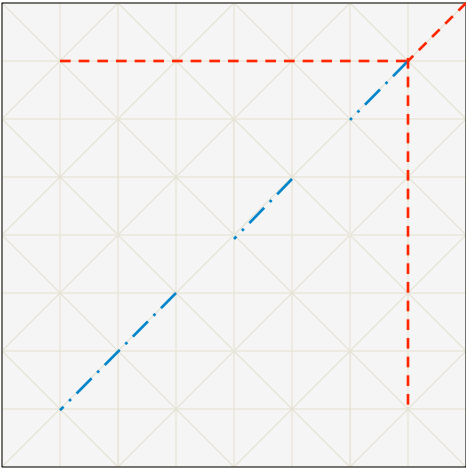


b) Target Shape
Hat Shape

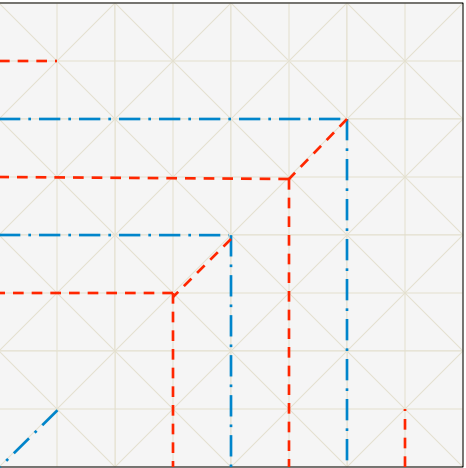


Line	Angle
	0
	+180
	+90
	-90
	-180

c) Actuator Group 1



d) Actuator Group 2



e) Actuator Group 3

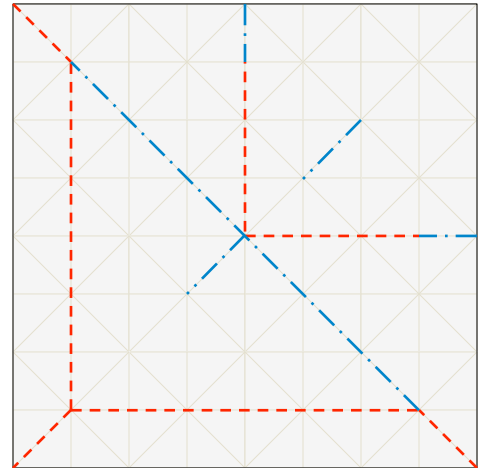


Fig 49. Smart Pebbles

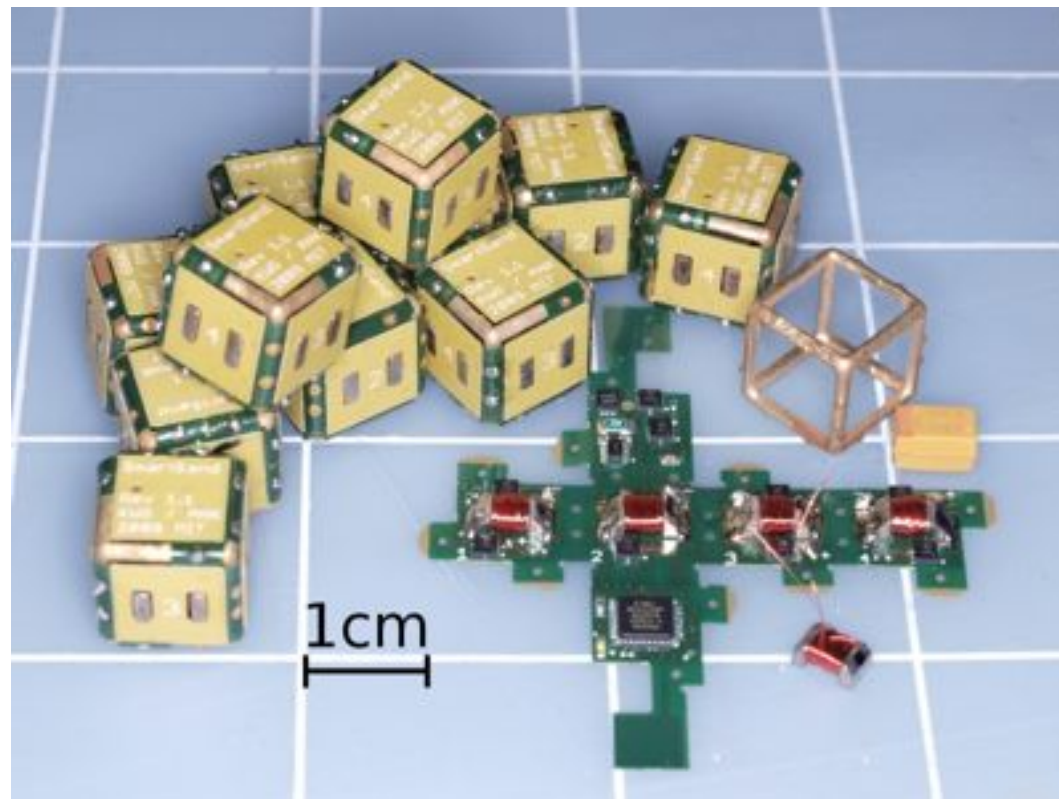
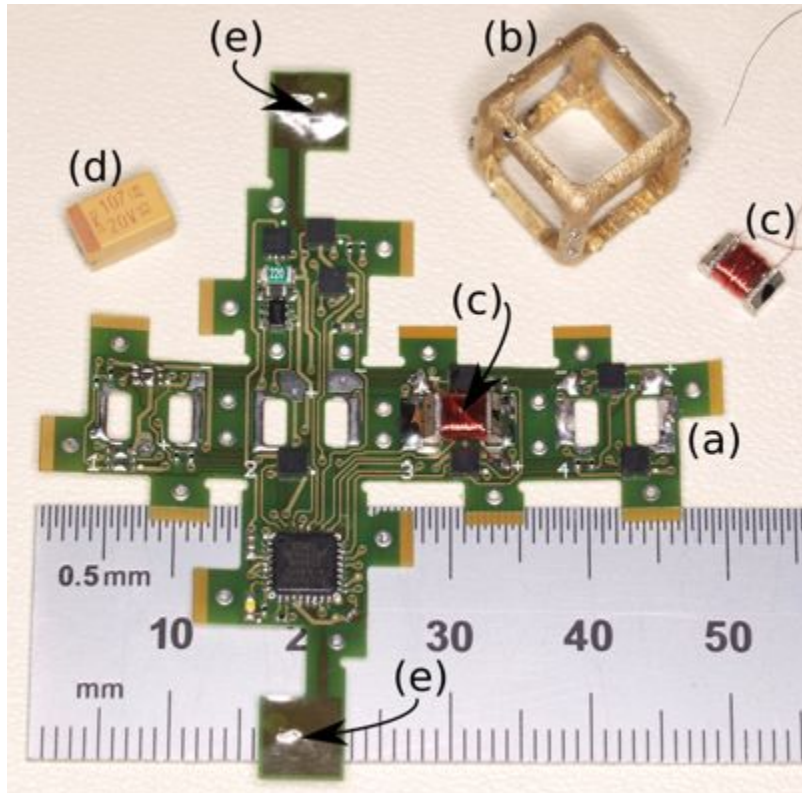


Fig 50. Pebbles Hardware



- 12mm, 4g cube with 4 active faces
- Rigid/flex with 7/7mil spacing, 15mil vias
- Investment casted brass frame
- Electropermanent (EP) magnets:
 - Latching
 - Communication
 - DC Power transfer
- 150uF 20V capacitor, *no battery*
- ATmega328 processor (32K Flash, 2-wire debug)
- 2x2 dual MOSFET packages

Assembly time: 2+ hours per module

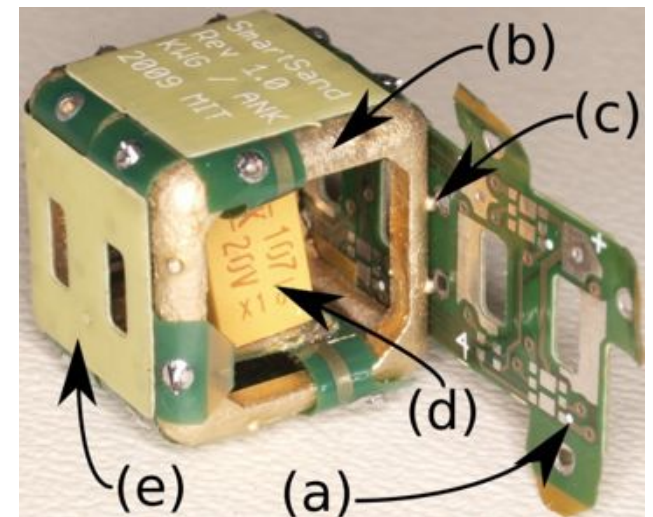
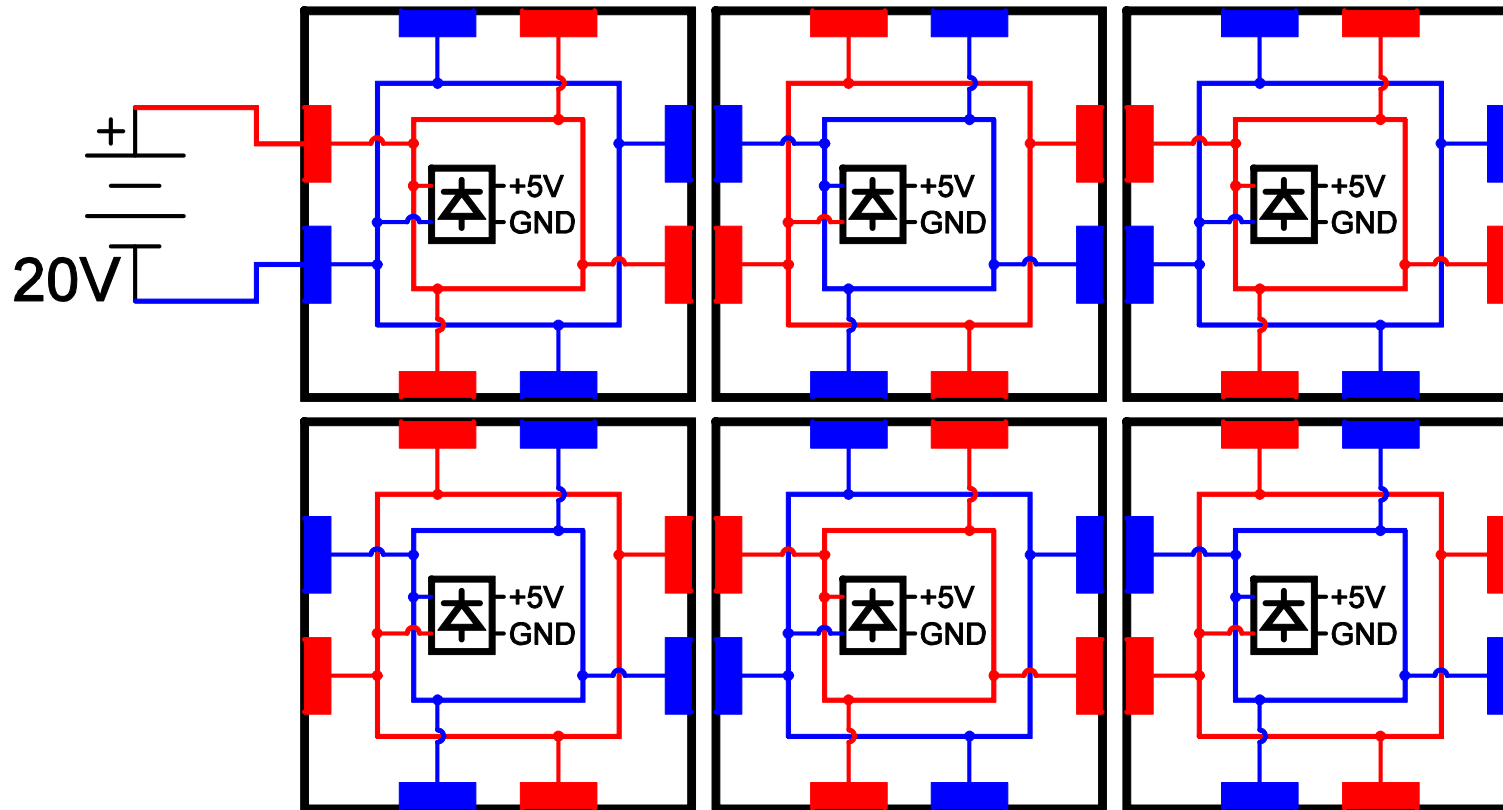
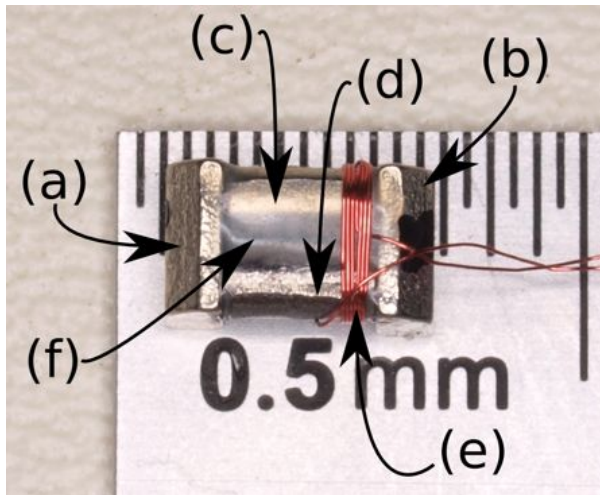


Fig 52. Pebbles Power Transfer



- Power flows through EP magnet poles
- Turning and swapping modules is okay
- 0.3 Ohm per module
- 15mA per module

Fig 53. EP Magnet Operation



- Alnico5 & NeFeB cylinders (0.125x0.625" dia)
- 5 μ m Parylene coating for electrical isolation
- 80 turns / #40AWG
- 20V, 4A, 300 μ s switching pulse (24mJ)

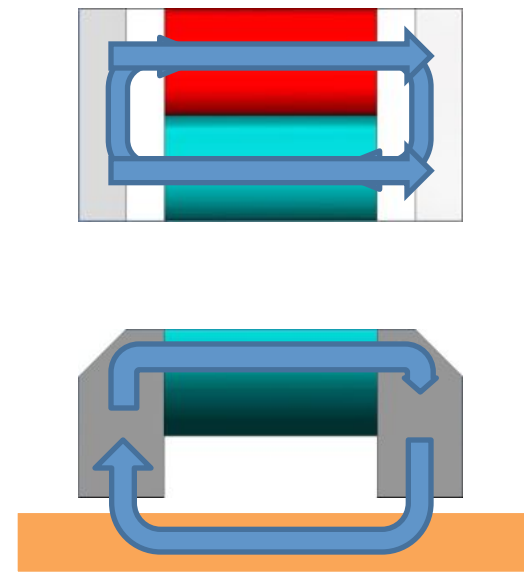
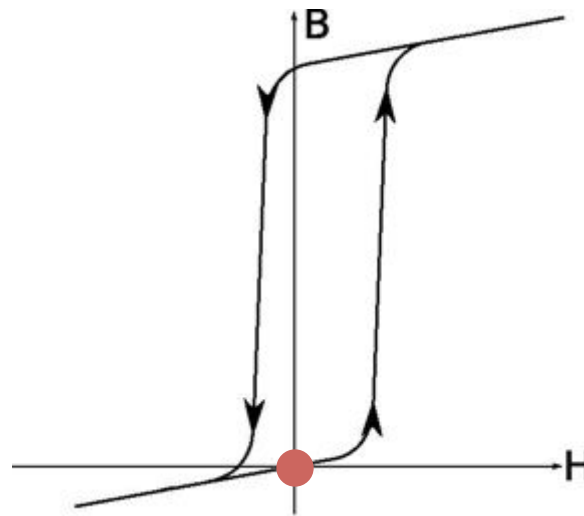
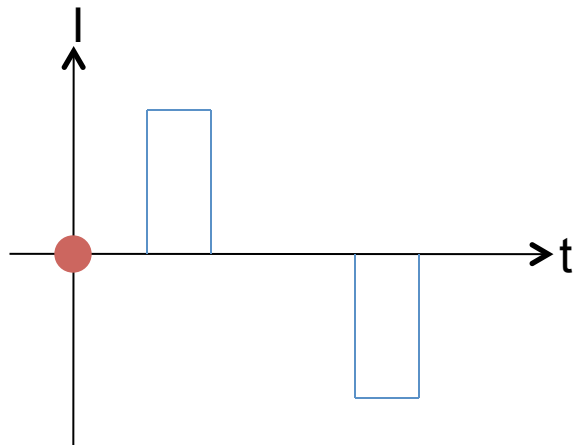


Fig 54. Humanoid Self-Disassembled from Pebbles

- Only self-disassembling system
- Smallest autonomous modular robot system
- EP magnets integrate latching, communication, and power transfer

